IMPLEMENTATION OF THE USE OF DRILL CUTTINGS IN HYDRAULIC FRACTURING RELATED OPERATIONS

A Dissertation

by

FABIÁN ALFREDO CARRASCAL DELGADO

Submitted to the Office of Graduate and Professional Studies of
Texas A&M University
in partial fulfillment of the requirements for the degree of

DOCTOR OF PHILOSOPHY

Chair of Committee,	Sara Abedi
Co-Chair of Committee,	A. Daniel Hill
Committee Members,	Ding Zhu
	Michael Pope
Head of Department,	Jeff Spath

December 2021

Major Subject: Petroleum Engineering

ABSTRACT

The objective of this study was to implement the use of drill cuttings in hydraulic fracturing-related operations. Two specific uses were studied: the use of drill cuttings as propping agents in hydraulic fracturing, and the use of drill cuttings to quantify proppant concentration in hydraulic fractures when drilling through them.

Drill cuttings as propping agents were evaluated by conducting fracture conductivity experiments utilizing a modified API fracture conductivity cell and flowing dry nitrogen. Eagle Ford drill cuttings were used as received from the field (with oil-based mud drilling fluid) and washed and dried at room temperature to eliminate the drilling fluid. The drill cuttings were mixed at different concentrations with sand proppants and they were tested. Three different sand proppants were used to investigate the effect of the sand proppant in the mixture of drill cuttings and sand proppant fracture conductivity response. The results show that the closer the sand proppant size particle distribution to the drill cuttings, the better the results; the drilling fluid present in the drill cuttings can improve the fracture conductivities results in the mixtures evaluated while keeping it lower than 5 wt%.

Quantification of sand proppant in drill cuttings was evaluated using synthetic samples made with Eagle Ford drill cuttings. A light reflection method was developed to identify, under microscope, the sand proppant particles and correlate their measured area with their mass. Knowing the total mass sample, it is possible to quantify the sand proppant mass in the drill cuttings. Blind samples were used to validate the method developed.

Finally, using a commercial hydraulic fracturing simulator, different hydraulic fractures in the Eagle Ford formation were simulated using a guar-borate cross-linked fracturing fluid to know the extent at which the sand proppant might be placed, and the distance at which a parallel well should be drilled to drill though the created hydraulic fractures and later quantify the sand proppant in the drill cuttings.

DEDICATION

I would like to dedicate this work and everything it represents to my family: Alfredo Carrascal Casadiegos (R.I.P.), who passed away shortly before my graduation, Nelly Delgado Contreras, Anyul Patricia and Mayerly Carrascal Delgado, and my girlfriend Jennifer Lemus. Without their continue support and sacrifices this milestone would not be possible. Thank you for your love and continue support.

Jennifer, from the distance, you were always there any moment I needed you.

Esta tesis también es de ustedes!

ACKNOWLEDGEMENTS

I would like to express my deepest gratitude and appreciation to Dr. A Daniel Hill and Dr. Ding Zhu for giving me the opportunity to be part of their research group. I feel, and will be forever, honored to have received countless learnings, guidance, motivation, support, and inspiration from you.

I would like to thank Dr. Sara Abedi and Dr. Michael Pope for her insight, patience, and guidance.

I would like to acknowledge and show my lasting gratitude to my parents Alfredo (R.I.P.) and Nelly, my siblings Patricia and Mayerly, and to my girlfriend Jennifer Lemus for their continue support, love, patience, sacrifices, and motivation to never give up, despite any adversity.

I would also like to thank all the members of the fracture conductivity research group.

CONTRIBUTORS AND FUNDING SOURCES

Contributors

This work was supervised by a dissertation committee consisting of Professor Sara Abedi, primary advisor, Professor A. Daniel Hill, co-advisor, and Professor Ding Zhu of the Harold Vance Department of Petroleum Engineering; and Professor Michael Pope of Department of Geology and Geophysics.

All other work conducted for the dissertation was completed by the student.

Funding Sources

Graduate study was supported in part by a graduate research assistantship from Texas A&M University.

This work was made possible in part by funding provided by NEXEN to complete the research presented in chapter 2, and by the Department of Energy's Office of Fossil Energy and the National Energy Technology Laboratory through the award "The Eagle Ford Shale Laboratory: A Field Study of the Stimulated Reservoir Volume, Detailed Fracture Characteristics, and EOR Potential," and its contributions from INPEX Eagle Ford, LLC to complete the chapters 3 and 4.

TABLE OF CONTENTS

Page

LIST OF FIGURES

Page

LIST OF TABLES

Page

1. INTRODUCTION

The hydrocarbons production from shale formations is identified by two main steps: the drill cuttings production while drilling through the formations and the hydrocarbons production through hydraulic fractures. Drill cuttings and hydraulic fracturing operations are used to be treated independently. In this dissertation, drill cuttings were correlated with hydraulic fracturing by implementing the use of drill cuttings in hydraulic fracturing-related operations.

This dissertation is divided into four chapters. The first chapter is a general overview to introduce drill cuttings and hydraulic fracturing operations. It is described how the drill cuttings, being an inevitable byproduct associated with drilling a well, constitute one of the most hazardous wastes of the petroleum industry. It provides the reader with the different toxicological problems associated with non-water drill cuttings so that when working with them healthy measurements can be taken. General concepts about hydraulic fracturing and history timeline are presented. The second chapter presents the study of the use of drill cuttings as propping agents in hydraulic fracturing operations by measuring the fracturing conductivity response using a modified API conductivity cell. The third chapter shows the use of drill cuttings to quantify sand proppant in hydraulic fractures. For this, synthetic samples were prepared using Eagle Ford drill cuttings. The final chapter exhibits the results of the simulated extent of sand proppant placement in hydraulic fractures in the Eagle Ford formation using a guar-borate high viscosity fracturing fluid.

This chapter introduces drill cuttings, describing its types, toxicity and disposal, and later move to hydraulic fracturing, doing a history and timeline description.

The general objective of this research is to implement the use of drill cuttings in hydraulic fracturing-related operations, and the specific objectives are:

- Use drill cuttings as propping agents in hydraulic fracturing.
- Use drill cuttings to quantify proppant concentration in hydraulic fractures.

1.1. General Overview.

Oil and gas production from shale formations has significantly contributed to the U.S. economy since the production boom started in 2008. As shown in the resource pyramid presented by Holditch (2006), unconventional resources, including shale oil and gas reservoirs, are found in larger volumes and require improved technologies to be developed (Elsarawy and Nasr-El-din, 2018).

There are more than 20 significant shale gas plays in the U.S. which are widely distributed; the most active plays are the Barnett, Woodford, Haynesville, Marcellus, and Fayetteville shales. Other active shale oil plays are the Bakken, Niobrara, Utica, and most recently, the Eagle Ford (Elsarawy and Nasr-El-din, 2018).

1.2. Drill cuttings.

Drill cuttings are an inevitable byproduct associated with drilling a well. Cuttings are a combination of different-sized geological materials and drilling fluids. Their characteristics depend on the type of rock drilled, the drilling process employed, the type of drill bit used, and the drilling mud fluid applied. The drilling mud fluid can be either water-based mud (WBM), oil-based mud (OBM), or synthetic mud (SBM) (Cedola et al., 2020). SBM are chemical formulations, while OBM is petroleum derivatives (Seixas et al., 2014). Drilling fluids are usually composed of the base fluid, weighting agents such as barite and clay, and also stabilizing, organic materials such as lignite. The main component of drilling fluid is bentonite clay. The clay is mixed with the base fluid, while several compounds are added to the mixture, such as cellulose polymers and barium sulfate, to increase viscosity. These additives increase the hazardous potential of the drilling fluid. In drilling operations, OBM and SBM are generally used because they offer comparative advantages over WBM in complex geological wells and horizontal wells. They are more suitable to drill sensitive shales, allowing drilling to be faster than the WBM, providing excellent shale stability, and high temperature and pressure stability (Xie et al, 2013; AlBeshr et al., 2016), high salt concentration resistance beneficial to the stability of the shaft wall, and small damage to the oil and gas layer (Wu et al., 2019).

1.2.1. Toxicity of the drill cuttings.

The main drawbacks of oil-based or synthetic-based cuttings produced, referred to as non-water cuttings (NWC), originate from the environmental impact

and worker safety issues associated with its chemical composition. NWC constitutes one of the most hazardous wastes of the petroleum industry, it can contain complex hydrocarbons, heavy metals, dissolved minerals, and naturally occurring radioactive materials, which released to the surrounding ground and aquatic environments can cause deleterious effects on them (Somee et al., 2018).

NWC are toxic pollutants due to poly aromatic hydrocarbon content of diesel, usually used as the base fluid of oil-based drilling fluids, which typically range between 5 to 10 vol% (Yousef et al., 2017). Complex mixtures of petroleum hydrocarbons, such as alkane and aromatic fractions, can be also found. Those compounds are carcinogenic and of mutagenic properties, and can lead to other health problems (Mandal et al., 2012).

The heavy metals contained in NWC can be harmful to the environment and humans. Some previous studies have shown that heavy metals present in NWC can cause inflammation, lung and heart disease, and DNA damage through ingestion, inhalation, and dermal contact (Xu et al., 2016). For example, excessive levels of Pb in the blood can induce inhibition of enzyme activity and destruction of the central nervous system (Gillis et al., 2012). Cr, Cu, and Zn can cause non-carcinogenic risks such as nerve damage, headache, and liver disease (Liu et al., 2013). Ni is closely related to cardiovascular disease and respiratory disease (Lippmann et al., 2006). Hg accumulated in adipose can also damage the central nervous system (Xu et al., 2018).

1.2.2. Drill cuttings cleaning and disposal.

Two of the biggest issues regarding NWC are cleaning and disposal. Cleaning and disposing of NWC is a costly operation. NWC are required to undergo cleaning to remove any remaining drilling mud fluid before disposal (Cedola et al., 2020). The treatment of NWC in an environmentally sound manner is a challenging task due to the complex nature of the wastes (AlBeshr et al., 2016). The NWC are treated first at the rig site, by a series of solid-control equipment, in order to remove the drilling fluid until getting fluid ranges between 15 to 20 vol%. Later, a secondary treatment is applied to reduce the drilling fluid content to less than 1% to satisfy most regional emission policies (Huang et al., 2018). Different techniques can be applied in this step, such as: solvent extraction, chemical washing, solidification/stabilization, etc. The most popular technique adopted for the treatment of NWC is thermal desorption, which uses heat to increase the volatility of contaminants to remove hydrocarbons and water from the solid matrix. Later, the NWC are Incinerated (Kleppe et al., 2009). However, environmental concerns due to the ash production of heavy metals and radioactive materials are still present (AlBeshr et al., 2016). Nonetheless, all these operations can be expensive, and accidental NWC spillage can occur with serious detrimental effects on humans and the environment (Siddique et al., 2017; Wu et al., 2019).

1.3. Hydraulic fracturing.

Hydraulic fracturing is a technique used for stimulating wells completed in low-permeability reservoirs. The process involves the pressurization of an isolated perforated section of the wellbore with a viscous fluid until the induced stress exceeds the formation strength, which causes a failure and thus creates the fracture. Proppants are then pumped into the newly created fracture with viscous fracturing fluid as a carrier. Once initiated, the fracture propagates as additional fracturing fluid is injected. Following the release of the fracturing pressure, the proppants hold the fracture open and provide a conductive channel through which the reservoir fluids flow to the wellbore (Acharya, 1988).

Hydraulic fracturing is one of the most important and enduring technologies ever developed by the oil industry. In the decades since its introduction in the late 1940s, the role of this technology in improving production and increasing recoverable reserves is probably second only to rotary drilling. Hydraulic fracturing is, today, the primary means of increasing and maintaining well productivity. The combination of horizontal wells and hydraulic fracturing has greatly expanded producers' ability to profitably recover natural gas and oil from low-permeability geologic plays—particularly, shale. Unlike drilling technology which has seen huge improvements over the last decade, fracturing technology still resides in the arena of technologies that were, for the most part, developed in the 1950s and 1960s (Smith and Montgomery, 2015).

1.3.1. History and timeline.

Fracturing can be traced back to the 1860s when liquid and later solidified nitroglycerin was used to stimulate shallow, hard rock wells in Pennsylvania, New York, Kentucky, and West Virginia. This principle proved to be effective in increasing the ultimate recovery of oil and can also be applied to water and gas wells. It was not until the 1930s that the idea of injecting fluid (acid) into the ground to stimulate a well was tried (Smith and Montgomery, 2015, Temizel et al., 2016). The “pressure-parting” phenomenon was recognized in well-acidizing operations as a means of creating a fracture, which would not completely close due to the acid etching. This would leave a flow channel to the well and enhance productivity. This phenomenon was confirmed in the field, not only from acid treatments but also during water injection and squeeze cementing operations. To understand “formation breakdown” during acidizing, water injection, and squeeze cementing, Floyd Farris of Stanolind Oil and Gas Corporation (Amoco) performed an in-depth study to establish a relationship between observed well performance and treating pressures. From this work, Farris originally conceived the idea of hydraulically fracturing a formation to enhance production from oil and gas wells. The first experimental treatment to “HydraFrac” a well, for stimulation, was performed in the Hugoton gas field in Grant County, Kansas, in 1947 by Stanolind. A total of 1000 gal of Napalm (naphthenic acid and palm oil-thickened gasoline was injected, followed by a gel breaker, to stimulate a gas-producing limestone formation at 2400 ft. The deliverability of the well was not changed appreciably. The HydraFrac process was first introduced to the industry in a paper written by J. B. Clark of Stanolind in 1948. A patent was

issued in 1949 with an exclusive license granted to the Halliburton Oil Well Cementing Co. (HOWCO) to pump the new “HydraFrac” process. HOWCO performed the first two commercial fracturing treatments in Stephens County, Oklahoma, and Archer County, Texas, on March 17, 1949, using crude oil or a blend of crude and gasoline and approximately 100–150 lbs. of sand. In the first 12 months, 332 wells were treated which resulted in an average production increase of 75% (Quentin, 2013). Applications of the fracturing process grew very rapidly and increased the supply of oil in the United States far beyond any anticipations. An average of 3000+ wells were treated per month during some years in the mid-1950s. The first one-half million-pound fracturing job in the world was performed in October 1968, by Pan American Petroleum and Transport Company (which became Amoco and now British Petroleum) in Stephens County, Oklahoma. Today, fracture treatments are performed regularly in all petroleum-producing countries. In 2008, there were over 50.000 frac stages completed worldwide. It is quite common to put anywhere from 8 to 40 frac stages into a single well. It is estimated that at least 30% of the recoverable oil and 90% of the gas reserves in the United States can be attributed to the application of hydraulic fracturing. Significant advancement has been made for more than six decades since the first commercial treatments. After the first few jobs, the average fracture treatment consisted of about 750 gal of fluid and 400 lbs. of sand for about a year. Treatments today average about 60.000 gal of fluid and 100.000 lbs. of propping agent with the largest treatments exceeding 1 million gal of fluid and 5 million lbs. of proppant. Some horizontal wells in unconventional shale plays receive as many as 20 stages requiring 6 million lbs. of proppant and 3.6 million gal of fluid. As a better understanding of the fracturing

process evolved, cleaner and more suitable fluid systems were developed, proppant type and quality improved, and higher concentrations were pumped, higher strength synthetic and resin-coated proppants were brought on the market for deep-well fracturing, pumping and monitoring equipment were computerized and improved, and fracture design and evaluation techniques grew in sophistication. It should be noted that since 2009, a dramatic increase in proppant usage has resulted from the advent of horizontal well fracturing of unconventional resources. To put this in perspective, to haul the amount of material used in 2013 would require 4600 trains with 100 hopper cars (100 tons each) for each train. The planning for hauling this amount of material is phenomenal (Smith and Montgomery, 2015).

2. DRILL CUTTINGS AS PROPPING AGENTS

This chapter presents the use of drill cuttings as propping agents in hydraulic fracturing operations. Oil-based drill cuttings were evaluated under different conditions as propping agents by measuring the resulting fracture conductivity.

2.1. Introduction.

Oil-based drill cuttings are contaminated with hydrocarbons, heavy metals, dissolved minerals, and naturally occurring radioactive materials, which released to the surrounding ground and aquatic environments can cause deleterious effects on them (Somee et al., 2018).

Drill cutting re-injection in disposal wells has been done for years. However, re-injection of oil-based drill cuttings poses additional issues due to their toxicity. The oil-based cuttings are usually disposed of by trucking them to an incineration plant, at considerable expense, and with some environmental risks.

Reinjecting the oil-base drill cuttings along with the proppant during the hydraulic fracturing operations has not been published yet. In this research, by evaluating the fracture conductivity this possibility was evaluated.

2.2. Literature review.

This section introduces the definition of proppant and its importance in hydraulic fracturing, and the concept of fracture conductivity, and its impact on well production performance.

2.2.1. Proppants.

Proppant is a granular material that is a constituent of hydraulic fracturing fluid. Proppants hold open the induced fractures (pack fractures) to provide the permeability needed to produce hydrocarbons from low permeable reservoirs.

Mechanical stress on the packed fractures is significantly greater during production when drawdown pressures are maximized and reservoir pressures begin to decline. These two pressures can lead to greater stresses on the proppant after closure. High closure stress also applies pressure to the proppant during production; consequently, the proppant has an increased tendency to crush. Proppant diagenesis is possible and can consequently contribute to reductions in conductivity. However, the application of liquid-modified resin creates a film on the proppant surface, resulting in significant reductions in proppant reaction with the formation of rock and fluid. This technique reduces diagenesis and helps to control fines generated from crushing which could plug the proppant pack and reduce conductivity. Modified liquid resin also increases pillar strength by creating a film on proppant grains. The application of different shear stresses enhances and stabilizes the strength of the pillar and keeps the newly created conduits open to flow (Suzart et al., 2016).

2.2.2. Fracture conductivity.

Fracture conductivity measures the total flow rate through a unit length of a fracture and it is calculated as the product of fracture permeability (Kf) and fracture width (W).

The dimensionless conductivity of a bi-wing vertical hydraulic fracture is defined as:

$$FCD = \frac{KfW}{kXf} \tag{2.1}$$

Where:

FCD: Dimensionless Fracture Conductivity

Kf is the fracture permeability in the formation

W is the fracture width

K is the formation (matrix) permeability

Xf is the fracture half-length

Sufficiently large fracture conductivity is critical for economically viable extraction of hydrocarbons from the reservoir. Fracture width and permeability depend closely on the amount of proppant placed in the fracture as well as the effective stress exerted on the proppant pack (Fan et al., 2019). The amount of proppant placed in a fracture is measured by proppant concentration, also known as proppant areal concentration, defined as the proppant mass per unit fracture-face area and usually in the unit of lbm/ft2

(Economides and Nolte 2000). To increase fracture conductivity, it is tempting to increase fracture width by placing multiple layers of proppant particles in the fracture. By increasing the proppant concentration, the fracture width increases. However, the fracture width alone does not control the overall flow capacity of the fracture, because fracture conductivity (i.e., the flow capacity of the fracture), by its definition, is determined by both the permeability of the proppant pack and the fracture width. Thus, increasing fracture permeability to obtain a larger flow capacity is as important as increasing fracture width. In addition, because the price of manufactured ceramic proppant is relatively high, ranging from USD 5/lbm to USD 10/lbm, it is of economic interest to use a lower proppant concentration. Decreasing proppant concentration to form a partial-monolayer proppant pack has the potential to increase the overall fracture conductivity, primarily because a partial-monolayer proppant structure has high porosity that leads to high fracture permeability (Fan et al., 2019).

The deterioration of fracture conductivity or poorly executed fracture treatment operations can have a significant effect on production performance. Hydraulic fracture conductivity in shale formations is a dynamic property and can vary adversely due to several mechanisms such as: clay swelling, surface softening, excessive proppant embedment, and fines migration due to failed proppant particles (Guerra, 2018).

Fracture conductivity data is obtained experimentally from relatively short-term laboratory measurements. The initial API RP 61 issued in October 1989 followed a concerted industry effort to standardize on a short-term testing procedure utilizing a standardized linear flow testing cell. Tests under this procedure lasted for two hours at ambient temperature between steel plates (API RP 61, 1989). This conductivity procedure

was quickly augmented (and later standardized in the procedures of API RP 19D, 2008; and ISO 13503-2:2006) into a long-term testing procedure in which each stress condition in the linear flow cell is held for fifty hours at 250°F between Ohio sandstone platens utilizing oxygen-free, silica saturated 2% KCl. Test results thus generated give the industry a standard set of Conductivity Vs. Stress curves. These curves are often referred to as the Reference Conductivity since they are obtained under standardized laboratory conditions with only 50-hours of time at each measured stress level (Pearson et al., 2020).

2.3. Methodology.

All measurements were conducted at room temperature, between two metal plates, using dry nitrogen gas, in short term, and high proppant loading conditions. Testing under these conditions allows for quick, comparable, and easily reproducible results.

The setup required to execute a fracture conductivity test is listed below.

1. Test Fluid Source (Nitrogen gas)
2. Gas Flow Meter
3. GCTS hydraulic press
4. Modified API Test Cell
5. Pressure Sensors
6. Back Pressure Regulator Valve

Figure 1 shows a schematic of the test setup used to measure a fracture conductivity test.

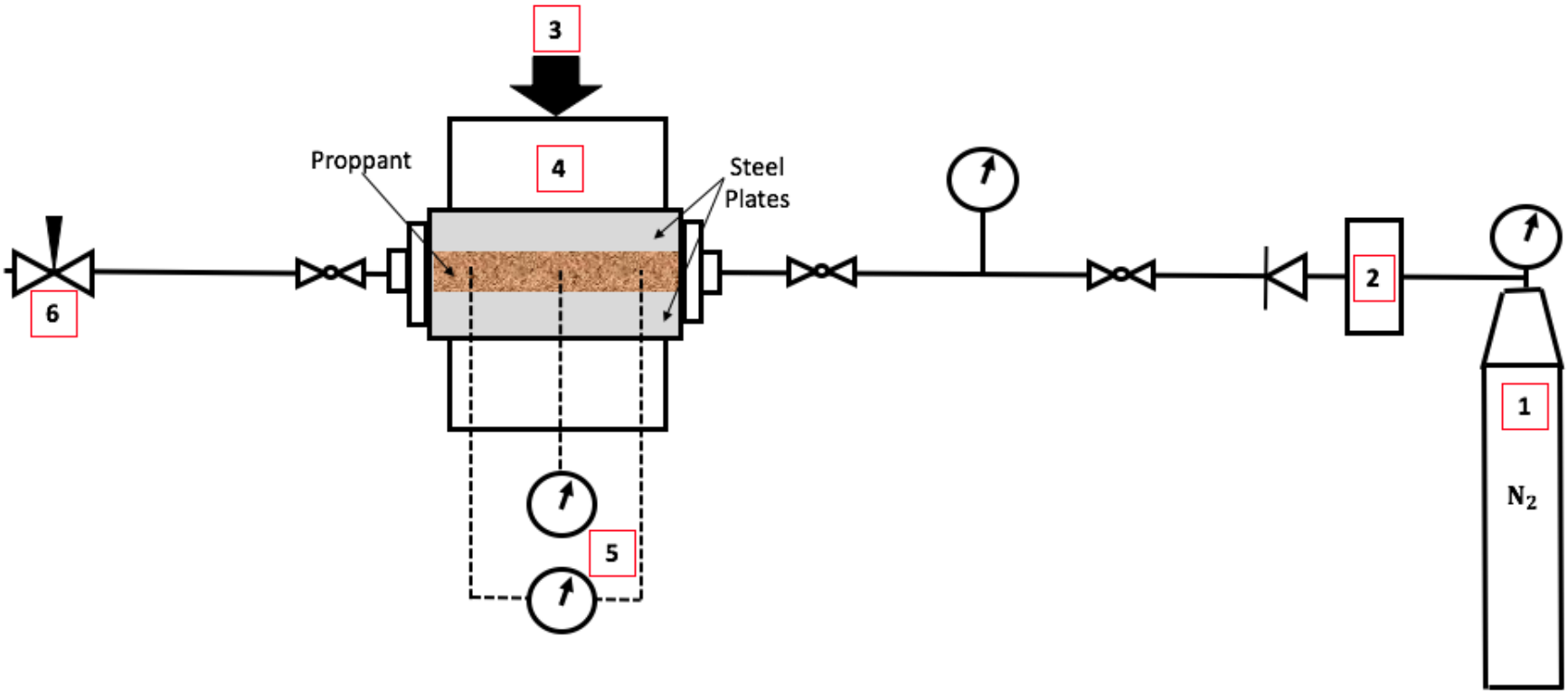

Figure 1.-Test setup schematic

All tests were conducted using steel plates under idealized conditions because proppant embedment and rock surface effects were not considered.

2.3.1. Steel plate design.

A modified API test cell, and steel plates used to confine the proppant in the modified API test cell, which was manufactured by CNC milling at the Texas A&M University Mechanical Engineering Machine Shop, were used. The Steel plates were designed to be 1-inch-thick and stacked three plates on top of each other to ease the manufacturing. In total, six steel plates were manufactured to fit the cell. **Figure 2** illustrates the engineering drawing and dimensions used for the steel plates.

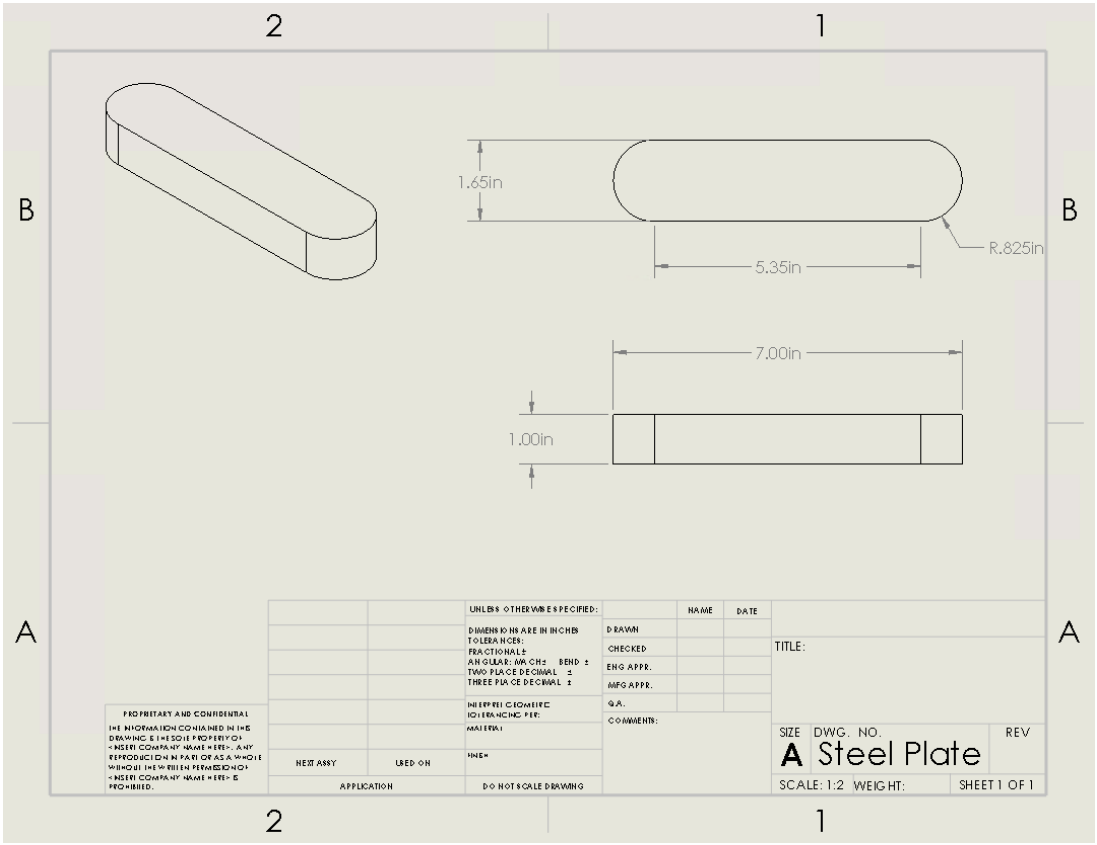

Figure 2.-Steel plates engineering drawing and dimensions

2.3.2. Steel plates assembly.

A total of six steel plates, 1-inch thick each, made up the sample assembly. Three steel plates are glued together on top of each other to confine the proppant from below, and the remaining three plates are glued on top of each other to confine the proppant from above. For both the top and bottom portions of the sample, a smooth alignment needs to be ensured. The plate assemblies act as pistons that apply stress to the proppant pack to simulate various closure stresses.

The steel plates are covered with a sealing epoxy which helps to allow for a tolerance that will inhibit the loss of proppant or gas leak-off, being that the mold is 0.003 inches wider than the steel plates.

2.3.3. Testing sample preparation procedure.

The preparation of the steel plates for use in the conductivity test cell assumes that three individual members have been molded to create one metal plate. The steel plate procedure is the same for both the bottom and top metal.

1. Apply a thin layer of Gorilla Glue to the top, middle, and bottom of the steel plate.
2. Place one layer of masking tape onto the out layer of the metal plate and make sure it is flush with the surface. Attempt to minimize overlapping tape as tolerance can become an issue (see **Figure 3**).
3. Apply another thin layer of Gorilla Glue on the outside of the masking tape and let it dry completely.

4. Softly, use steel wool to scratch the glue on the outside of the masking tape, creating dimension on the surface that allows for better binding with epoxy.
5. Apply Momentive SS4155 Primer to masking tape surface of steel plate. Allow drying for fifteen minutes or until the surface becomes white. Repeat this process three times.
6. Clean all surfaces of the metal mold.
7. Apply EZ aluminum tape onto the side wall of the metal mold. This minimizes the width of the sample when epoxy is applied, maintaining tolerance, and allowing for a snug fit into the conductivity cell.
8. Spray Silicon Mold Release to the aluminum tape surface. Allow drying for five minutes. Repeat this process three times. Silicon Mold release helps to reduce shear stress when removing the sample from mold.
9. Place sample evenly within the mold to ensure that an equal layer of epoxy is found on all sides of the sample.
10. Tighten all sides of the mold with screws.
11. Mix Momentive RTV627 parts A and B equal weight ratios. Use 50 grams of both.
12. Pour Momentive RTV627 mixture from one end of the sample, at a very slow rate. This helps to reduce the formation of air bubbles in the epoxy, which can bring into question the integrity of the epoxy. Pouring of the mixture should take between 15-20 minutes.
13. Place mold in the oven for four hours at a temperature of 120 °F.
14. Remove all screws from mold.

15. Remove one side and bottom of the mold.
16. Use hydraulic press to shear sample from remaining side of the mold. The resulting sample will look like what is shown in **Figure 4**.

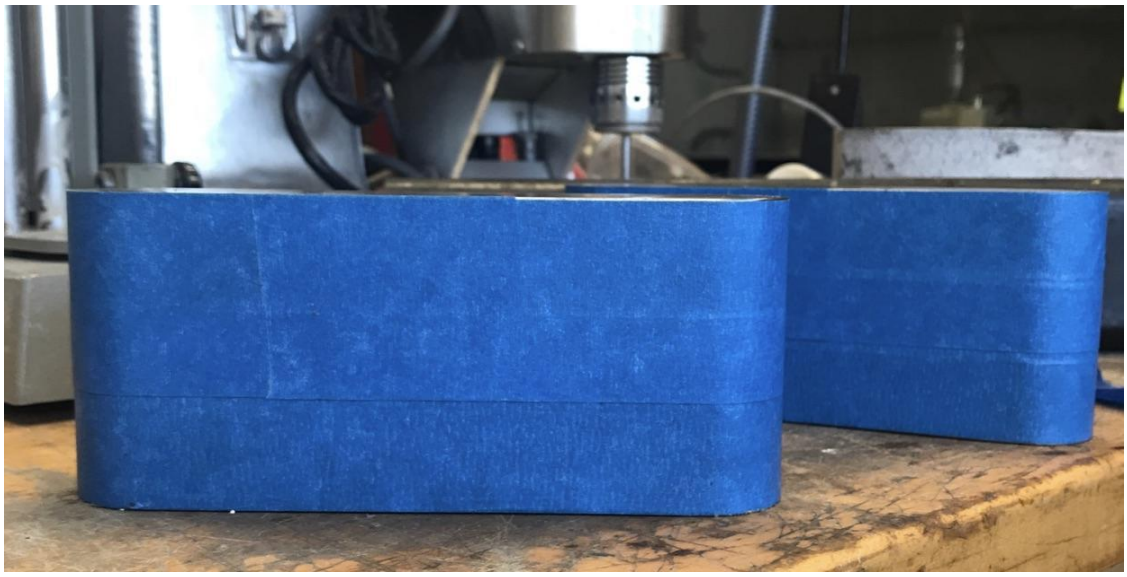

Figure 3.-Steel plate assemblies covered in blue painter's tape

Figure 4.-Steel plate sample assembly covered in rubber epoxy and ready for testing

2.3.4. Sieve analysis.

To determine the particle size distribution of a sample, 30, 40, 50, 70, 80, and 100 mesh sieves are typically used. However, any desired sieve assortment can be used. The test procedure is presented below.

1. Remove any particles from the sieves by using high-pressure air.
2. Weight the sieves independently and register their weights.
3. Arrange the set of sieves in the shaker equipment.
4. Around 100 grams of sample is placed on the top sieve.
5. Place the top cap and secure the sieve assembly to the sieve shaker.
6. Turn on the shaker for 10 minutes to guarantee that the sample successfully travels through all mesh sizes until being withheld by a mesh size that is too small for the proppant to fall through.
7. Weight the mass of each sieve containing the retained mass of sample.
8. Express the particle distribution in weight percent.

2.3.5. Drill cuttings removing of oil-based drilling fluid.

The following procedure is designed to wash and dry the drill cuttings at room temperature to remove the oil-based drilling fluid.

Steps 1 to 5, and 9-10, must be done inside a fume hood.

1. Mix 250 grams of drill cuttings with 250 mL of paint solvent.
2. Stir the mixture with a spatula for 5 minutes.
3. Filtrate the mixture through a 200-mesh.

4. Take the particles retained in the 200-mesh and spread them on 3 layers of paper towel.
5. Let the particles dry at room temperature, inside the fume hood, for 12 hours.
6. Do a sieve distribution analysis of the dried particles
7. Take the filtrated liquid from step 3 and filtrate it through a 400-mesh.
8. The resulted filtrated liquid from step 9 can be re-utilized to wash the drill cuttings in step 1.
9. Discard the particles with size 200/400-mesh.

2.3.6. Drill cutting evaluations.

Eagle Ford drill cuttings were used in two different conditions, containing oil-based drilling fluid, as received from the field (wet), and drill cuttings washed and dried at room temperature to remove the oil-based drilling fluid (dried).

Sand proppant 40/70 mesh and two sand proppants 100-mesh were used.

2.3.6.1. Sand proppant 40/70 mesh.

A baseline for only sand proppant was tested. Next, mixtures of the sand proppant with the wet drill cuttings, and the dried drill cuttings, at concentrations of 12.5, 20, 25, and 50 wt% were evaluated for fracture conductivity.

2.3.6.2. Sand proppant-A 100 mesh.

A baseline for only sand proppant was tested. Following, mixtures of the sand proppant with the wet drill cuttings at concentrations of 12.5, 25, and 35, and 50 wt%

were tested for fracture conductivity. The dried drill cuttings were tested at concentrations of 12.5, 25, 35, and 50 wt%.

2.3.6.3. Sand proppant-B 100 mesh.

Sand proppant-B 100 mesh was used to test fracture conductivity measurements for different sand proppant-cuttings mixtures. Initially, a baseline for only sand proppant was tested and used to compare the results obtained for each mixture.

a. Sand proppant mixed with wet drill cuttings.

Mixtures of the sand proppant with the wet drill cuttings at concentrations of 12.5, 25, and 35 wt% were evaluated for fracture conductivity.

b. Sand proppant mixed with specific size particles.

Fracture conductivity measurements using specific size particles were run. Size particles 8, 8/20, 20/40, 40/70, and >100 mesh from Eagle Ford, and Austin Chalk, formation at a concentration of 12-5 wt% were tested.

c. Sand proppant mixed with mixtures of drill cuttings from different formations.

The wet and dried drill cuttings from the different formations were mixed in and tested for fracture conductivity after mixing them with the sand proppant. The drill cuttings from the different formations were mixed according to the volume

percentage shown in **Table 1**, which corresponds to the volume proportions obtained after drilling an Eagle Ford well.

FORMATION	%V
Midway	15.3
Navarro	6.5
Olmos	11.2
Anacacho	0.3
Upson	0.3
Austin Chalck	3.0
Upper Eagle Ford	3.8
Middle Eagle Ford	11.1
Lower Eagle Ford	48.3
TOTAL	100.0

Table 1.-Volume percentage of rock by formation drilled in a typical Eagle Ford well

- ***Wet mixture of drill cuttings from different formations.***

200 grams of the wet mixture of drill cuttings from the different formations were prepared. 100 grams of it were used to prepare a mixture at 12.5 wt% with the sand proppant and tested for fracture conductivity.

The additional 100 grams of the wet mixture of drill cuttings were washed and dried to eliminate the oil-based drilling fluid, and later mixed with the sand proppant at 12.5 wt%, and tested for fracture conductivity.

- ***Dried mixture of drill cuttings from different formations.***

The dried drill cuttings from all formations were mixed according to Table 1 volumes. The dried mixture of drill cuttings from all formations were mixed at 5, 10, and 20 wt% with the sand proppant and tested for fracture conductivity.

- ***Dried mixture of drill cuttings from different formations added with oil-based drilling fluid.***

The mixture of dried drill cuttings from all formations was added with oil-based drilling fluid in two different concentrations at 5 and 10 wt%. The mixture containing 5 wt% oil-based drilling fluid was tested at 5 and 10 wt% with respect to the sand proppant, and the mixture containing 10 wt% oil-based drilling fluid was tested at 5 wt% with respect to the sand proppant.

2.3.7. Placement of mixtures of sand proppant and oil-based drill cuttings.

As recommended by API RP 61 for fracture conductivity testing of a short-term proppant pack, each test was run on a basis of 2 lb./ft^2 (PPF) loading which relates to a quarter-inch proppant pack. The mass of the proppant and oil-base drill cutting mixtures samples are calculated from the blueprints provided in Figure 2 which represents an area of 10.966 in^2.

Oil-base drill cutting sample concentrations of 12.5, 25, 35, and 50 wt% to the proppant mass were evaluated. The samples to evaluate for fracture conductivity are as described below.

1. Load the bottom steel plate assembly through the bottom opening of the modified API test cell.

2. Assure that the lower piston is loaded until the top of the steel plate assembly is visible through the inlet, outlet, and pressure ports of the modified API test cell.
3. As recommended by API RP 61, place screens of a mesh filter in the inlet, outlet, and pressure ports
4. Attach the respective fittings of the API test cell to confine the proppant, and prevent it from spilling over the edge of the steel plate assembly, and prevent sensor interference.
5. Pour the proppant and NWC mixture down a funnel onto the surface of the steel plates.
6. Distribute the mixture evenly across the entire plate, smooth with a straight edge.
7. Take multiple measurements across the surface of the mixture pack to guarantee the equal distribution of the mixture. Figure 5 shows a top view of an evenly distributed proppant pack sample.
8. Secure the fittings to prevent the blowout of the mixture.
9. Put in place the top steel place carefully into the API conductivity cell. **Figure 6** illustrates the complete setup of the API conductivity cell.

Figure 5.-Top view of an evenly distributed proppant pack

Figure 6.-Complete setup of the API test cell

2.3.8. Fracture conductivity procedure.

Once the sample has been properly loaded into the modified API cell, the test procedure can begin. The test procedure is listed below.

1. Calibrate differential pressure sensors using pressure pump and GTCS software using the 2-point option.
2. Assure that the back pressure regulator is completely open to allow any air that may be trapped within the proppant pack to escape while increasing load to desired closure stress.
3. Increase GCTS press load to initial closure stress (1000 psi).
4. Check all fittings are tightened.
5. Zero pressure sensors.
6. Close back pressure regulator.
7. Slowly open the gas valve, ensuring that the gas flow rate never exceeds 0.2 L/min.
8. Continue opening the gas valve until cell pressure reaches 30 psi.
9. Check for leaks in the system.
    a. Cell pressure should maintain 30 psi.
    b. There should be no pressure drop across the sample.
    c. The gas flow meter should read 0 L/min.
    d. If one or more of these conditions is not met, spray soap solution on fitting and cell openings to find the leak.
    e. If the leak is detected, tighten necessary fittings until conditions a, b, and c are satisfied.

10. Slowly open the backpressure regulator, make sure the gas flow rate does not increase too quickly. Introducing a large increase in flow rate may rearrange the proppant and create a conductive channel in or around the proppant pack.
    a. Ensure that the cell pressure does not reach less than 26 psi, and the differential pressure does not exceed 1.2 psi. Pressures beyond these limits can damage pressure sensors.
11. Once the desired pressure drop has been reached, allow the system to reach a steady-state with a constant gas flow rate, cell pressure, and differential pressure.
12. Record gas flow rate, cell pressure, and differential pressure.
13. Slowly close the back-pressure regulator until the pressure drop reaches three-quarters of the original pressure drop.
14. Once the desired pressure drop has been reached, allow the system to reach a steady-state with a constant gas flow rate, cell pressure, and differential pressure.
15. Record gas flow rate, cell pressure, and differential pressure.
16. Slowly close the back-pressure regulator until the pressure drop reaches one-half of the original pressure drop.
17. Once the desired pressure drop has been reached, allow the system to reach a steady-state with a constant gas flow rate, cell pressure, and differential pressure.
18. Record gas flow rate, cell pressure, and differential pressure.

19. Slowly close the back-pressure regulator until the pressure drop reaches one-quarter of the original pressure drop.
20. Once the desired pressure drop has been reached, allow the system to reach a steady-state with a constant gas flow rate, cell pressure, and differential pressure.
21. Record gas flow rate, cell pressure, and differential pressure.
22. Slowly close the gas valve.
23. Slowly open the back-pressure regulator until it is fully open and the gas flow rate, cell pressure, and differential pressure all reach a value of zero.
24. Increase GCTS press to next desired closure stress (2000, 3000, 4000 psi).
25. Repeat steps 6-24 for each desired closure stress.
26. After final closure stress, unload the GCTS press to 500 psi.
27. Untighten all fittings.
28. Return GCTS press to relative zero displacements.
29. Remove the test cell from the hydraulic press.
30. Disassemble the test setup and remove the sample.

Figure 7 displays the fully assembled modified API conductivity cell.

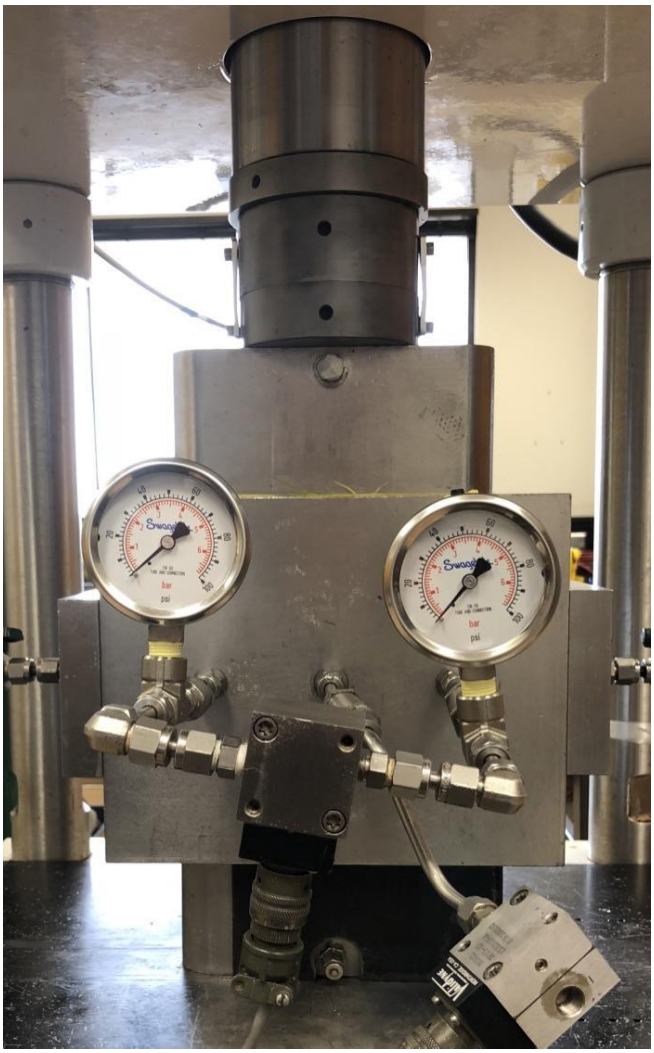

Figure 7.-Fully assembled test setup

2.3.9. Fracture conductivity calculations.

At each closure stress-tested, four separate gas flow rates and corresponding cell pressure and differential pressure combinations were recorded. These values will be used to evaluate the conductivity of the proppant and oil-base drill cutting mixtures pack at given closure stress.

The fracture conductivity of a mixture sample pack was determined based on two-equation, the Forchheimer equation, and the Darcy equation. The use of these two equations has independent stipulations for its use. Darcy flow for a sample pack is considered at flow rates less than 2 L/min (McGinley, 2015). For flow rates above 2 L/min, the use of the Forchheimer equation is suggested. The experiments will be based solely on the derivation of the Darcy equation is that the flow rates rarely exceed 1 L/min. The derivation is shown above using the relationship between known values and the unknown values measured in the laboratory (gas flow rate, cell pressure, and differential pressure).

Darcy's Law equation is shown in 2.2:

$$\frac{q}{A} = u = -\frac{k}{\mu}\frac{dP}{dL} \tag{2.2}$$

Rearranging and separation of variables leads to the form:

$$dP = -\frac{\mu u}{k}dL \tag{2.3}$$

Definition of cross sectional area:

$$A = wh \tag{2.4}$$

Both sides of equation 2.2 are multiplied by density.

$$\rho dP = -\frac{\mu u}{k}\rho dL \tag{2.5}$$

Using the ideal gas law, density can be expressed in known variables.

$$Pv = znRT \tag{2.6}$$

$$PM = zRT\frac{m}{v} = zRT\rho \tag{2.7}$$

$$\rho = \frac{PM}{zRT} \tag{2.8}$$

Equation 2.8 is substituted into the left-hand side of Darcy's Law equation (2.5):

$$\frac{PM}{zRT}dP = -\frac{\mu u}{k}\rho dL \tag{2.9}$$

Integrate and multiply each side by -1:

$$\frac{M}{zRT}\int_{P_1}^{P_2} PdP = -\frac{\mu u}{k}\rho\int_0^L dL \tag{2.10}$$

$$\frac{M}{zRT}\frac{[{P_1}^2-{P_2}^2]}{2} = \frac{\mu u}{k}\rho(L-0) \tag{2.11}$$

By definition of flow rate per area (2.1) and area (2.3):

$$\frac{M}{zRT}\frac{[{P_1}^2-{P_2}^2]}{2} = \frac{\mu}{kwh}q\rho L \tag{2.12}$$

Assumptions about test cell and pressure measurement locations:

$$\Delta P = P_1 - P_2 \tag{2.13}$$

P_{cell} is located halfway between P1 and P2:

$$P_1 - P_{cell} = P_{cell} - P_2 = \frac{1}{2}\Delta P \tag{2.14}$$

Using the above assumptions (2.13 and 2.14):

$$P_1 = \frac{1}{2}\Delta P + P_{cell} \tag{2.15}$$

$$P_2 = P_{cell} - \frac{1}{2}\Delta P \tag{2.16}$$

After substitution of equations 2.15 and 2.16 into equation 2.12, the altered Darcy's Law equation becomes:

$$\frac{M}{zRT}\frac{\left[\left(\frac{1}{2}\Delta P + P_{cell}\right)^2 - \left(P_{cell} - \frac{1}{2}\Delta P\right)^2\right]}{2} = \frac{\mu}{kwh} q\rho L \tag{2.17}$$

Equation 2.17 simplifies to:

$$\frac{M}{zRT}\frac{2P_{cell}\Delta P}{2} = \frac{\mu}{kwh} q\rho L \tag{2.18}$$

Equation 2.18 can be rearranged in a useful linear format.

$$\frac{P_{cell}\Delta PM}{LzRT} = \frac{\mu q\rho}{h}\frac{1}{kw} \tag{2.19}$$

Definition of fracture conductivity:

$$C_f = kw \tag{2.20}$$

The final form of the equation relating known and unknown variables used to calculate proppant pack conductivity is formed by the final step of substituting equation 2.20 into equation 2.19:

$$\frac{P_{cell}\Delta PM}{LzRT} = \frac{\mu q\rho}{h}\frac{1}{C_f} \tag{2.21}$$

Above is the final form of the equation used (2.21) to determine conductivity in a lab setup. The unknowns which were measured in the lab are the cell pressure (P_{cell}), the differential pressure across the length L (ΔP), and the fluid flow rate (q). At any given fracture closure stress, the conductivity of the fracture and proppant pack was determined by flowing fluid at several different rates and using the corresponding cell pressure and differential pressure to plot the left-hand side of the equation vs. the right-hand side of the above equation which will have a slope that is inverse of conductivity at that closure stress **(Figure 8).**

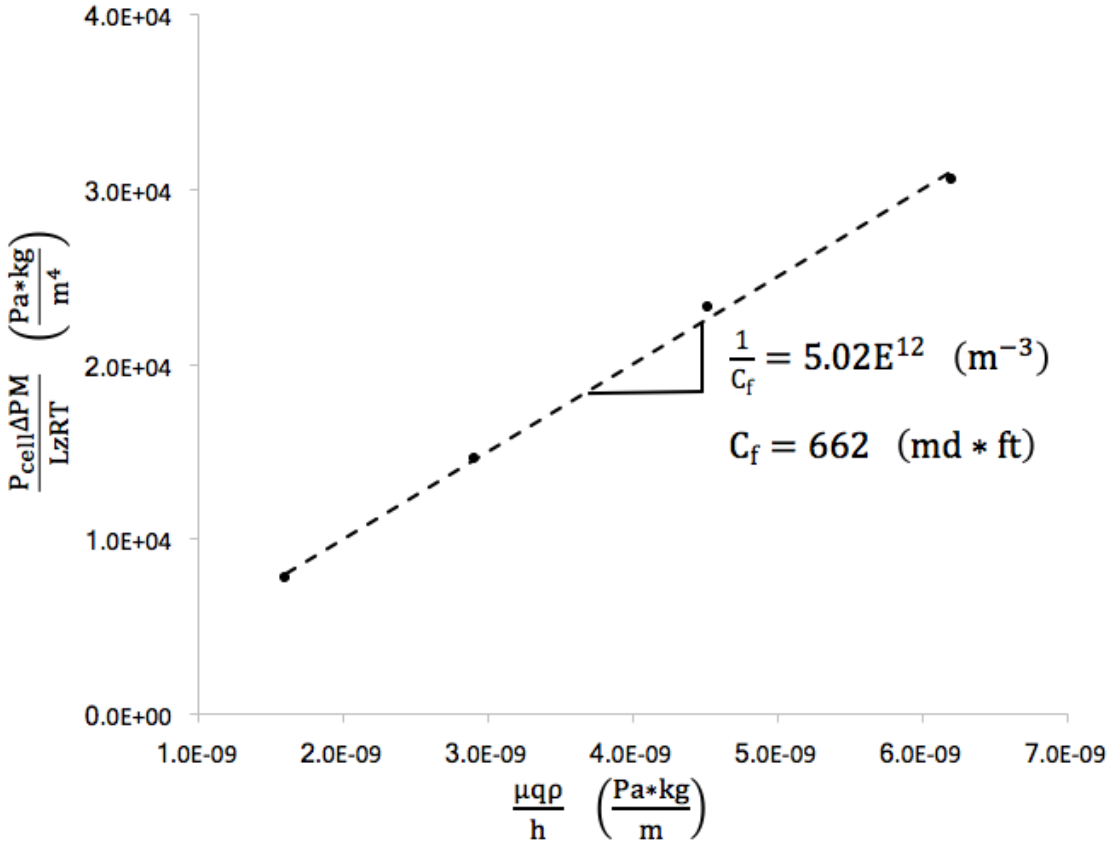

Figure 8.-Experimental results used to determine the conductivity of a proppant pack

It is important to note that the conductivity values measured in the lab are higher than the actual fracture conductivity observed downhole. However, the lab conductivity measurements serve as a means of comparison between proppant types, concentration, flow fluid, and many other variable testing factors. Even though the conductivity downhole will be less than that determined in the lab, multiple lab tests can be used to determine which treatments will perform better than others.

2.4. Results.

The oil-based drill cuttings were classified as wet or dried. Wet corresponding to the drill cuttings as received, and dried to the drill cuttings after being washed to remove the oil-based mud drilling fluid and dried at room temperature.

Preliminary fracture conductivity tests were done using only wet cuttings from the Eagle Ford zone, obtaining impermeable layers in all cases. **Figure 9** shows an example of a produced layer after applying 500 psi closure stress, and **Figure 10** displays its thickness.

Figure 9.-Layer obtained using Eagle Ford wet cuttings and 500 psi closure stress

Figure 10.-Thickness of the layer obtained using Eagle Ford cuttings and 500 psi closure stress

2.4.1. Drill cuttings particle size distributions.

Samples from different depths were washed to remove the drilling fluid and dried at room temperature. **Figure 11** shows some of these samples by formation. The depths correspond to the measured depth.

			
Midway (11200 ft)	**Olmos (12550 ft)**	**Austin Chalk (13590 ft)**	**Eagle Ford (14040 ft)**
			
Eagle Ford (14880 ft)	**Eagle Ford (15680 ft)**	**Eagle Ford (16300 ft)**	**Eagle Ford (17380 ft)**

Figure 11.-Oil-based drill cuttings washed and dried at room temperature

Drill cuttings from the vertical section of the well, drilled using a water-based drilling fluid, were analyzed for particle size distributions. Results are shown in **Figure 12.**

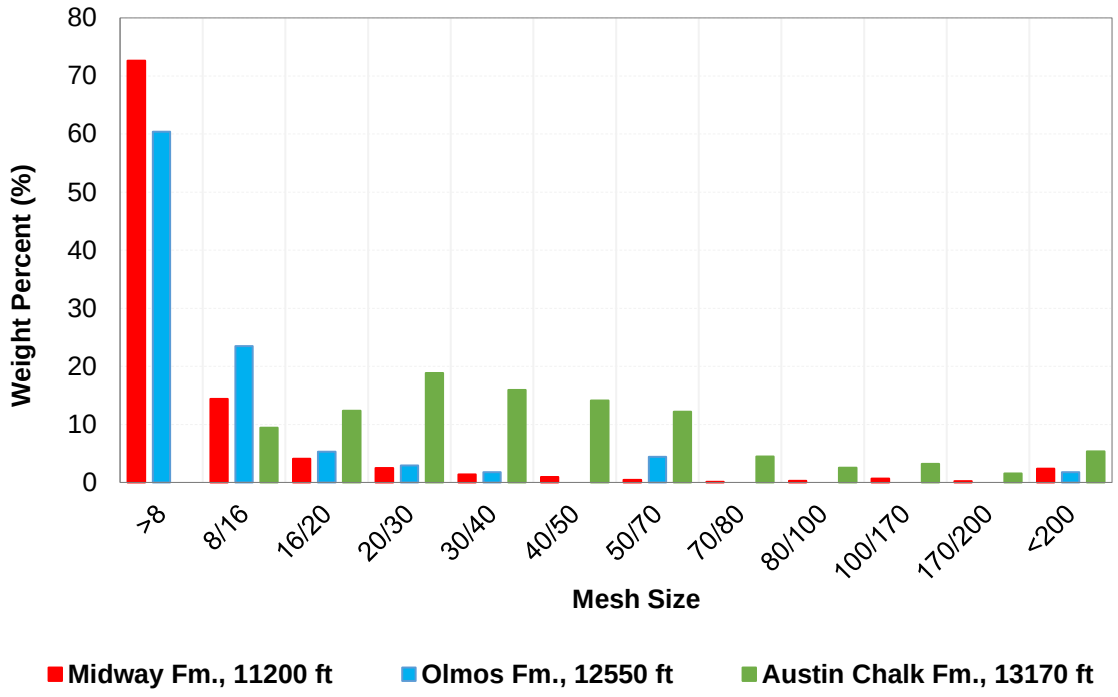

Figure 12.-Particle size distribution of drill cuttings from the vertical section of the well

Drill cuttings from the horizontal section of the well, drilled using oil-based drilling fluid, were washed using an organic solvent and dried at room temperature. **Figure 13** and **Figure 14** show the results of the particle-sized distribution from different measured depths corresponding to the upper and lower Eagle Ford formation, respectively.

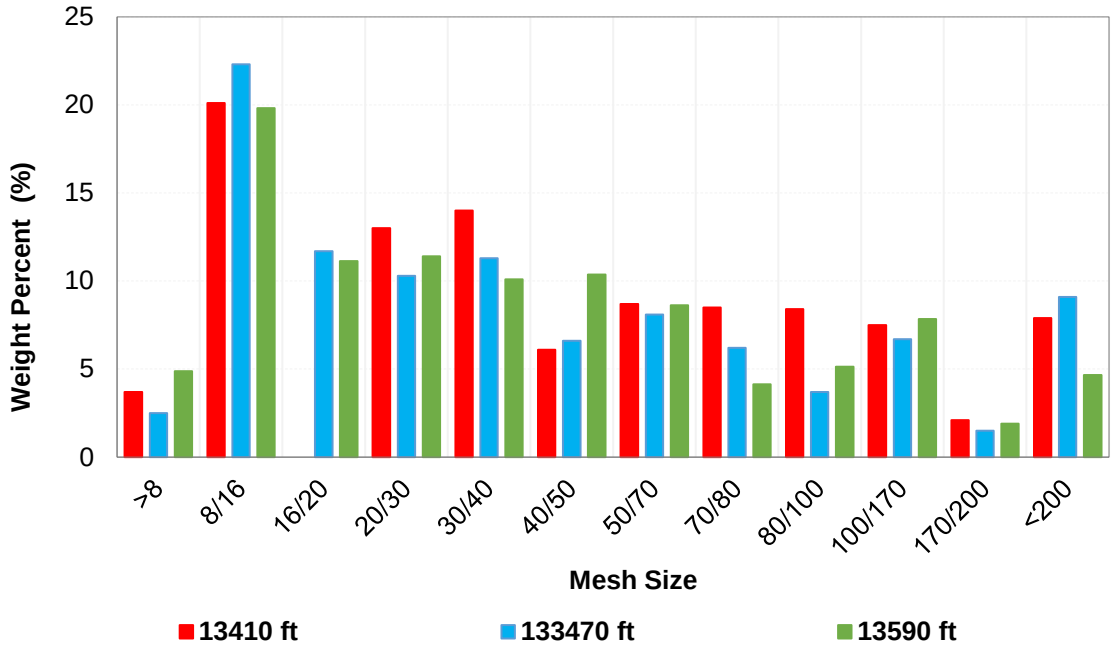

Figure 13.-Particle size distribution of the drill cuttings from Eagle Ford formation, upper zone

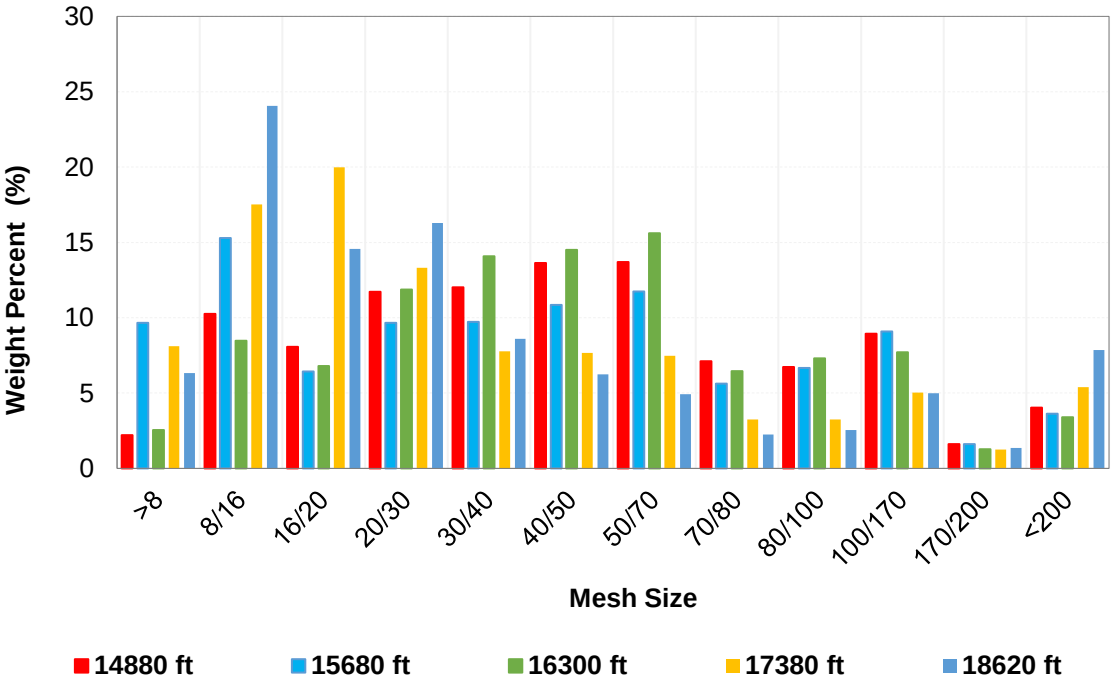

Figure 14.-Particle size distribution of the drill cuttings from Eagle Ford formation, lower zone

Drill cuttings in the measured depth that could not be identified as either upper or lower Eagle Ford were denominated as middle Eagle Ford. Their particle size distribution is displayed in **Figure 15**.

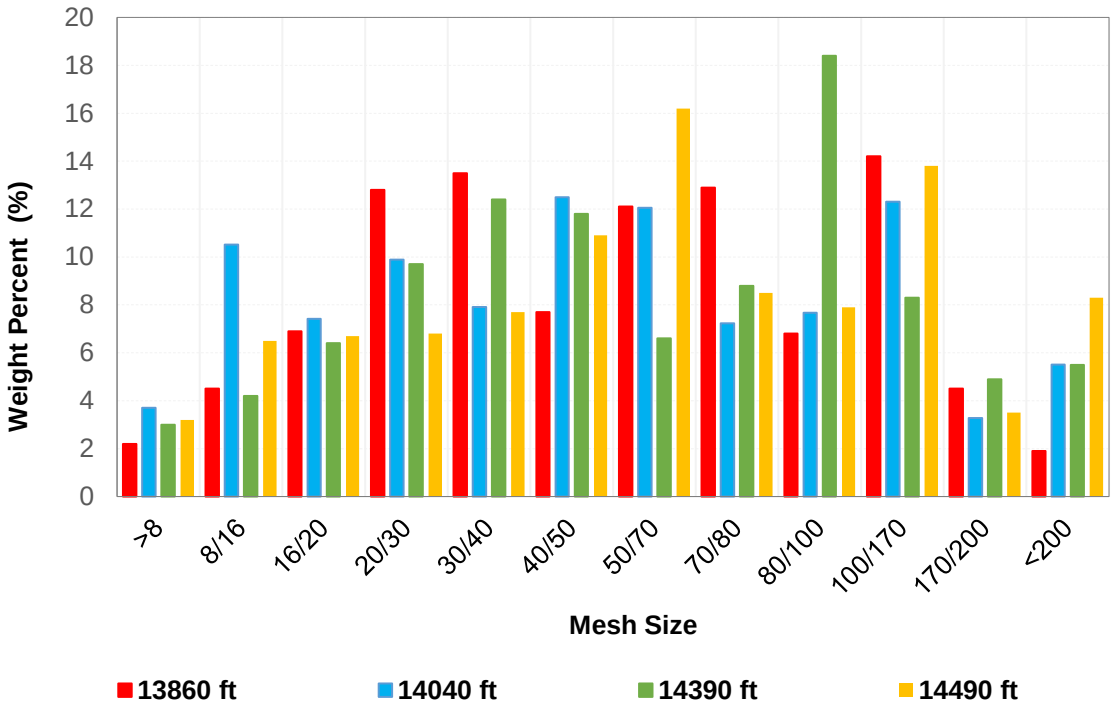

Figure 15.-Particle size distribution of the drill cuttings from Eagle Ford formation, middle zone

Figure 16 shows the average particle size distribution values for the Eagle Ford formation drill cuttings. There are no large differences between particle sizes within the zones in this formation.

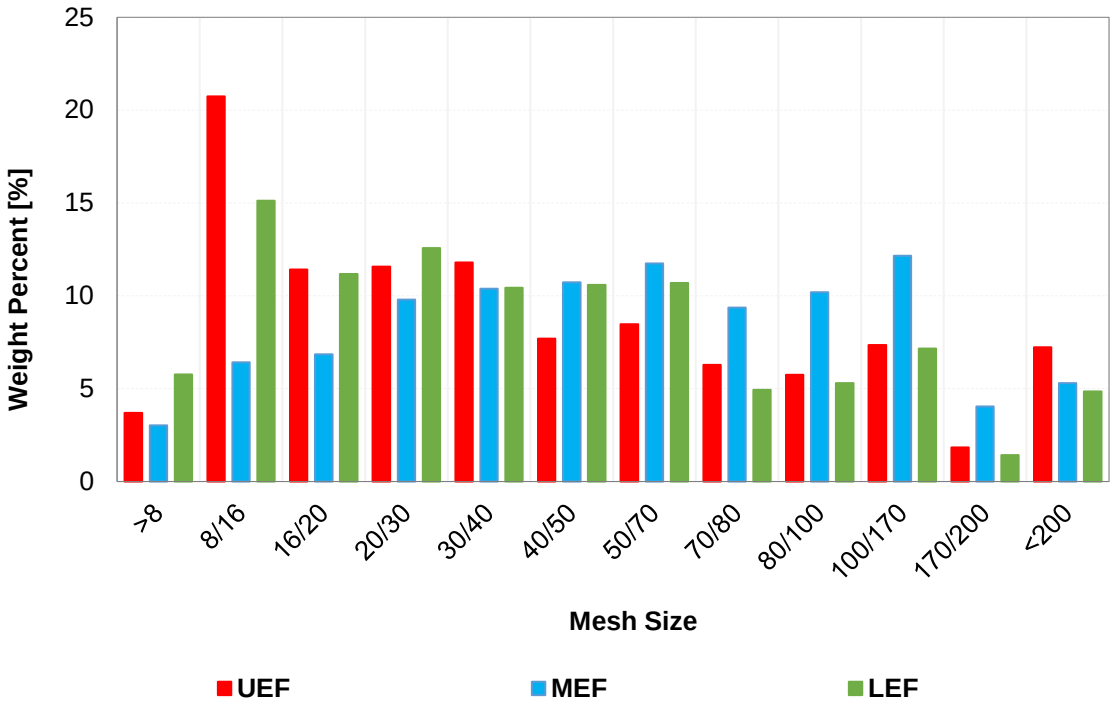

Figure 16.-Average particle size distribution of the drill cuttings from Eagle Ford formation

The drill cuttings particles corresponding to the vertical zone of the well (Midway and Olmos formation, for example) were larger and well defined into a mesh size, in contrast with those from the horizontal zone, which are widespread from particles 8-mesh to smaller than 200-mesh. These results are common in deviated wells. The driving forces that clean up the well are different from the driving forces in vertical and high angled wells. Specific differences in size particles in the horizontal section of the well could be related to the formation rocks, drilling bit type (Yi, 2013), rate of penetration, and weight on bit (Reyes, 2015). **Figure 17** exhibits the average particle size distribution of the drill cuttings received from the well Gus Tips Runge 1-D3H.

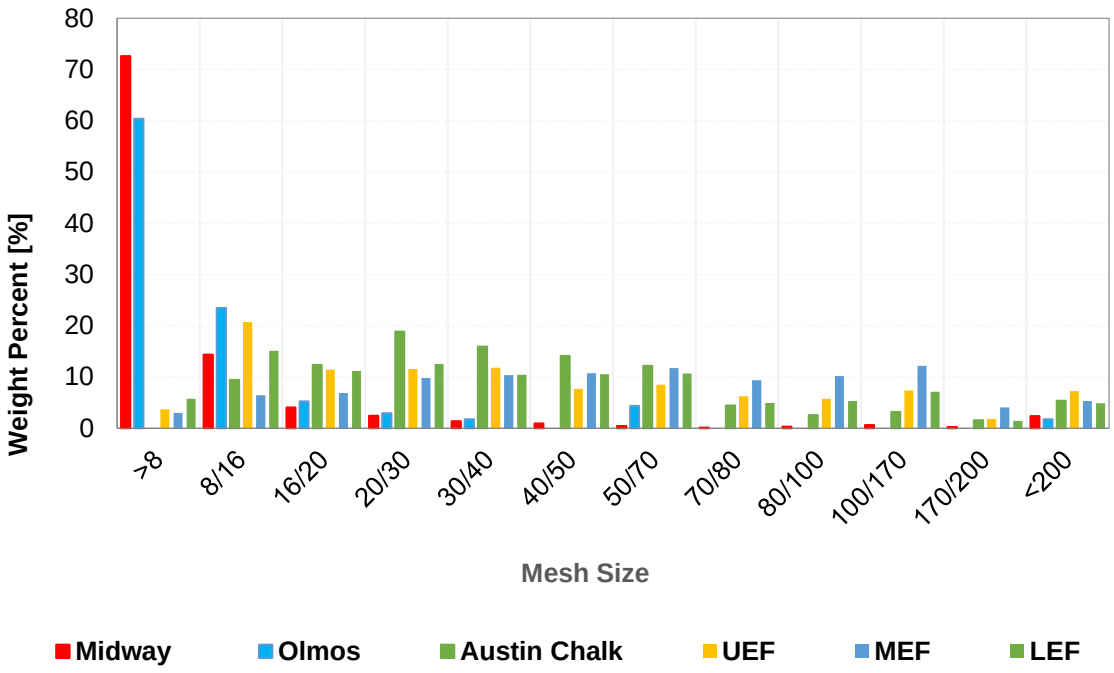

Figure 17.-Average particle size distribution of drill cuttings from the well Gus Tips - Runge 1- D3H

2.4.2. Sand proppant 40/70 mesh.

First, the particle size distribution of the sand proppant was analyzed. Then, the drill cuttings were mixed with the sand proppant in two different conditions: wet and dried.

The drill cuttings were mixed in different mass proportions (weight percent) with the sand proppant. The wt% values in the legends of the figures correspond to the weight percent of drill cuttings used in the mixtures with the sand proppant.

The fracture conductivity was measured in 1000 psi incremental steps, from 1000 up to 6000 psi closure stress.

2.4.2.1. Sand proppant particle size distribution.

The particle size of the sand proppant corresponds to a 40/70 mesh distribution. More than 80 wt% of the sand proppant was retained in the 50/70 mesh configuration. The results are shown in **Figure 18**.

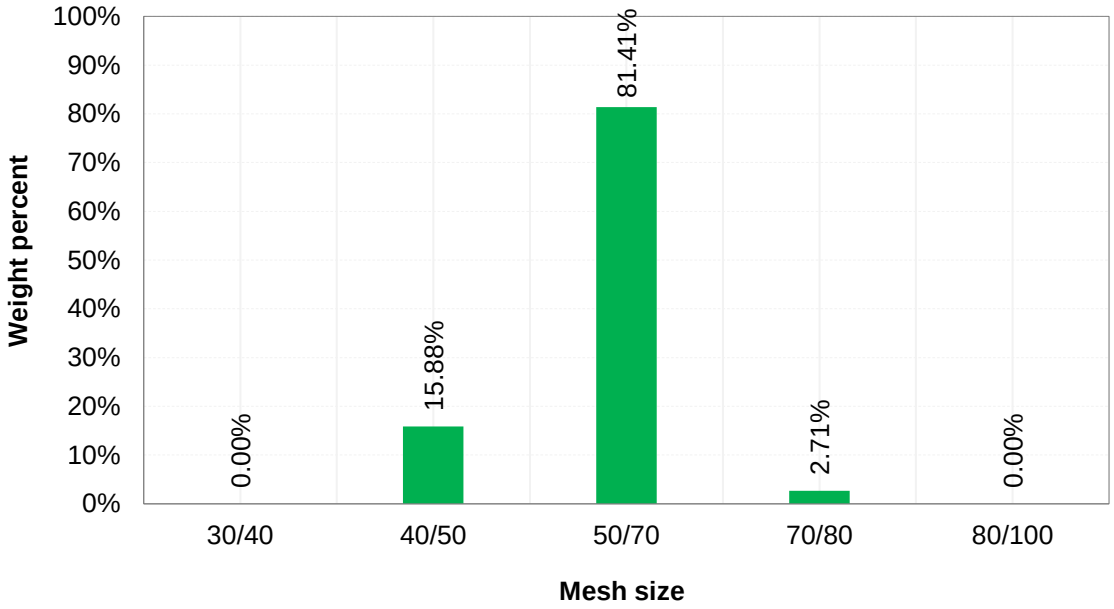

Figure 18.-Sand proppant 40/70 mesh - particle size distribution

2.4.2.2. Wet drill cuttings.

After obtaining the baseline for the sand 40/70 mesh, the mixtures of drill cuttings with sand proppant were tested. The fracture conductivity for the 50 wt% drill cutting concentration was measured up to 3000 psi closure stress. After this

closure stress, the fracture conductivity was close to zero. The results are shown in **Figure 19**.

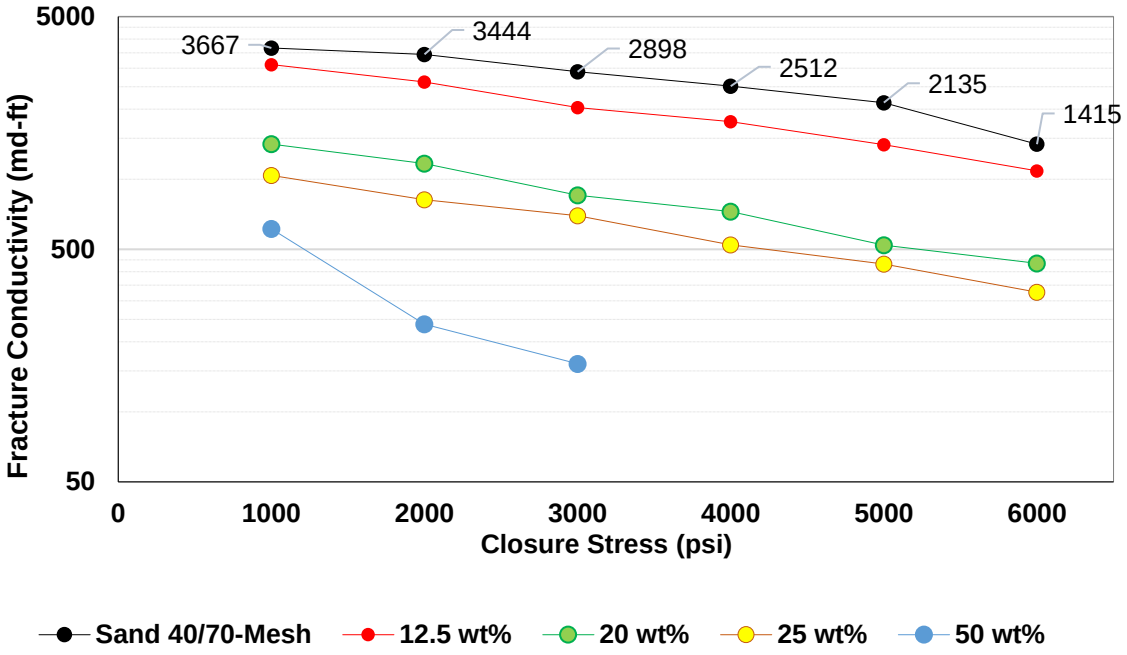

Figure 19.-Fracture conductivity results of 40/70-mesh sand proppant and wet Eagle Ford drill cuttings

There is an inverse relationship between fracture conductivity and drill cuttings concentrations. By increasing the mass of drill cuttings in the mixture, the fracture conductivity decreases. A 12.5 wt% drill cuttings concentration produced a result close to the baseline. A drill cutting concentration of 50 wt% is too large to maintain good fracture conductivity. Probably, the fines generated by crushing after 3000 psi closure stress produce a blockage of the void proppant space.

2.4.2.3. Dried drill cuttings.

The fracture conductivity for the 50 wt% drill cutting concentration was measured up to 3000 psi closure stress. After this closure stress, the fracture conductivity was close to zero. The results are shown in **Figure 20**.

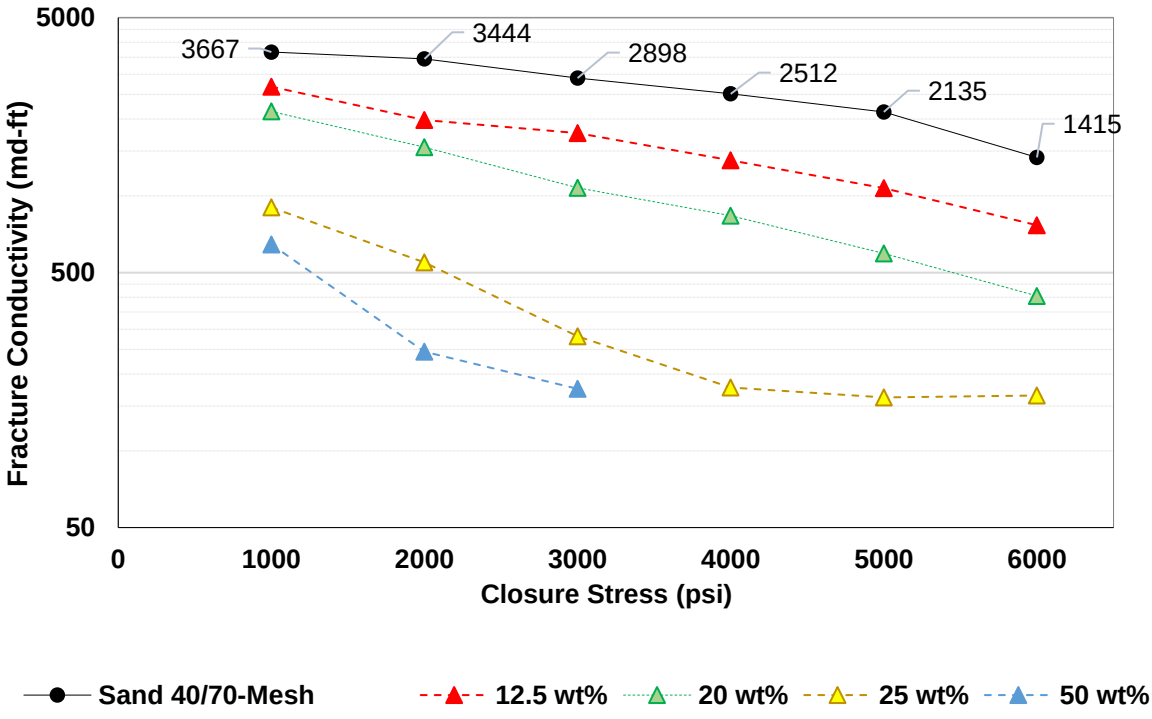

Figure 20.-Fracture conductivity results of 40/70-mesh sand proppant and dried Eagle Ford drill cuttings

A drill cuttings concentration of 12.5 wt% produced fracture conductivity results closer to the baseline. The drill cuttings concentration of 25 wt% produced close results for closure stresses ranging from 4000 to 6000 psi. It is believed that the drill cuttings particles crushed at 4000 psi closure stress, producing the maximum amount of fines. No more fines were produced when the closure stress was

increased, resulting in constant fracture conductivity response after increasing closure stress.

Drill cuttings concentrations of 50 wt% produced an excessive amount of fines after 3000 psi closure stress, blocking the void space in the proppant and producing a decrease in the fracture conductivity.

2.4.3. Sand proppant 100 mesh.

Two different 100 mesh size sand proppants were used, identified as “Sand proppant -A” and “Sand proppant-B”, respectively.

The drill cuttings were mixed in mass proportions with the sands in two different conditions: wet and dried. Additionally, mixtures of dried specific drill cutting sizes from the Eagle Ford and Austin Chalk formations at 12.5 wt% with sand proppant-B were tested. Finally, cuttings from the different formations of the well were mixed in volume percentage according to the volumes drilled from the well. These preparations were mixed in wet, wet/dried, dried, and dried and added with oil-based drilling fluid. Later, they were mixed with sand proppant-B and tested for fracture conductivity.

2.4.3.1. Sand proppant particle size distributions.

The particle sizes of the two sand proppants 100-mesh were tested. The results are shown in **Figure 21**. The two sand proppants correspond to 100 mesh distribution, with sand proppant A with larger particles, 50 wt% in the 50/70 mesh

distribution. The sand proppant B is mainly distributed between 50/170 mesh sizes, with more than 75 wt% particles smaller than 100 mesh.

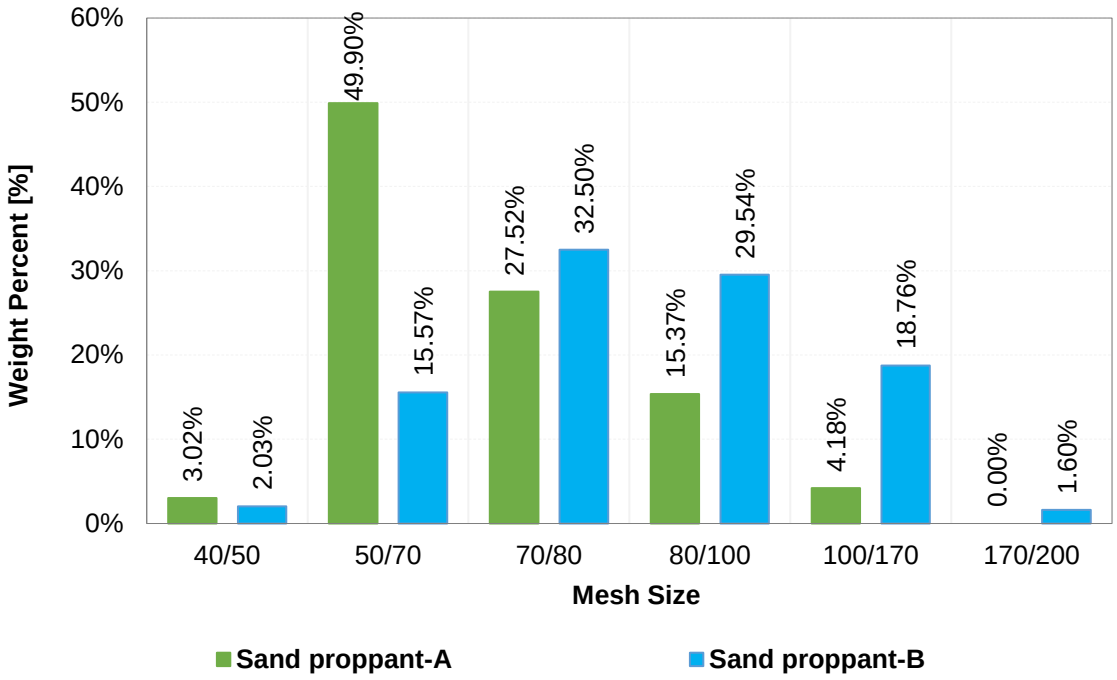

Figure 21.-Sand proppants 100 mesh - particle size distribution

2.4.3.2. Wet drill cuttings.

After obtaining the baseline for the sand proppants, the mixtures of drill cuttings were tested.

The fracture conductivity for the 50 wt% drill cutting concentration mixed with the sand proppant-A was measured up to 3000 psi closure stress. After this closure stress, the fracture conductivity was close to zero. The results are shown in **Figure 22**.

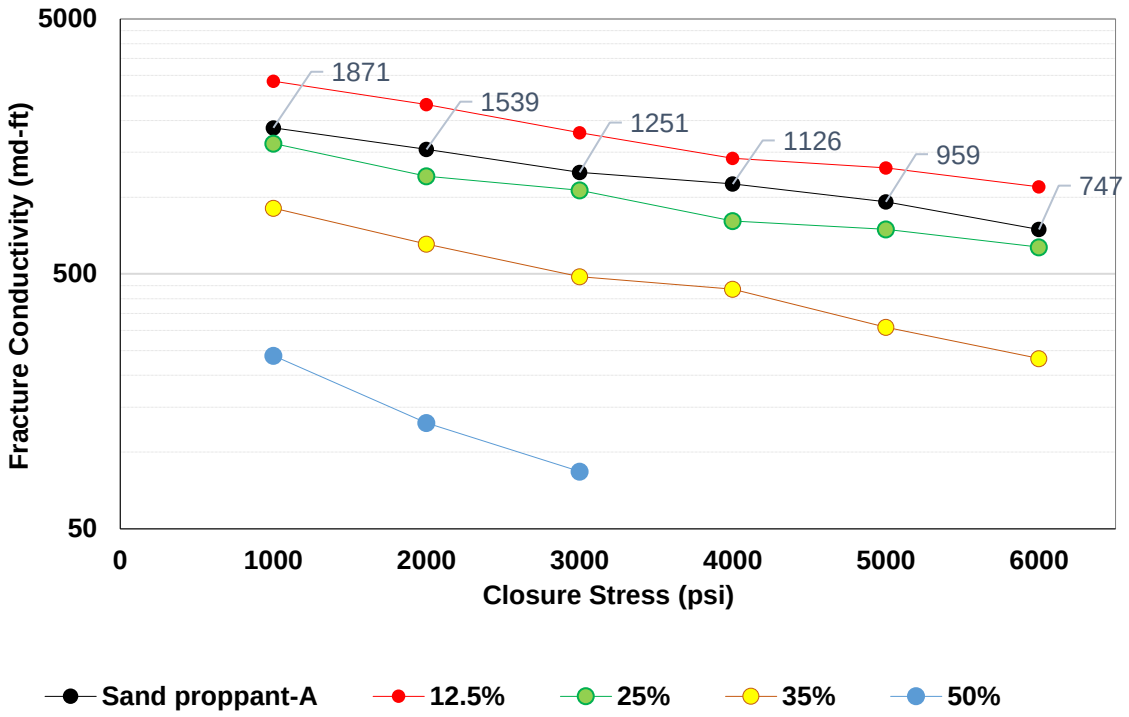

Figure 22.-Fracture conductivity results of sand proppant-A 100-mesh and wet Eagle Ford drill cuttings

An increase in the fracture conductivity baseline was obtained by using a drill cutting concentration of 12.5 wt%. Experimental results that were close to the baseline were obtained using a drill cutting concentration of 25 wt%. The 35 wt% drill cutting concentration could produce more fines when increasing closure stress, resulting in the reduction of fracture conductivity

The sand proppant-B baseline was established, and the fracture conductivities of the mixtures were tested. Drill cutting concentrations of 12.5, 25, and 35 wt% were evaluated. **Figure 23** presents the results obtained.

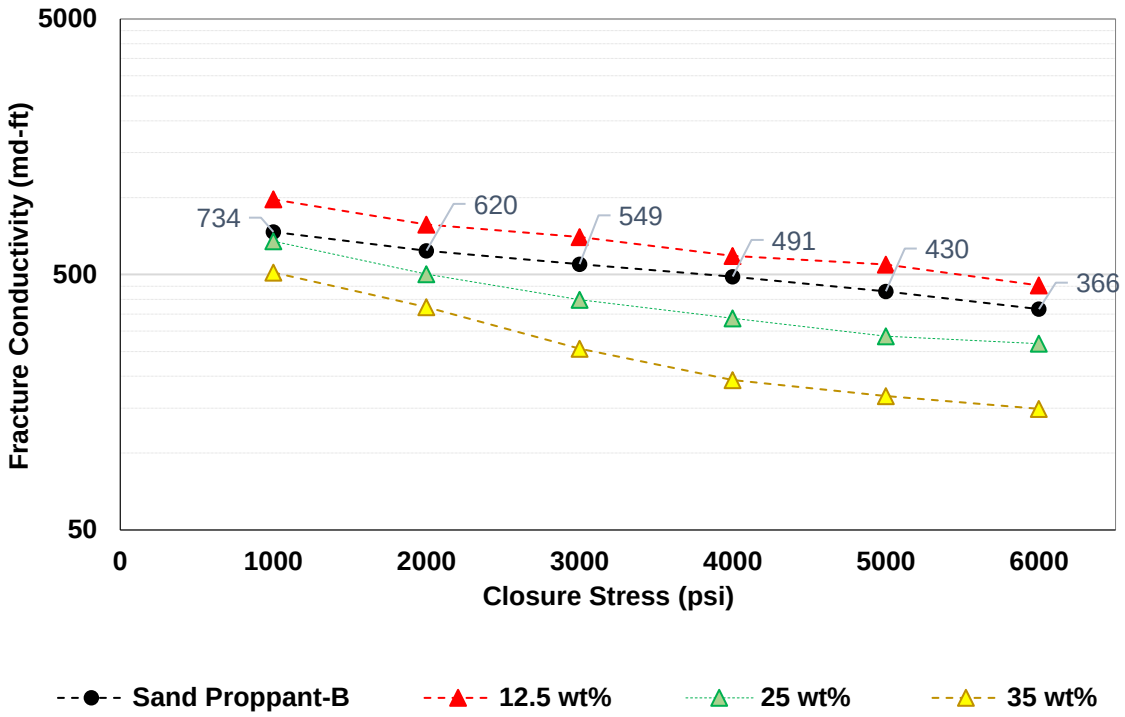

Figure 23.-Fracture conductivity results of sand proppant-B 100-mesh and wet Eagle Ford drill cuttings

The results show similar trends to those obtained for sand proppant-A. A drill cutting concentration of 12.5 wt% produced an increase in fracture conductivity with respect to the baseline. Fracture conductivities closer to the baseline were produced by using drill cuttings at 25 wt%. Drill cutting concentration of 35 wt% produced a larger reduction in fracture conductivity.

2.4.3.3. Dried drill cuttings.

Sand proppant-A was used. The fracture conductivity for the 50 wt% drill cutting concentration was measured only for 1000 psi closure stress. After this value, the fracture conductivity was close to zero. The results are shown in **Figure 24**.

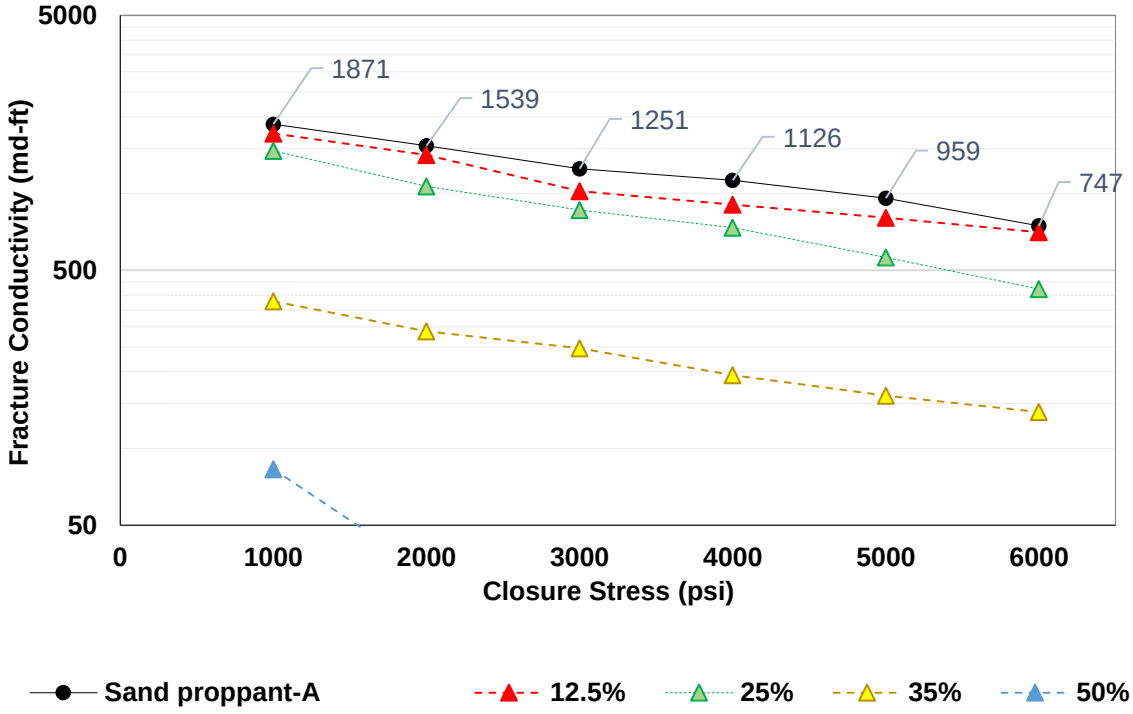

Figure 24.-Fracture conductivity results of sand proppant-A 100-mesh and dried Eagle Ford drill cuttings

A drill cutting concentration of 12.5 wt% produced closer values to the baseline. The drill cuttings at 25 wt% produced acceptable results. The 35 wt% produced a larger reduction in the fracture conductivity, probably due to the fines generation by the closure stress. The 50 wt% concentration was measured only at 1000 psi closure stress, after this value, the fracture conductivity was close to zero.

It is believed that the drill cuttings could produce a larger amount of fines after applying the closure stress, moving through the void space, and decreasing the fracture conductivity.

2.4.3.4. Eagle Ford size particles.

Five different size particles were evaluated. In all cases, the size particle concentration was 12.5 wt%. **Figure 25** presents the results obtained.

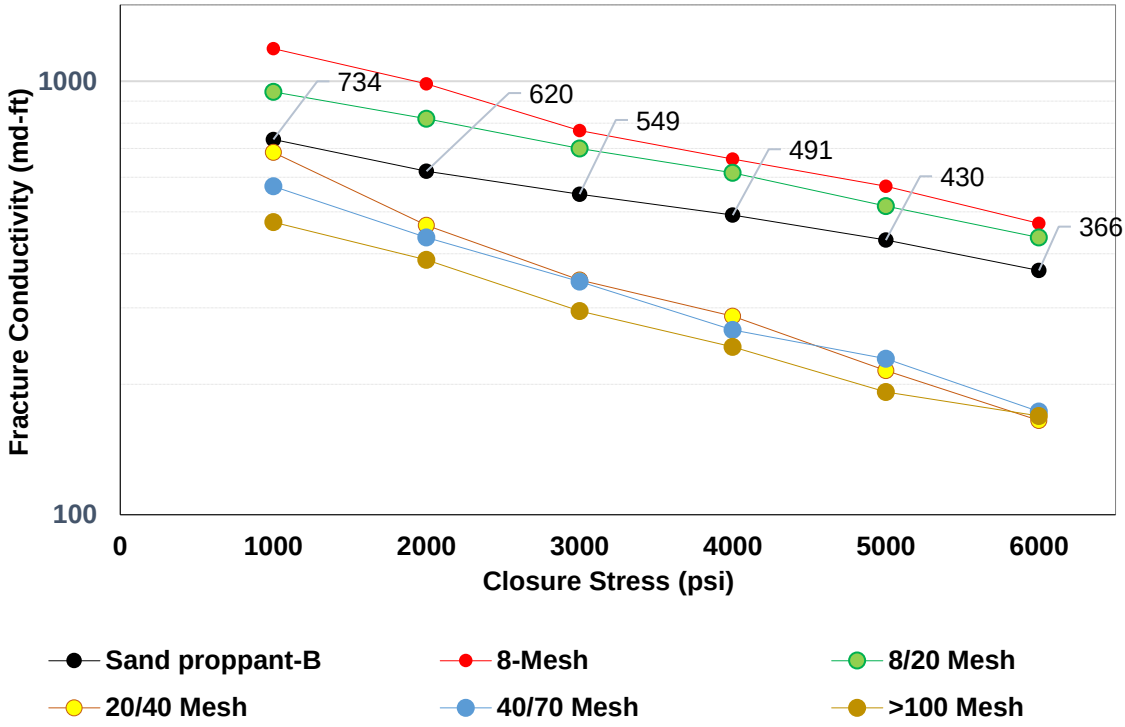

Figure 25.-Fracture conductivity results of sand proppant-B 100-mesh and Eagle Ford size particles

As expected, there is a trend between drill cutting size particle and fracture conductivity. Larger particle sizes, like 8-mesh or 8/20-mesh, increased the fracture

conductivity baseline. On the other hand, particles 20/40-mesh, or smaller, decreased the fracture conductivity baseline.

2.4.3.5. Austin Chalk size particles.

Five different size particles were evaluated. In all cases, the particle concentration was 12.5 wt%. the results are shown in **Figure 26**.

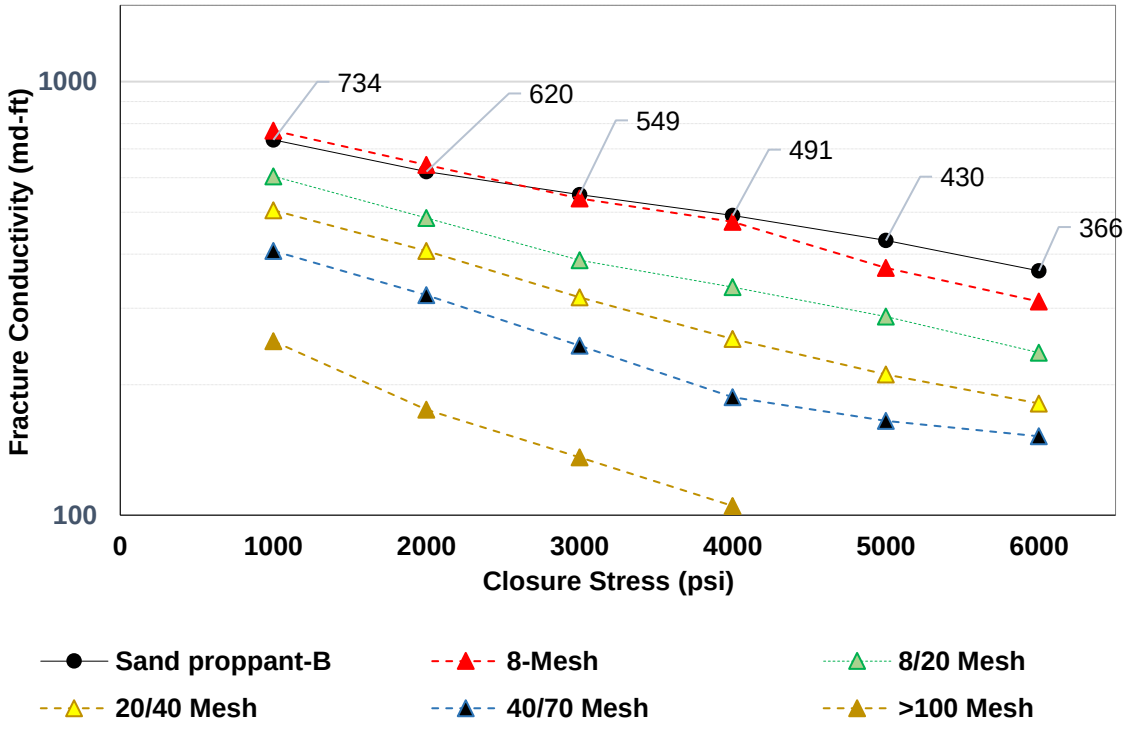

Figure 26.-Fracture conductivity results of sand proppant-B 100-mesh and Austin Chalk size particles

A defined trend between size particle and fracture conductivity was found: the larger the drill cutting particles the best the fracture conductivity result. The 8-mesh particle sizes produced results close to the baseline.

2.4.3.6. Wet mixtures of drill cuttings.

The drill cuttings were mixed by rock type formation in volume percentage according to the volumes drilled from the well, as explained in the methodology of this chapter. They were mixed in wet, and the resulting mixture was mixed at a concentration of 12.5 wt% with sand proppant-B and tested. **Figure 27** shows the results got.

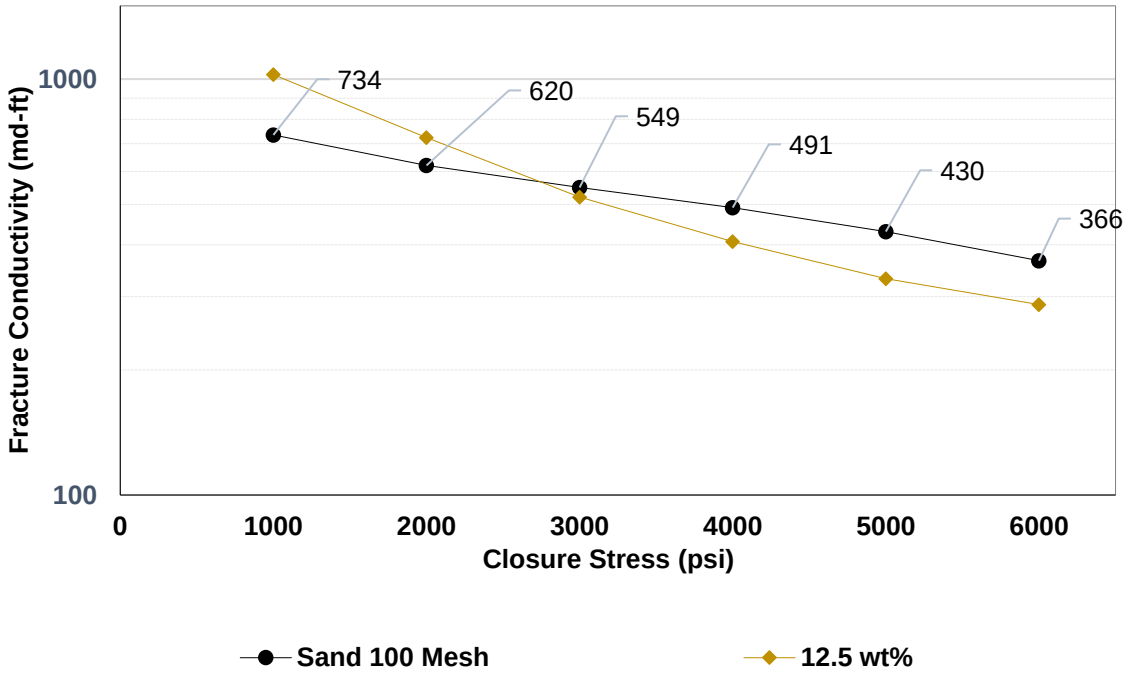

Figure 27.-Fracture conductivity results of sand proppant-B 100-mesh and wet mixture of drill cuttings

The mixture of drill cuttings produced a fracture conductivity close to the baseline, being larger for closure stresses of 1000 and 2000 psi, and smaller for closure stresses between 4000 to 6000 psi.

When preparing this mixture of cuttings, it was observed that the bags containing the drill cuttings presented variable amounts of oil-based drilling fluid. Considering this, different approaches were taken, such as mixing them in wet and later washing the oil-based drilling fluid or mixing the dried drill cuttings.

2.4.3.7. Wet/dried mixtures of drill cuttings.

The wet drill cuttings were mixed and then washed and dried to remove the oil-based drilling fluid. The resulting mixture was mixed at a concentration of 12.5 wt% with sand proppant-B and tested. **Figure 28** shows the results.

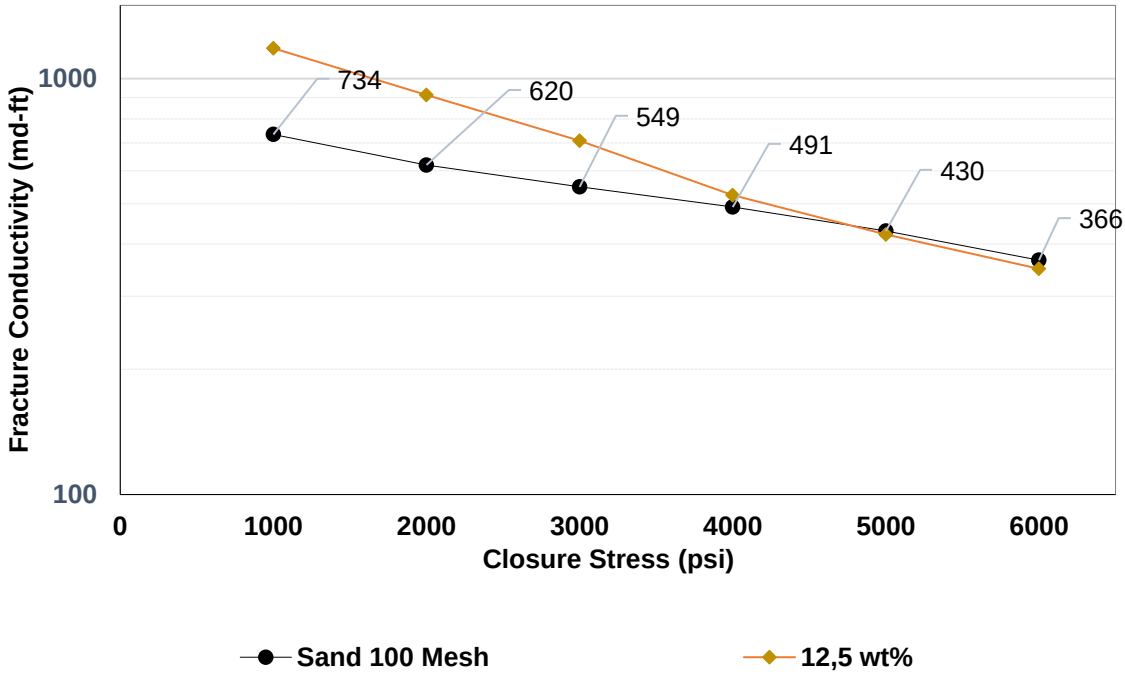

Figure 28.-Fracture conductivity results of sand proppant-B 100-mesh and wet/dried mixture of drill cuttings

The cuttings mixture produced an increase in fracture conductivity with respect to the baseline. This test is an ideal condition where there is not oil-based drilling fluid in the cuttings

2.4.3.8. Dried mixtures of drill cuttings.

The drill cuttings were mixed in dried because it was observed that the bags containing the drill cuttings had different amounts of drilling fluid. The resulting mixture was mixed at a concentration of 5, 10, and 20 wt% with sand proppant-B and tested. **Figure 29** shows the results.

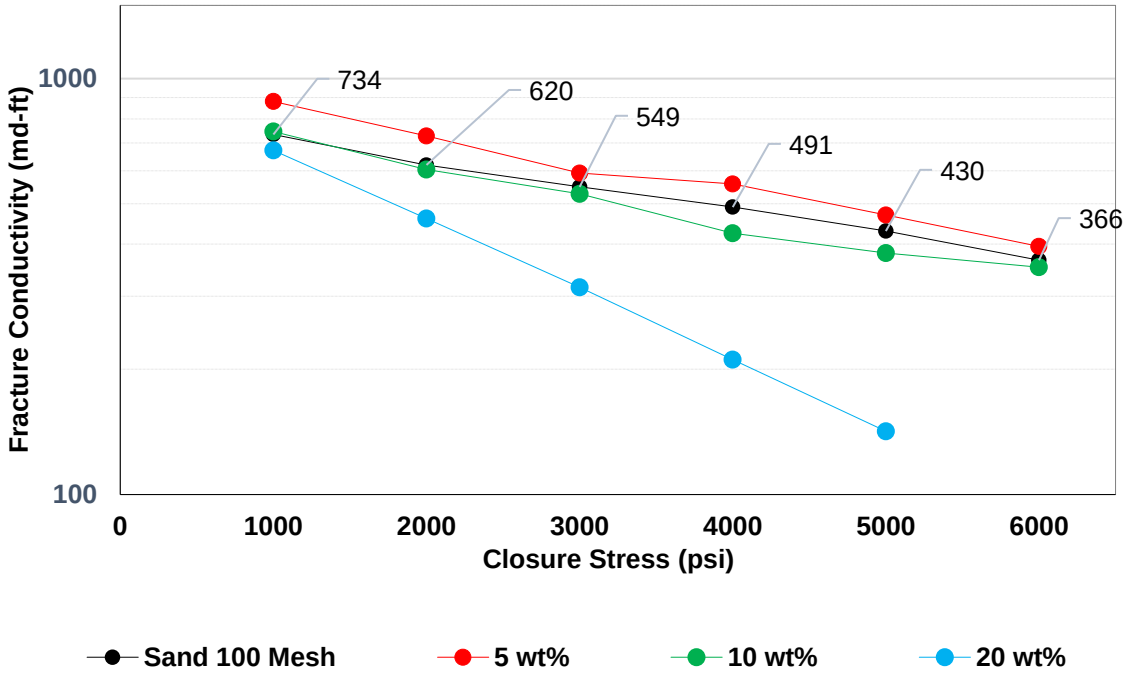

Figure 29.-Fracture conductivity results of sand proppant-B 100-mesh and dried mixtures of drill cuttings

Drill cutting concentrations of 5 and 10 wt% produced close results to the baseline. The 20 wt% produced a drastic decline in the fracture conductivity after increasing the closure stress.

2.4.3.9. Dried mixtures of drill cuttings added with oil-based drilling fluid.

The drill cuttings were mixed in volume percentage according to the volumes drilled. They were mixed in dried. Then, part of the resulting mixture was dosed with oil-based drilling fluid (OBM) at a concentration of 5 wt%. This mixture was mixed at a concentration of 5 and 10 wt% with sand proppant-B. The other part of the dried mixtures of drill cuttings was dosed at 10 wt% of OBM, and the resulting mixture was prepared at 5 wt% with sand proppant-B. the results are shown in **Figure 30**.

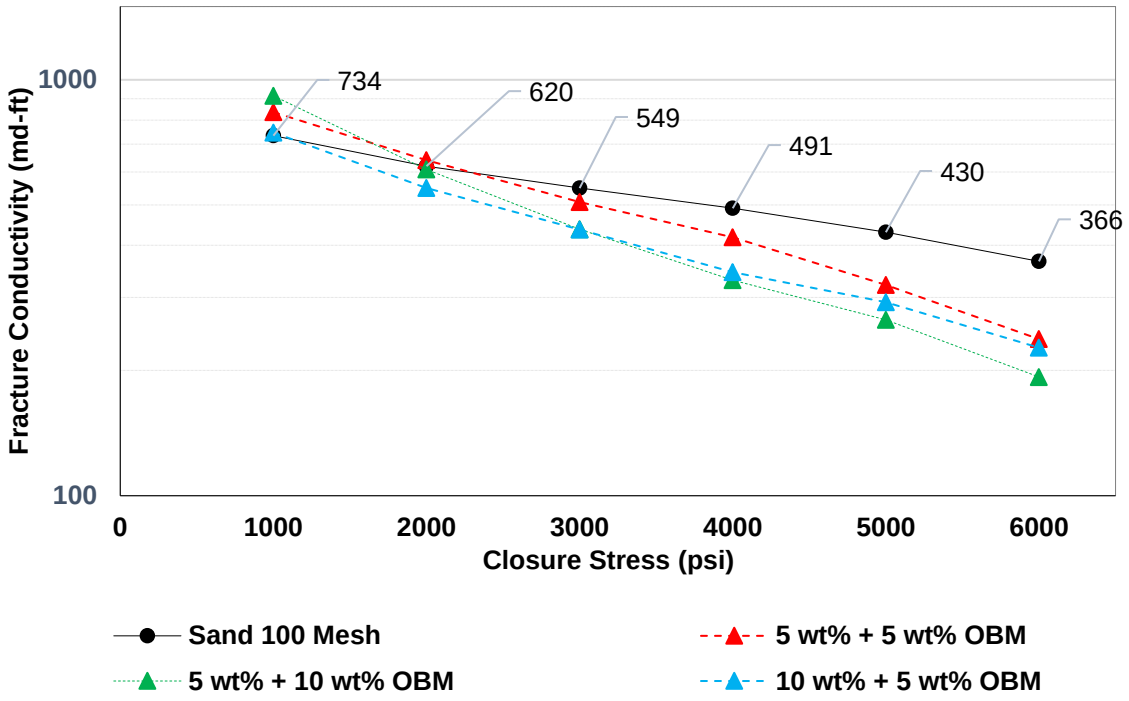

Figure 30.-Fracture conductivity results of sand proppant-B 100-mesh and dried mixtures of drill cuttings dosed with OBM

Close results were obtained for the conditions tested. However, the results indicate that the oil-based drilling fluid content is more relevant than the percentage of drill cuttings in the mixture. When increasing the oil-based drilling fluid in the sample, the fracture conductivity decreased.

2.5. Analysis of results.

The exponential decline curve was used to better understand the behavior of the fracture conductivity results. When the fracture conductivity is presented as a function of varying stress, a linear relationship on a semi-log plot is produced (Jansen, 2014). This is represented in equation 2.22.

$$Cf \cong Cf_0 e^{-\lambda \sigma c} \tag{2.22}$$

where Cf is the predicted fracture conductivity (md-ft) across the closure stress range, Cf_0 is the initial fracture conductivity at zero closure stress, λ is the exponential decline rate constant (psi^{-1}), and σc is the closure stress (psi).

2.5.1. Proppant size effect.

A direct relationship between proppant size and the fracture conductivity of the mixtures was observed: the closer the sand proppant particle sizes to the drill cutting sizes, the best the results obtained. The mixture of drill cuttings at 12.5 wt% with 40/70 mesh sand, resulted in a reduction of the baseline (see **Figure 31**). By comparing the initial fracture conductivity (Cf_0) there is a reduction of 29%. There is also a difference in the exponential decline rate constants (λ). This value was 1.8 E-

4 psi^{-1} for the sand, and 2.4 E-4 psi^{-1} for the mixture. These values indicate that the fracture conductivity in the mixture is decreasing faster than in the sand when increasing the closure stress. This can be caused by two reasons. The drill cuttings are generating fine particles (crushing), which can move through the sample, blocking the void spaces and decreasing the fracture conductivity. The second reason may be related to the wide particle size distribution of the drill cuttings, specifically the smaller size fraction which can move and accommodate in the void spaces of the sand proppant, affecting the fracture conductivity.

On the other hand, when using sand proppant 100 mesh, the mixture of drill cuttings and the sand resulted in fracture conductivity values close to the baseline. In this case, the drill cutting particles did not show a negative effect on the sand proppant fracture conductivity. The exponential decline rate constants were close, 1.7 E-4 psi^{-1} and 1.8 E-4 psi^{-1} for the sand and the mixture, respectively. This suggests that not much damage was induced in the frack pack mixture with respect to the baseline.

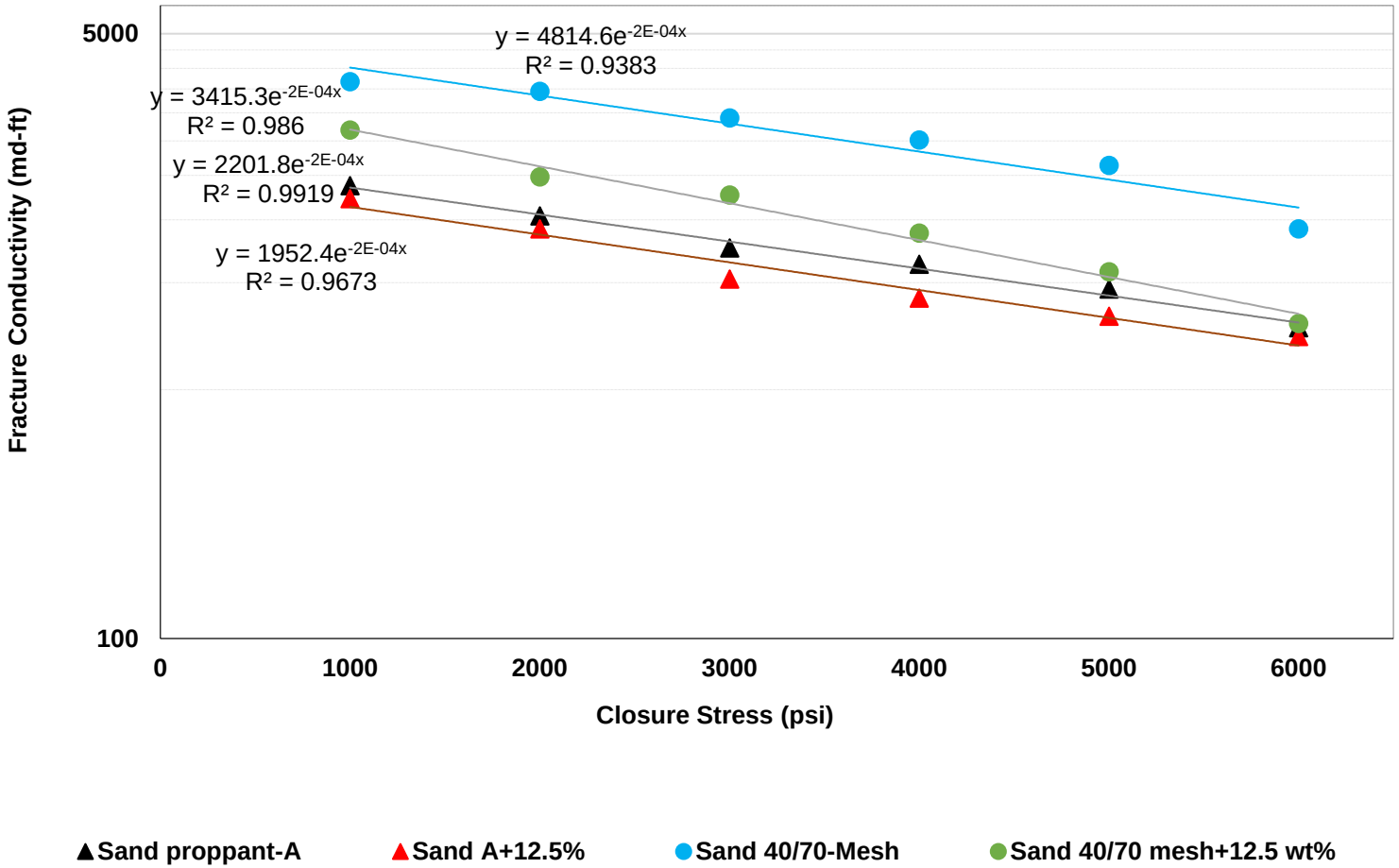

Figure 31.-Fracture conductivity exponential decline function for dried drill cuttings mixed with sand proppants

2.5.2. Oil-based drilling fluid effect.

The best result was obtained using wet drill cuttings. 100 mesh sands mixed with wet drill cuttings showed an increase in fracture conductivity, with respect to the baseline **(Figure 32).** The increase in fracture conductivities seems to be because of the oil-based drilling fluid. There are two possible mechanisms to explain the fracture conductivities increase. First, it is believed that the oil-based drilling fluid content in the drill cuttings creates a pathway for the gas to flow through the sample. Second, it is theorized that the oil-based drilling fluid agglomerates the fines produced, either by the sand or the drill cuttings, after increasing the closure stress. After being agglomerated, they cannot move through the void spaces, resulting in an improvement of the fracture conductivity.

The fracture conductivity decline rate constants for the mixtures were larger than for the sand proppant. Sand A and B have λ values of 1.7 E-4 psi^{-1} and 1.3 E-4 ps^{-1}, respectively. When adding the 12.5 wt% wet drill cuttings, the λ values for the mixtures A and B were 1.9 E-4 psi^{-1} and 1.5 E-4 psi^{-1}, respectively. For sand 40/70 mesh, an increase of the fracture conductivity decline rate constant was also noted, from 1.8 E-4 psi^{-1} for only sand to 2.1 E-4 psi^{-1} for the mixture. These results suggest that more damage was caused to the mixture sand 40/70 mesh pack than for the 100 mesh pack. As explained before, it is also related to the relationship between the drill cuttings and sand particle size distributions.

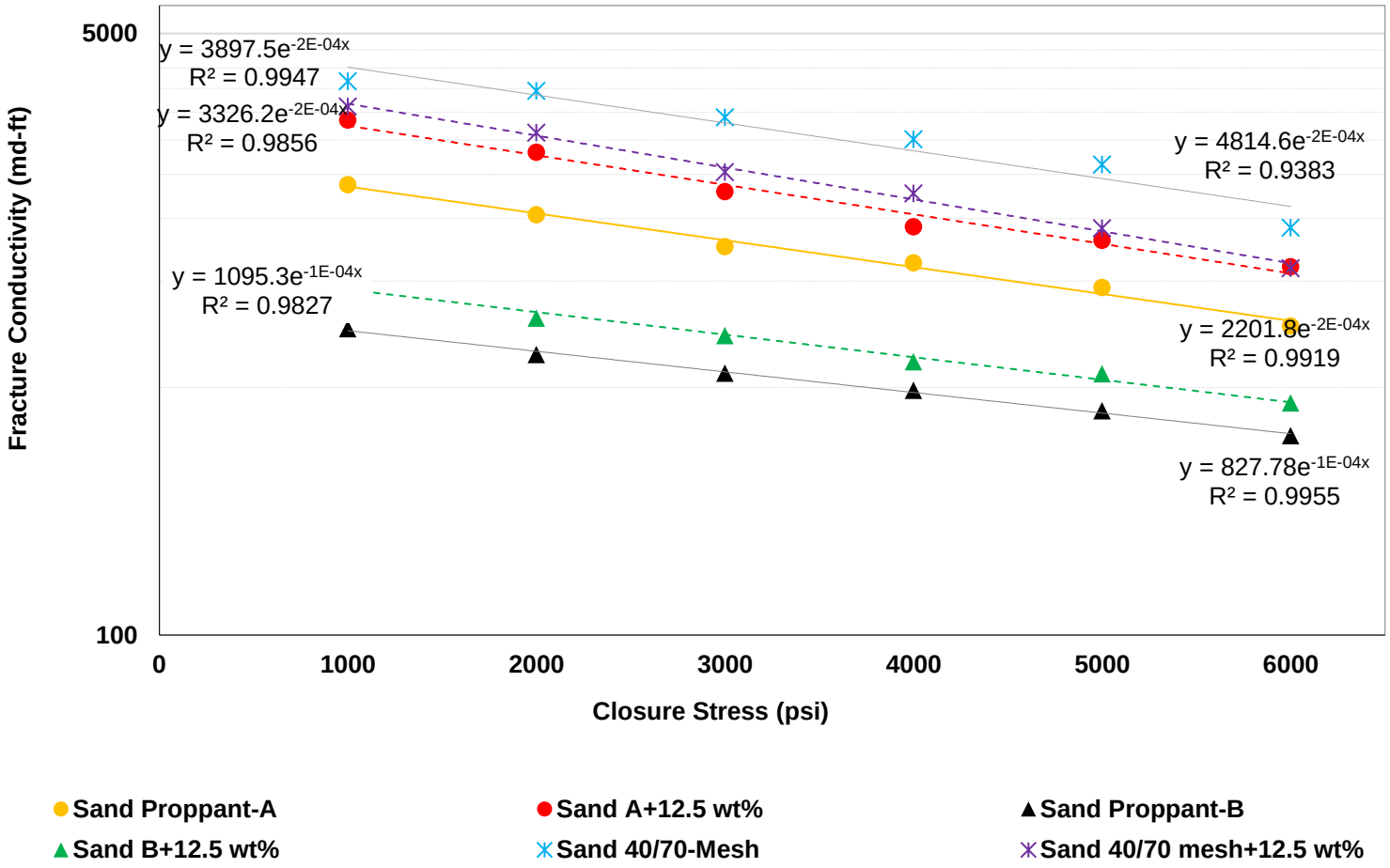

Figure 32.-Fracture conductivity exponential decline function for wet drill cuttings mixed with sand proppants

2.5.3. Proppant particle size distribution effect.

The results for the two sand proppants 100 mesh are shown in **Figure 32**. This displays similar trends for the mixtures with drill cuttings. When comparing the ratio of the initial fracture conductivity at zero closure stress (Cf_0) of the mixtures to the sands, similar results are obtained for both sand proppants. These results indicate that reproducible trends might be obtained when using different sand 100 mesh mixed with wet drill cuttings.

The difference in the fracture conductivity results between the two sands 100 mesh is a function of their particle size distribution, shape, and resistance to crushing.

2.5.4. Drill cutting particles size effect.

As expected, larger drill cutting particle sizes produced higher fracture conductivities. **Figure 33** shows that drill cutting particles 8/20 mesh produced higher fracture conductivities than particles 40/70 mesh, in both formations evaluated. The increase of the particle size in the frack pack increase the void space, resulting in a higher area for the gas to flow.

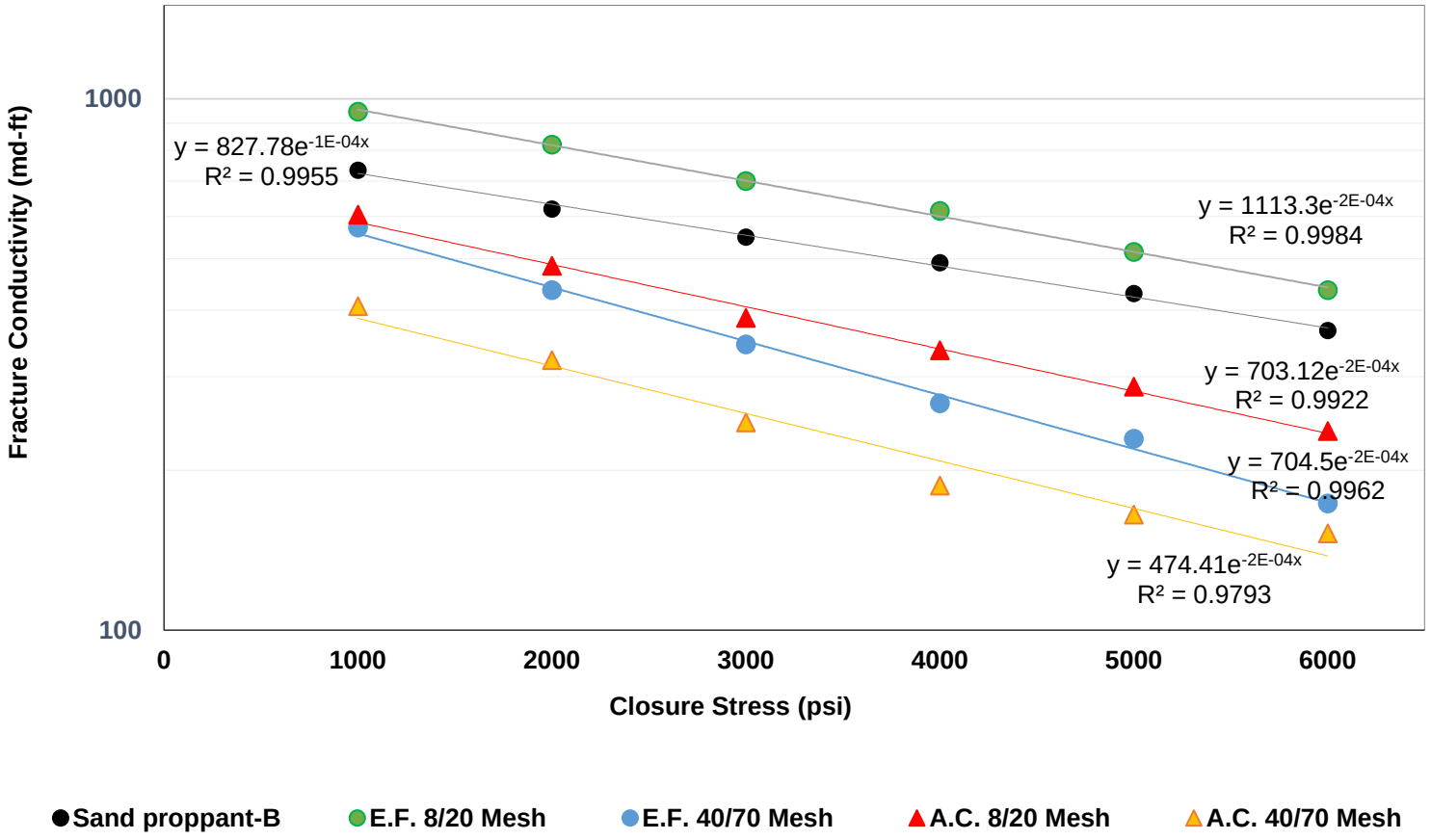

E.F.: Eagle Ford A.C.: Austin Chalk

Figure 33.-Fracture conductivity exponential decline function for dried drill cuttings from Eagle Ford and Austin Chalk (12.5 wt%) mixed with sand proppant-B

2.5.5. Drill cuttings formation effect.

Drill cuttings from the Eagle Ford showed better results than Austin Chalk drill cuttings (see Figure 33). Austin Chalk and Eagle Ford formations are composed mainly of calcium carbonate. However, the strength of the chalk is lower than calcite, which explains the results obtained. Additionally, Eagle Ford drill cuttings are composed of quartz particles (up to 30 wt%), which add strength against the crushing of the drill cuttings.

2.5.6. Combined effects of drill cutting mixtures from different formations and oil-based drilling fluid content.

The oil-based drilling fluid content has major relevance in the fracture conductivity decline rate constant of the mixtures **(Figure 34).** This value for the mixtures of drill cuttings at 5wt% and 10 wt%, mixed with 5 wt% oil-based mud produced close λ values (2.4 E-4 psi^{-1}). When the 5 wt% drill cuttings sample was added with 10 wt% oil-based drilling fluid, the λ was higher (3.0 E-4 psi^{-1}). These results suggest that the drilling fluid proportion must be kept lower than 10 wt% (the lower the best) to avoid a negative impact on the fracture conductivity.

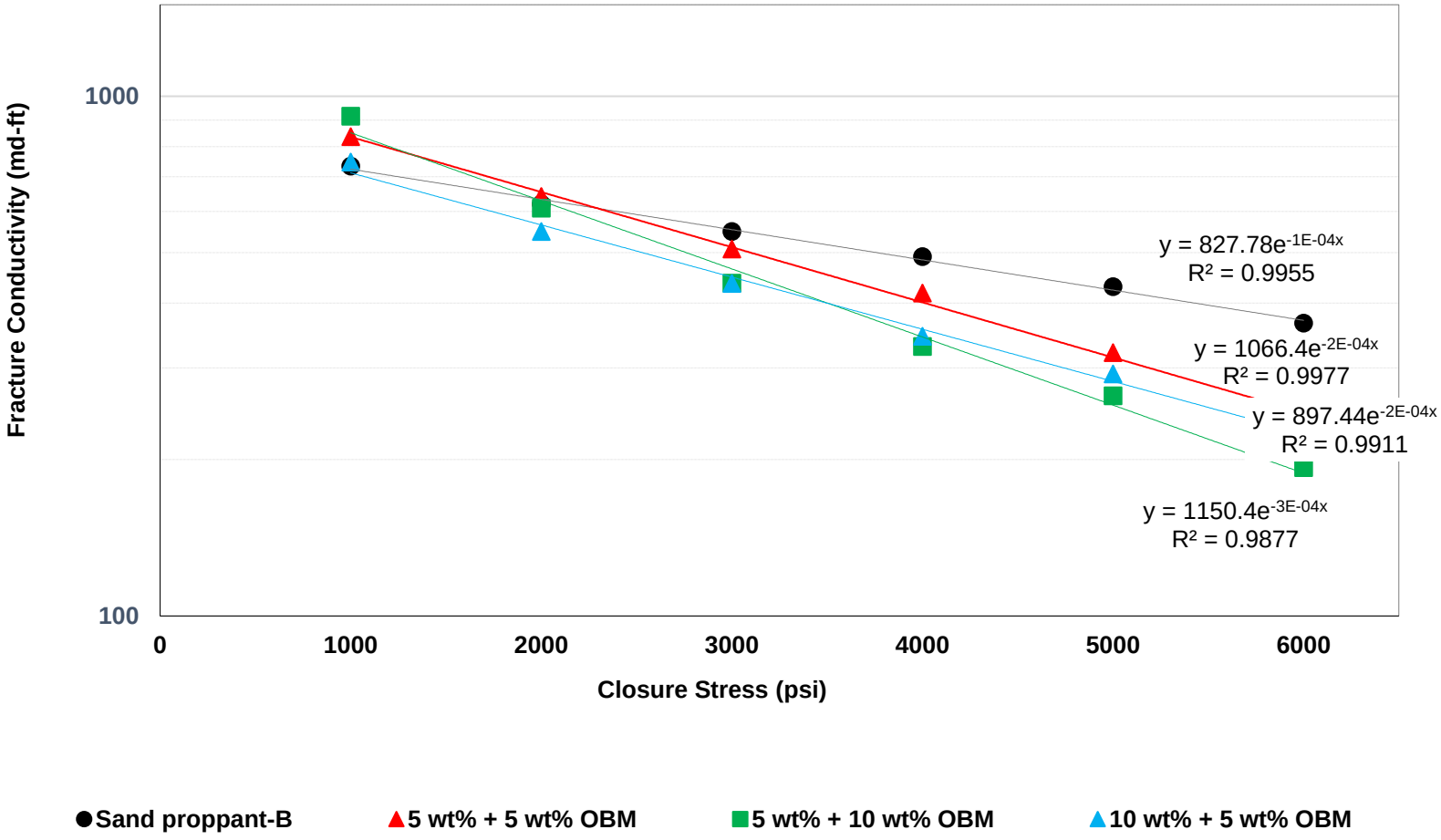

Figure 34.-Fracture conductivity exponential decline function of mixtures of drill cuttings from the well, added with oil-based drilling fluid, with sand proppant-B

2.6. Field application.

When using a 6-inch drill bit in the horizontal section of an unconventional well, approximately 33 lb/ft of oil-based drill cuttings are produced. According to the results obtained, a 12.5 wt% wet drill cuttings concentration mixed with sand proppant 100 mesh can be used. For 33 lb/ft of produced drill cuttings, 231 lb/ft of sand proppant is required, producing a total proppant intensity of 264 lb/ft.

The proppant intensity for the Eagle Ford formation was in average 7500 lb./ft (see **Figure 35**).

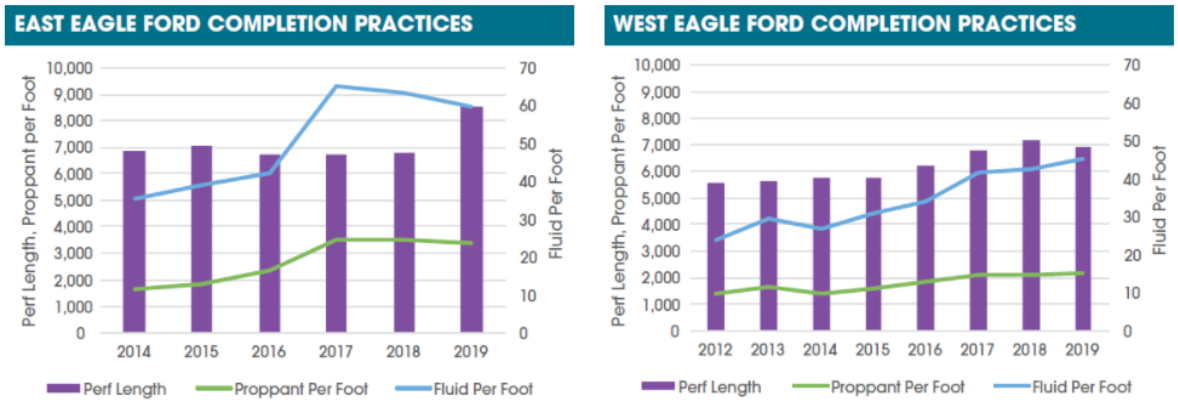

Figure 35.-Eagle Ford completion practices (Reprinted from Presley 2019)

This trend shows that all oil-based drill cuttings can be reinjected along with the sand proppant 100 mesh without affecting the productivity index of the well.

If the oil-based drill cuttings would be reinjected in the first stages, at a concentration of 12.5 wt%, when completing a horizontal well, with a proppant intensity of 7500 Lb/ft, they would be re-injected in the first 217 ft of the horizontal

section of the well, this will reduce the economic operating costs and the environmental impacts associated with oil-based drill cuttings disposal treatment.

2.7. Conclusions.

The best results were obtained using sand 100 mesh than 40/70 mesh. Probably, since the 40/70 mesh sand particles are much larger than the drill cuttings particles, the latter, tend to migrate with the gas flow through the void spaces of the proppant, decreasing its conductivity.

Wet cuttings mixed with sand proppants showed, in general, better results than dried cuttings. One possible explanation is that the oil-based drilling fluid in the wet cuttings is creating a path way for the gas to flow. A second reason might be related to the agglomeration of the fines particles generated by the crushing of the drill cuttings after increasing closure stress. The oil-based drilling fluid might act as an agglomerating agent to avoid the fines particles to move across the sand.

In general, 12.5 wt% drill cuttings concentration in sand proppant produced fracture conductivity results close to the base line. Drill cuttings concentration up to 25 wt% produced acceptable results.

The physical properties of sand, like shape and proppant size distribution, and the resistance to crushing, are important factors affecting the fracture conductivity response when mixed with drill cuttings.

Drill cutting size and mineral composition showed to be important factors in the fracture conductivity of the mixtures. The larger the drill cutting particles, the best the fracture conductivity results.

The oil-based drilling fluid content is more important than the mass of the drill cuttings used in the mixture for the fracture conductivity response. The oil-based drilling fluid content should be lower than 5 wt% in the mixture to obtain acceptable results.

3. PROPPANT QUANTIFICATION IN DRILL CUTTINGS

This chapter presents the use of drill cuttings to measure the proppant concentration in hydraulic fractures by quantifying sand proppant particles in the drill cuttings. Synthetic samples were used to test and validate the method.

3.1. Introduction.

The general approach to estimate the proppant concentration in the hydraulic fractures, and the fracture conductivity, is by using hydraulic fracturing simulations. Modeling of hydraulic fracturing is a complex problem, which includes the description of many physical processes, including the fluid flow in the fracture, deformation of the rock, fracture of the rock, proppant flow, etc. An effective solution to this problem requires a considerable number of simplifications and assumptions (Khasanov et al., 2017).

Proppant transport and placement poses an additional challenge to the modeling of hydraulic fracturing. The fluid-solid two-phase system is often modeled under the Eulerian-Eulerian framework (Ouyang et al., 1997), while sometimes the Eulerian-Lagrangian approach is used to allow models to track individual proppant particles (Zhang, et al., 2017). The slurry is usually represented as a fluid-solid mixture of prescribed rheology and density with differential settling enabled from the suspension. It is also assumed that the proppant is distributed homogeneously across the fracture. However, flows of non-Brownian particles, such as proppant,

often result in nonhomogeneous flows (Meeker et al., 2020). Proppant tends to migrate transversely away from the fracture walls to accumulate at the fracture center, where shear stress is the lowest and flow velocity is the highest (Wang and Elsworth, 2019).

The previous arguments can be summarized by stating that hydraulic fracturing is not very predictable because of the strong uncertainties concerning subsurface heterogeneities (Chen et al., 2015), and proppant transport mechanism. Understanding of the mechanisms and effects of the coupled fracture/proppant system is greatly limited by insufficient direct observations (Chen et al., 2015) to calibrate the models (Raterman et al., 2018), and justify any intent to measure the proppant concentration in the hydraulic fractures.

In this research, it was investigated the use of drill cuttings to quantify the proppant concentration in hydraulic fractures when drilling through it. Synthetic samples, using Eagle Ford drill cuttings, were used to test and validate the methodology developed. The field application of the results obtained will be useful as direct observation to determine the proppant concentration in the hydraulic fractures, and to calibrate the hydraulic fracture models.

3.2. Literature review.

A description of the reported works on quantification of proppant particles in hydraulic fractures is first presented, then some parameters used for particle detection are presented.

3.2.1. Proppant measurements in drill cuttings.

Previous work measured qualitatively the sand proppant in drill cuttings (Raterman et al., 2018). They also reported a “semi-quantitative” concentration of sand proppant in the hydraulic fractures by counting the number of proppant particles in a mass of sample obtained after scratching the fracture faces from downhole cores. However, they reported several hydraulic fractures without proppant, and they claimed that “it is unknown whether these sand grains were in-situ or had been washed into the hydraulic fractures along with drilling mud”. Gale, et al. (2018) claimed that the proppant grains may be removed from the fractures by the action of the drilling mud. Maity, et al. (2018) reported the estimation of proppant particles number by mass of a sample. They also used downhole core samples and scraped the proppant from the fracture faces.

3.2.2. Sand Proppant.

Sand proppant, also known as silica sand, quartz sand, white sand, or industrial sand, is made up of two main elements: silica and oxygen. Silica sand, specifically, is made up of silicon dioxide (SiO_2). To be considered silica sand, the material must contain at least 95% SiO_2 and less than 0.6% iron oxide. If the sand does not meet these criteria, it will be qualified as what is often called ‘regular’ sand (Shaw Resources, 2021). It has two of the most prominent attributes critical for classification: “blue hue” and “translucence” (Maity et al., 2018).

Sand particles are expected to be translucent when imaged under transp||||arency. These depend on the particle size, its cleanliness (from sample preparation), and the kind of mineralization within the sand particle, i.e., its crystal structure. Since light absorption is also influenced by particle size, larger particles tend to be darker (more absorption) and vice versa (Maity et al., 2018).

In contrast, aluminum, calcite, and clay particles are very dark. The aluminum and clay particles tend to show a reddish hue (Maity et al., 2018). Additionally, as reported by Maity et al. (2018), calcite particles have rougher edges than sand particles.

3.2.3. Proppant detection.

The basic problem with detecting and classifying proppant particles from sub-sample images is essentially an image processing problem aimed at object detection and classification. Various attributes can be used to identify whether the object is a proppant particle, calcite particle, or other miscellaneous material. These attributes include particle darkness, “hue”, “continuity”, particle roundness, size, shape factors, roughness, etc. (Maity et al., 2018).

3.2.3.1. Visible molecular spectroscopy

When the matter interacts with an incident electromagnetic radiation (beam), it experiences a change in its properties. The Figure 36 exhibits the electromagnetic spectrum radiation and the types of electronic transitions after an incident beam interacts with the matter.

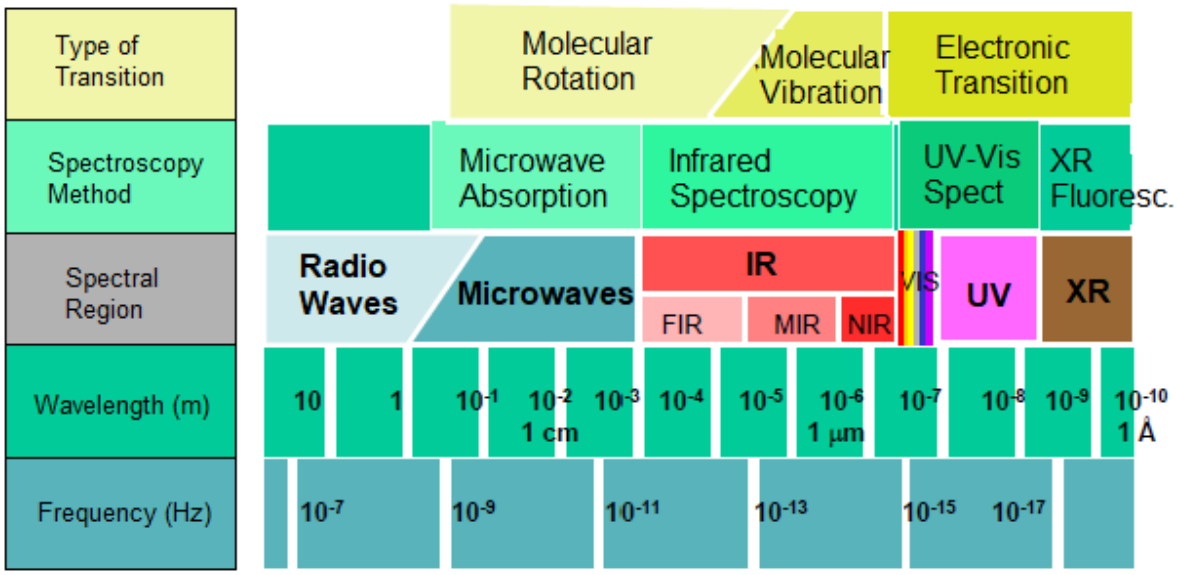

Figure 36.- Electromagnetic spectrum radiation: type of electronic transitions and spectroscopic methods (modified from Todoli, 2008)

When the matter interacts with a beam in the visible region of the electromagnetic spectrum, the spectroscopic method is referred as to visible molecular spectroscopy. It can lead to light absorption, scattering, diffraction or emission of radiation at certain wavelengths. When the silicon dioxide interacts with a beam in the visible region of the electromagnetic spectrum, it leads to light absorption.

3.2.3.2. Light Absorption

The light absorption is produced by the electron excitation of the bonding or nonbonding electrons. Figure 37 is a schematic representation of the electronic transition during light absorption. σ, π, and n makes references to the external electros.

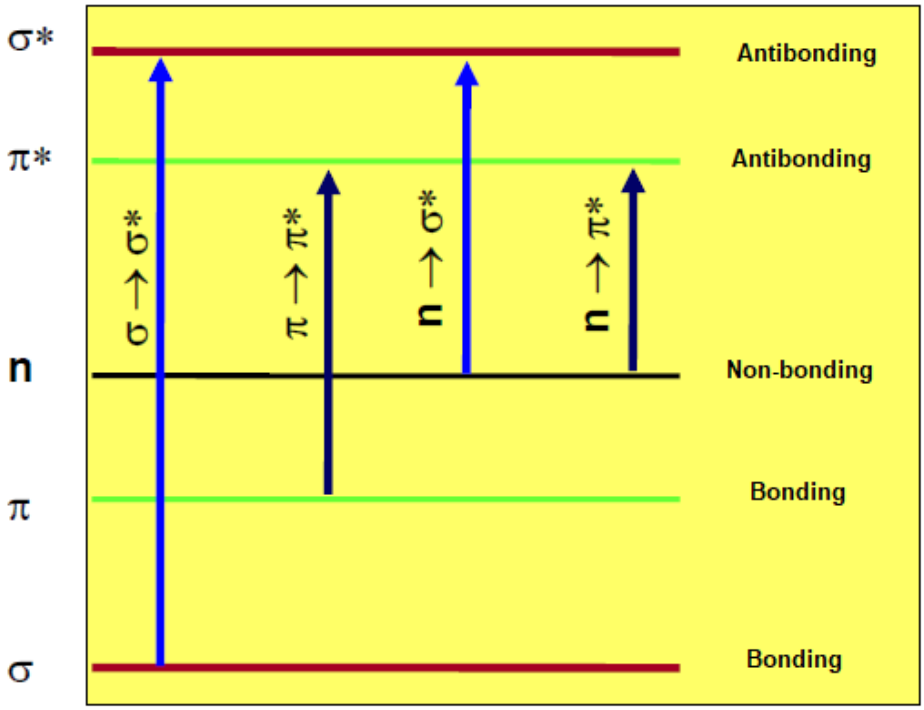

Figure 37.-Representation of the electronic transition during light absorption (Reprinted from Todoli, 2008)

Light absorption is a two steps process: absorption and relaxation (Todoli, 2008).

a) Absorption: a beam interacts with the external electrons of the matter, changing its energy levels, generating a transition state of the matter and producing light absorption of specific wavelength.

$$M + h\upsilon \quad M^*$$

The transition state (M*) has a lifetime of 10-8 – 10-9 seconds.

b) Relaxation: the transition state of the matter liberates the absorbed energy and returns to its originally state, generating heat, photochemical reactions or luminescence.

M* M + Heat

M* B (Photochemical reactions)

M* M + hυ (Luminescence)

Every atom (and molecule) has its specific wavelength absorption values. It is determined by their external electron configuration. It is useful to identify atoms or molecules. As example, **Figure 38** to **Figure 40** show the electron transition levels of energy for different atoms.

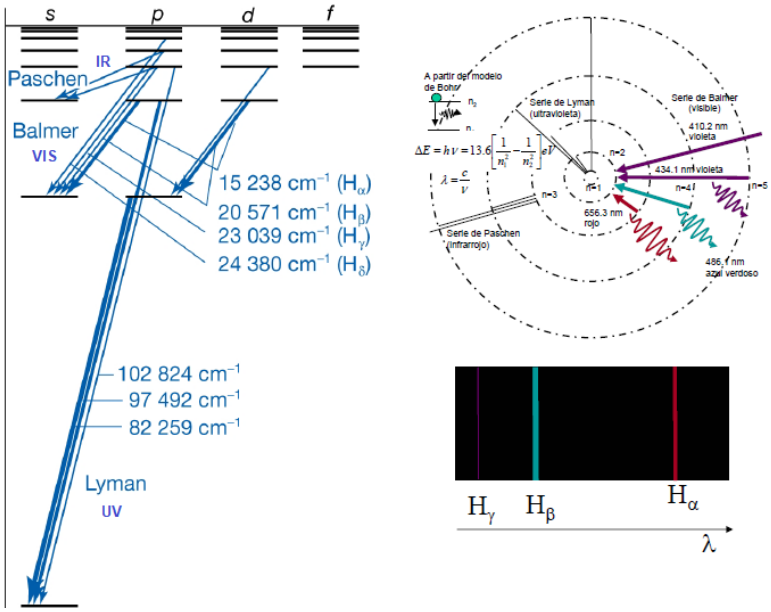

Figure 38.-Electron transition levels of energy of a hydrogen atom after interacting with photons of different energy levels (Reprinted from Todoli, 2008)

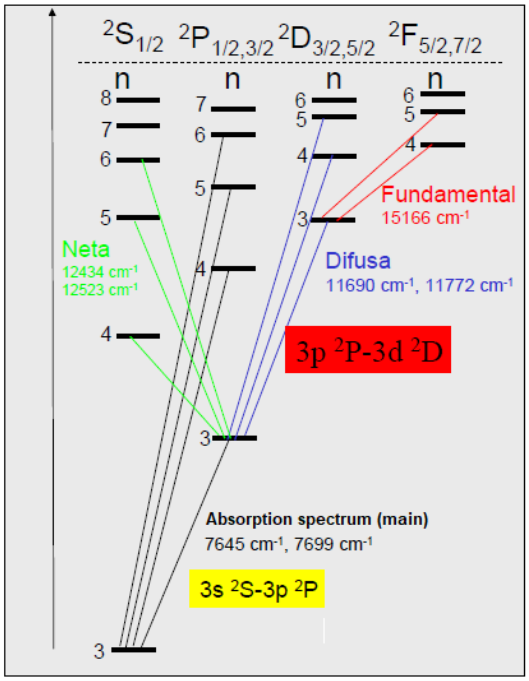

Figure 39.-Electron transition levels of energy of a sodium atom after interacting with photons of different energy levels (Reprinted from Todoli, 2008)

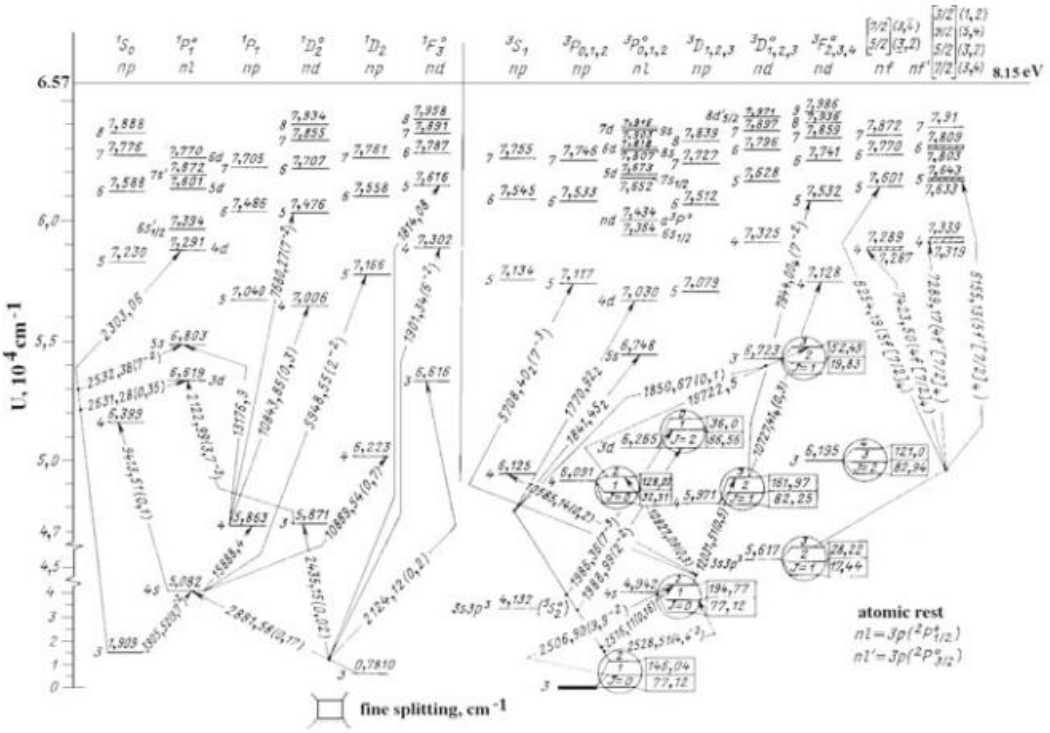

Figure 40.-Electron transition levels of energy of a silicon atom after interacting with photons of different energy levels (Reprinted from Smirnov, 2018)

The silicon dioxide molecule has σ electrons, corresponding to the electrons in the σ bonding between silicon and oxygen, and nonbonding electrons (called n electrons) which are the lone pair in the oxygen atom (see **Figure 41**). These electrons are involved in the light absorption process of the silicon dioxide.

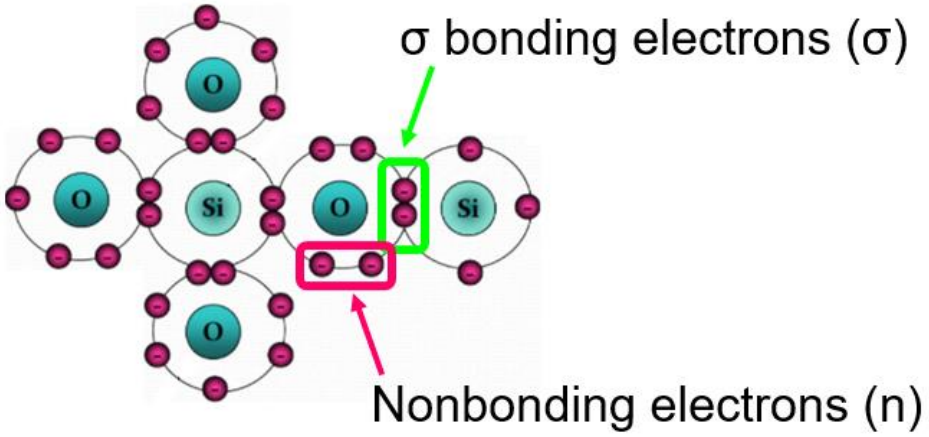

Figure 41.-External electrons in the silicon dioxide

Light absorption measurements of silica sand, in various silica sand samples, showed that more absorption takes place around in the blue range of the visible light within the visible region of the electromagnetic spectrum (Coblentz, 1912, Ketheeswaren, 2004; Kitamura, 2007; Kowalsky, 2009; Yang et al., 2010; Rodríguez, 2018). Figure 42 shows an absorption curve for silica sand at room temperature. This absorption occurs because when a beam (photon) with the appropriate energy interacts with a silica crystal, then the photon is absorbed by the external electronic configuration of the system, increasing their kinetic and vibration random movement.

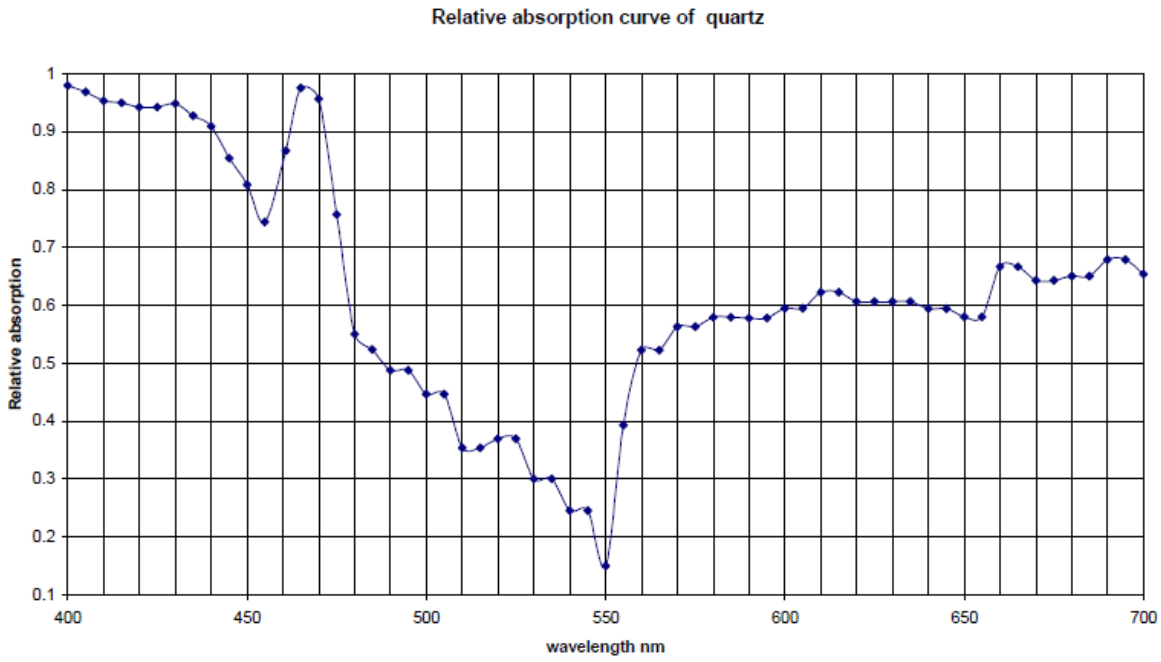

Figure 42.-Absorption curve of silica sand (Reprinted from Ketheeswaren, 2004)

3.3. Methodology.

This section presents a methodology to sample the drill cuttings in the field, and the step by step for the proppant quantification in the drill cuttings, a method based on light absorption.

3.3.1. Field sampling.

The sampling procedure will be presented for drilling an infill well through the stimulated reservoir volume of a legacy well. It is represented in Figure 43.

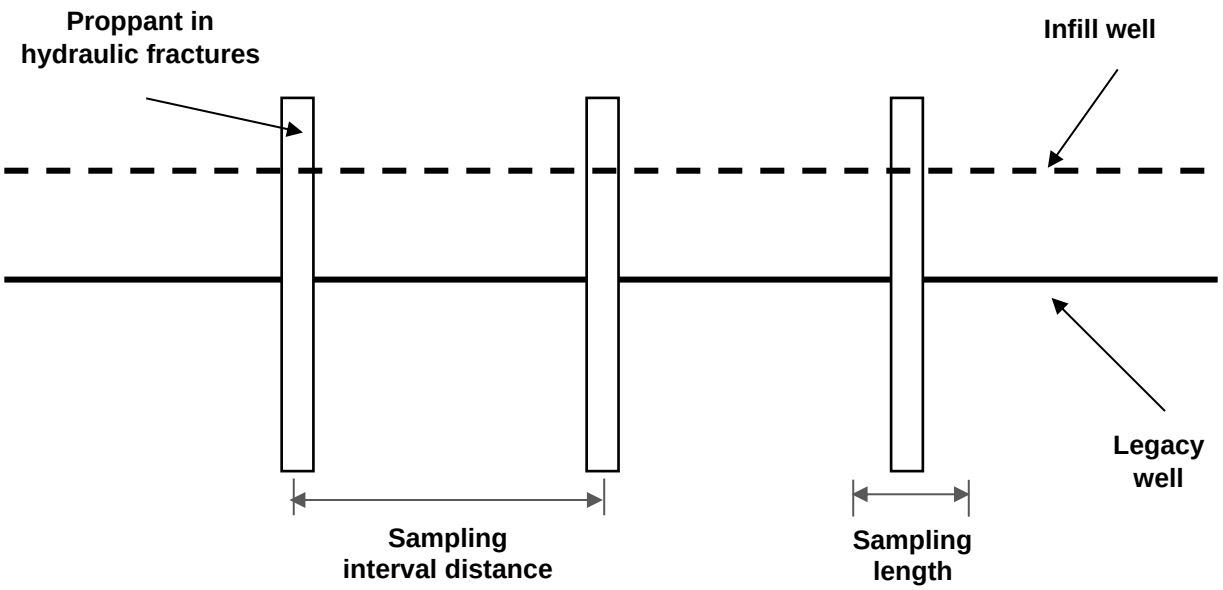

Figure 43.-Top view representation of the infill drilling well

The well Klattenhoffunitlas-1H, called in this chapter the legacy well, has a 7000 ft horizontal wellbore length. For assumed values of rate of penetration (138 ft/h) and circulation rate (300 gpm), a total of 233 samples were calculated. Sampling can be done following the following procedure:

1. Sampling interval distance: 30 ft.
2. Sample length: 10 ft.
3. Take a sample of around 1 during a time no longer than 4 minutes.
4. Filtrate each sample through a 200-mesh to eliminate as much drilling fluid as possible.
5. Collect approximately 500 grams of drill cuttings per sample.
6. Package the samples and label them properly.

Two possible locations to take the samples are recommended. Both are part of the drilling shaker fluid separation.

1. Possum belly. It is recommended to sample at this location because it contains the whole mud (see green highlighted area in **Figure 44**).
2. Off the shaker screen & “catch board”. To sample at this location is an alternative. However, fine particles can be separated during the process, affecting the mass balance to calculate the proppant concentration in the fracture (see blue highlighted area in Figure 44).

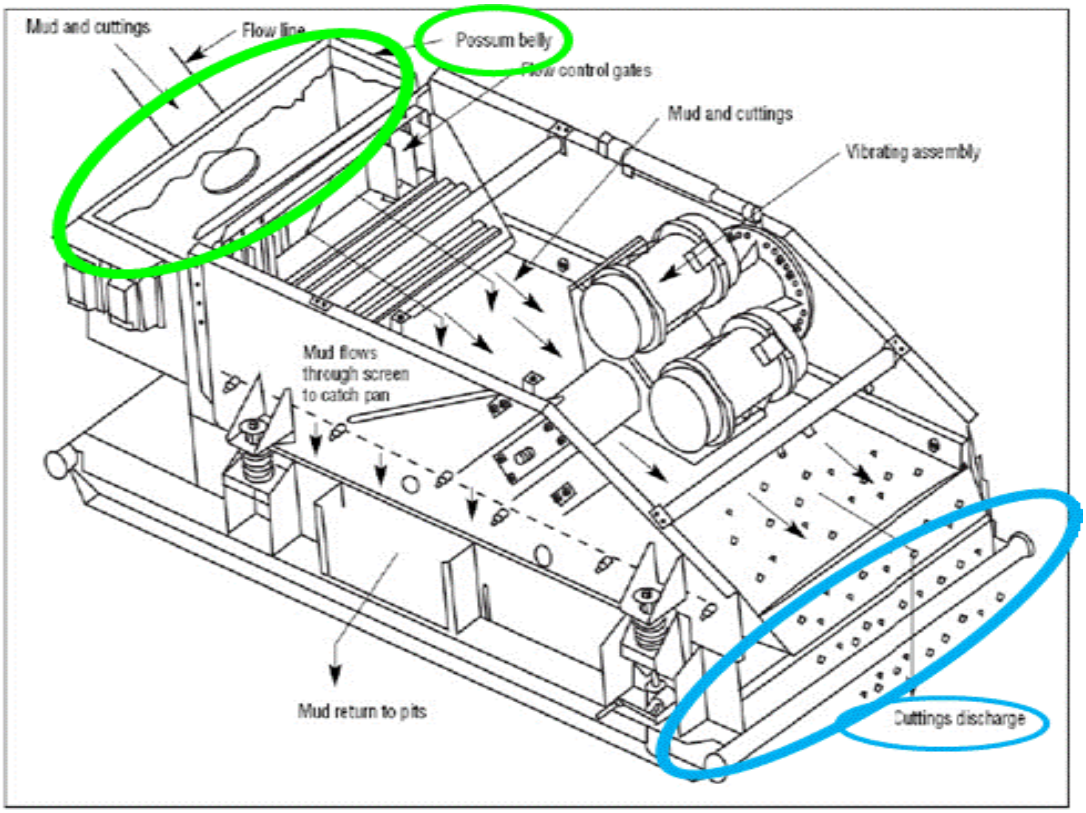

Figure 44.-Recommended locations to sample drill cuttings

3.3.2. Sample preparation.

Before quantifying the sand proppant in drill cuttings, it is necessary to prepare the samples by removing the drilling fluid.

Steps 1 to 5, and 9-10, must be done inside a fume hood.

10. Mix 250 grams of drill cuttings with 250 mL of paint solvent.
11. Stir the mixture with a spatula for 5 minutes.
12. Filtrate the mixture through a 200-mesh.
13. Take the particles retained in the 200-mesh and spread them on 3 layers of paper towel.
14. Let the particles dry at room temperature, inside the fume hood, for 12 hours.
15. Do a sieve distribution of the dried particles?
16. Separate the particles by mesh size into 4 groups:
    a. 40-mesh.
    b. 40/70 mesh
    c. 70/100 mesh
    d. 100/200 mesh

    Particles 40/70 mesh will be used to quantify sand proppant 40/70 mesh. Particles 70/100 mesh will be used to quantify the amount of crushed sand proppant.
17. Weight the mass of the particles retained in every mesh group.
18. Take the filtrated liquid from step 3 and filtrate it through a 400-mesh.

19. The resulted filtrated liquid from step 9 can be re-utilized to wash the drill cuttings in step 1.
20. Discard the particles with size 200/400-mesh.

3.3.3. Sand proppant concentration measurements in drill cuttings.

A procedure based on light reflection on particles was used to quantify the amount of sand proppant in drill cuttings. A microscope, SMZ-168 SERIES **(**Figure 45**)**, was used to magnify and to take pictures of sand proppant and cutting particles. Using the Fiji-Image G software, a code was developed to automatically quantify the sand proppant in drilled cuttings.

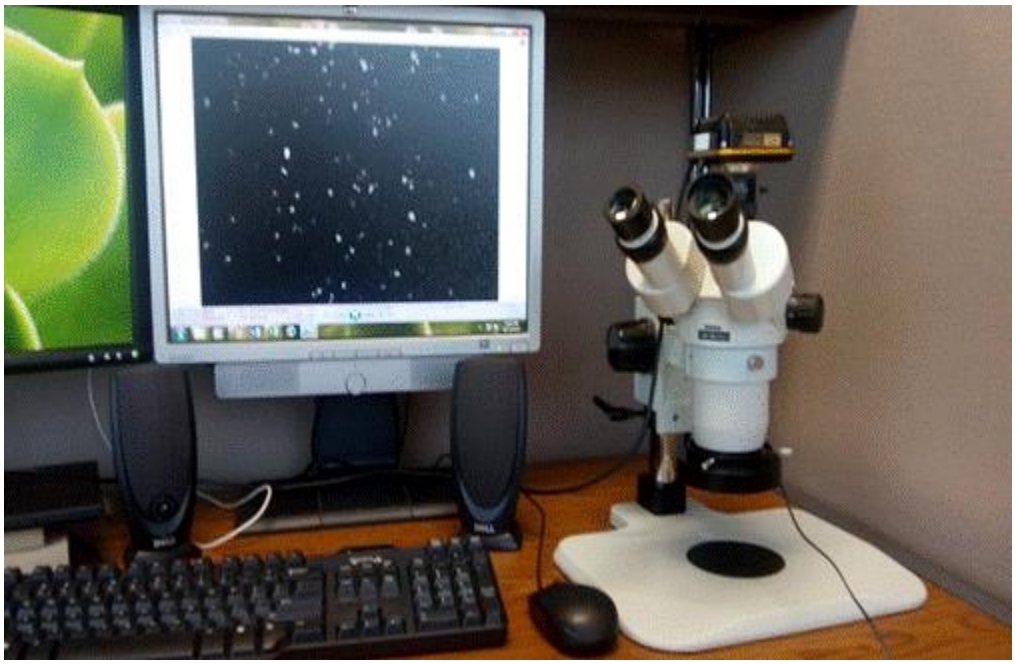

Figure 45.-Microscope SMZ-168 SERIES

3.3.3.1. Microscope configuration.

The microscope configuration is adjusted to make the rock drilling particles similar to the black background, and the sand proppant particles are adjusted with the “white balance”.

1. Open the ToupView software to control the camera on the microscope. A window like shown in Figure 46 will display.
2. Select “Exposure & Gain” and configure it as follow (see Figure 47).
    a. Exposure Target: 120.
    b. Exposure Time: 45.812ms.
    c. Gain 100%.
3. Select “White Balance”, and modify its configuration as shown in Figure 48:
    a. Color Temperature: 8160.
    b. Tint: 920.
4. Finally, configure “Black Balance” as in **Figure 49**.
    a. Red: 89.
    b. Green: 117.
    c. Blue: 91.

If necessary, the black configuration can be modified to make darkness the rock drill cuttings.

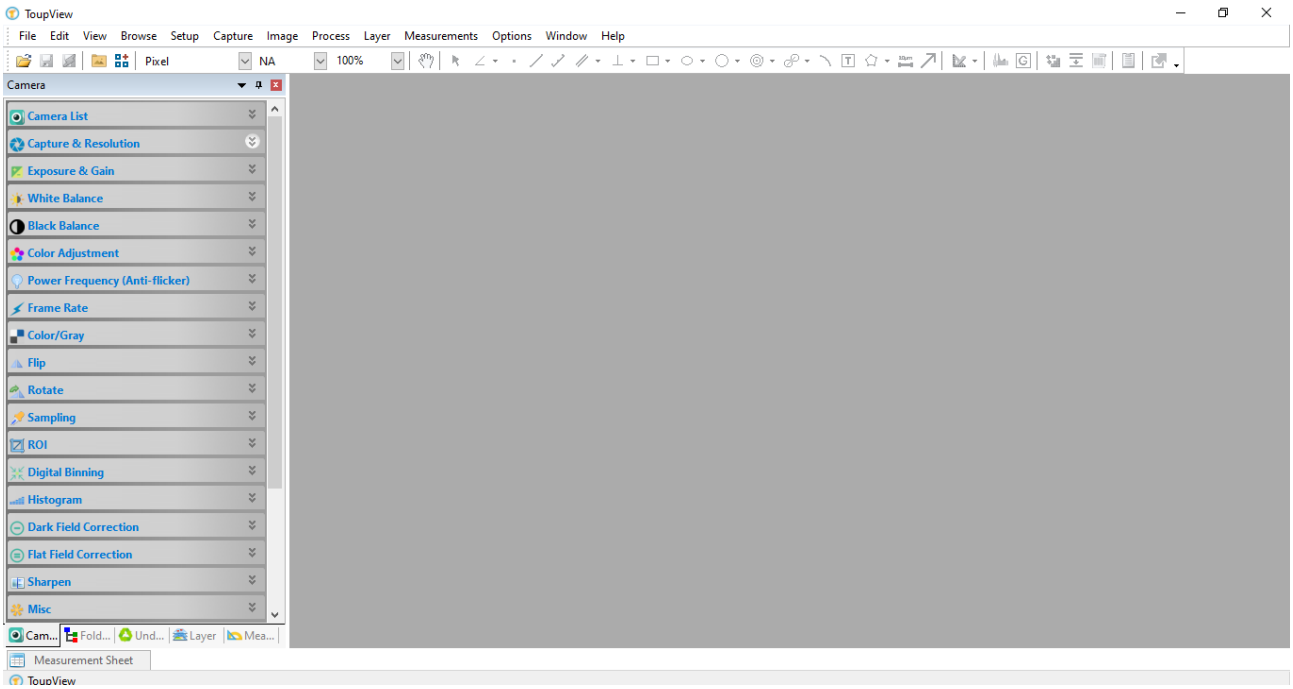

Figure 46.-Window display after opening ToupView software

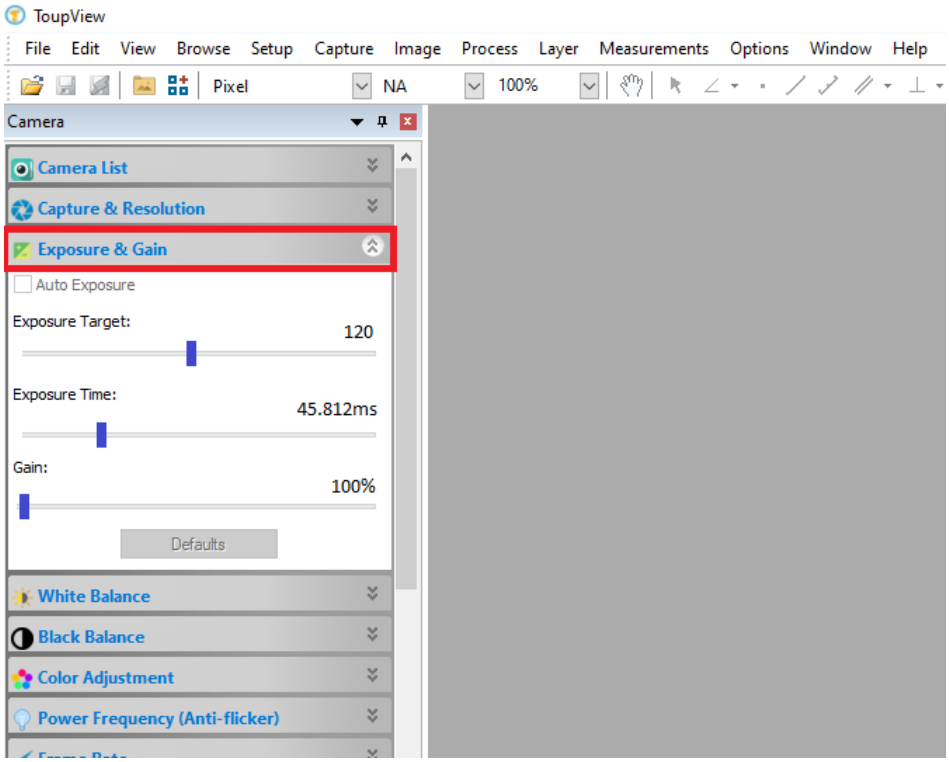

Figure 47.-Exposure & gain configuration

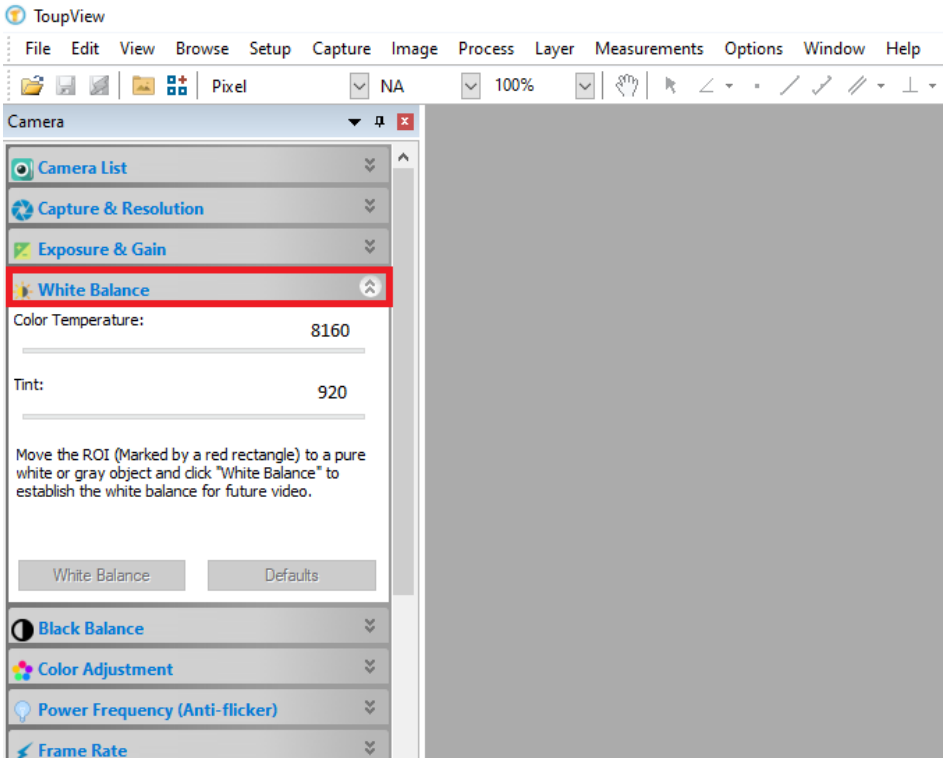

Figure 48.-White Balance configuration

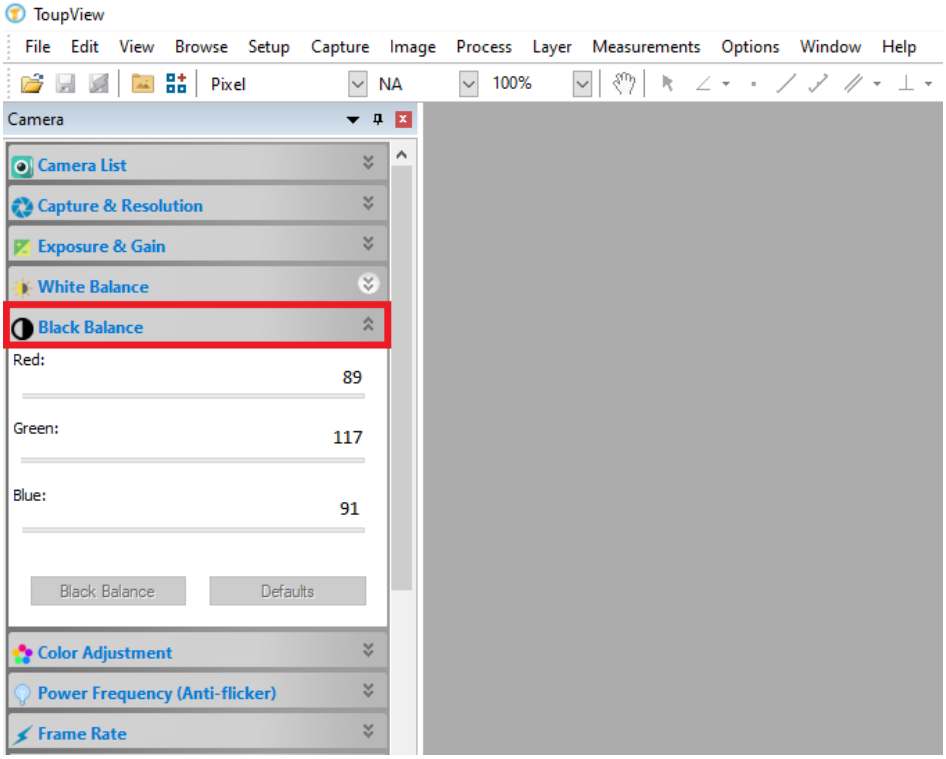

Figure 49.-Black Balance configuration

3.3.3.2. Sand proppant measurements.

Two different microscope magnifications were used: 1X and 2X for particles size 40/70 and 70/100 mesh, respectively. The general procedure is shown below:

1. Prepare a millimeter paper with rectangles of 1.2 mm * 0.8 mm for the 1X magnification, and 0.7 mm * 0.45 mm for the 2X magnification.
2. Fix the millimeter graph paper on a table surface.
3. Take a black surface paper and place it over the millimeter paper.
4. Take a sample and spread it on a black surface paper like in **Figure 50**.

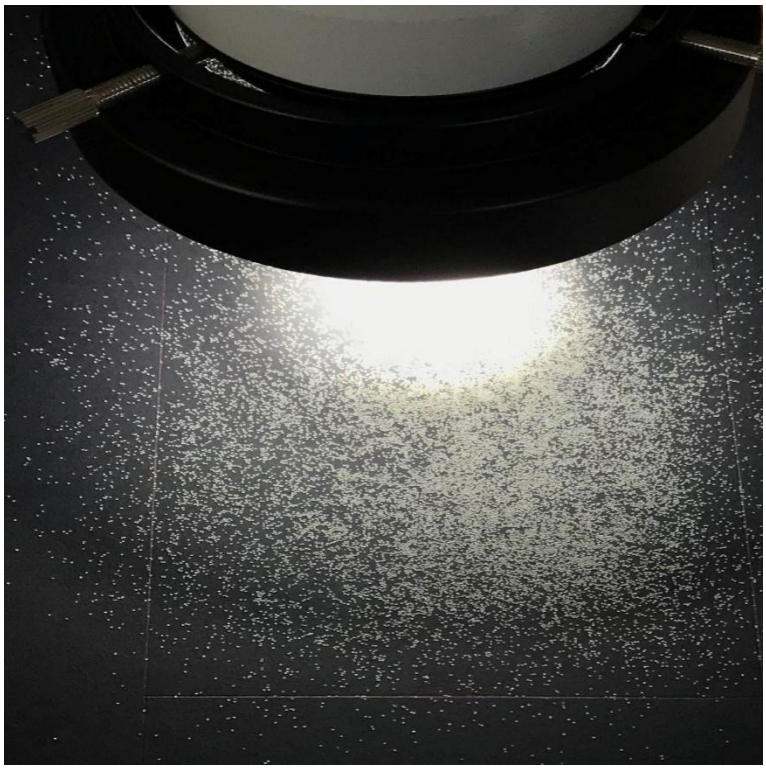

Figure 50.-Proppant sample spread on a black surface paper

5. Using the squares on the millimeter paper as a guide, carefully, move the black paper, without moving the particles on it, from one rectangle to another and then take a picture of the particles.
6. Repeat step 5 until cover all the rectangles in all the rows and columns. Doing so, all the surfaces where the particles are spread will be covered (see **Figure 51**).
7. Save the pictures in a unique folder for every sample measured.
8. Use the Fiji-Image G code to process and quantify the sand proppant concentration in the sample.

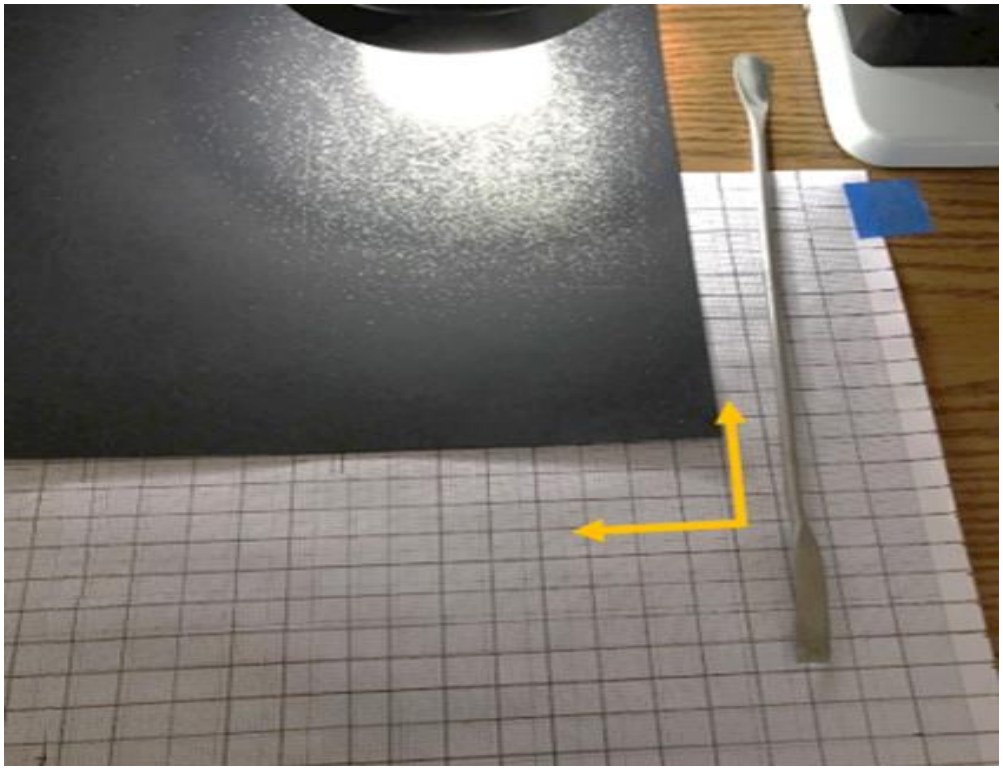

Figure 51.-Squares on the paper used as a guide to cover the entire area of black paper while taking pictures of every square area

3.3.3.3. Fiji Image-G code.

A general procedure was developed to quantify the area of the sand proppant particles in the sample:

1. Run split channels to separate the picture into the three main channels: red, green, and blue.
2. Blue channel is selected to quantify only sand proppant.
3. The threshold is adjusted for only sand proppant particles.
4. Fill holes are run.
5. Eroded particles.
6. Watershed is run to separated particles.
7. Measure particles are run and the obtained area is saved.
8. Measure the weight of the amount of sample used to calculate the area in step 8.
9. Correlate the area obtained in step 8 with the weight of the sample measured in step 9.

The macro used to automatize the sand proppant particles area measurements is as follows:

```
//run("Brightness/Contrast...");
run("Enhance Contrast", "saturated=0.35");
run("Split Channels");
//run("Brightness/Contrast...");
run("Apply LUT");
```

```
setAutoThreshold("Default dark");
//run("Threshold...");
//setThreshold(253, 253);
setOption("BlackBackground", false);
call("ij.plugin.frame.ThresholdAdjuster.setMode", "Over/Under");
setAutoThreshold("Default dark");
//setThreshold(129, 255);
run("Convert to Mask");
run("Convert to Mask");
run("Erode");
run("Fill Holes");
run("Watershed");
run("Set Measurements...", "area mean standard modal min centroid center perimeter bounding fit shape feret's integrated median skewness kurtosis area_fraction stack limit display redirect=None decimal=4");
run("Analyze Particles...", "size=250-Infinity circularity=0.60-1.00 show=[Overlay Masks] display summarize in_situ");
```

The threshold was adjusted when drilled cuttings from different depths were used. This depends on the mineral concentration of the rock drill cuttings.

The procedure to run the Fiji Image-G software is presented below:

1. Download the Fiji Image-G software. This is free software and can be downloaded from: https://imagej.net/Fiji/Download.
2. Open the software.

3. Run the macro, go to Process, next to Batch, and finally clink on Macro (see **Figure 52**).
4. On the window displayed, the input box refers to the folder where the pictures are saved (see **Figure 53**).
5. The output box will be the folder where the picture results will be saved.
6. Paste the code in the white empty box.
7. Click on Run to execute the code.
8. A window called “summary” will display the results of the measured area of the proppant particles.

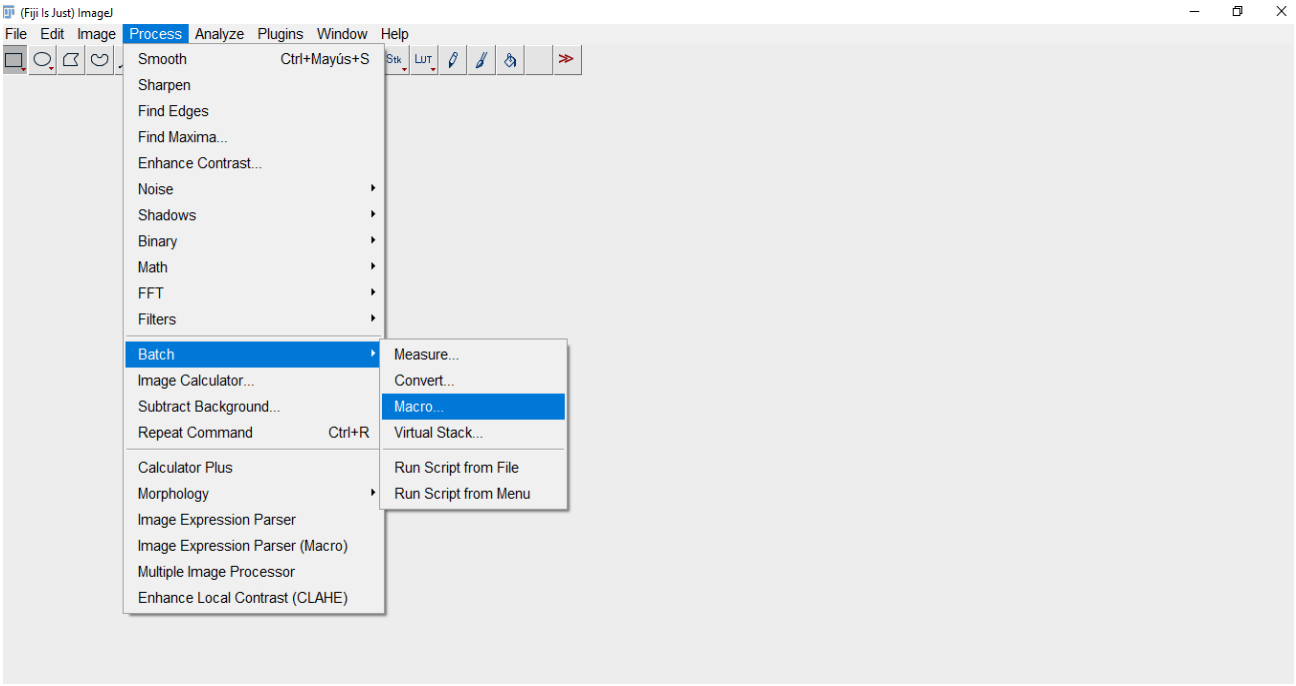

Figure 52.-Fiji Image-G: running a macro. Step 1

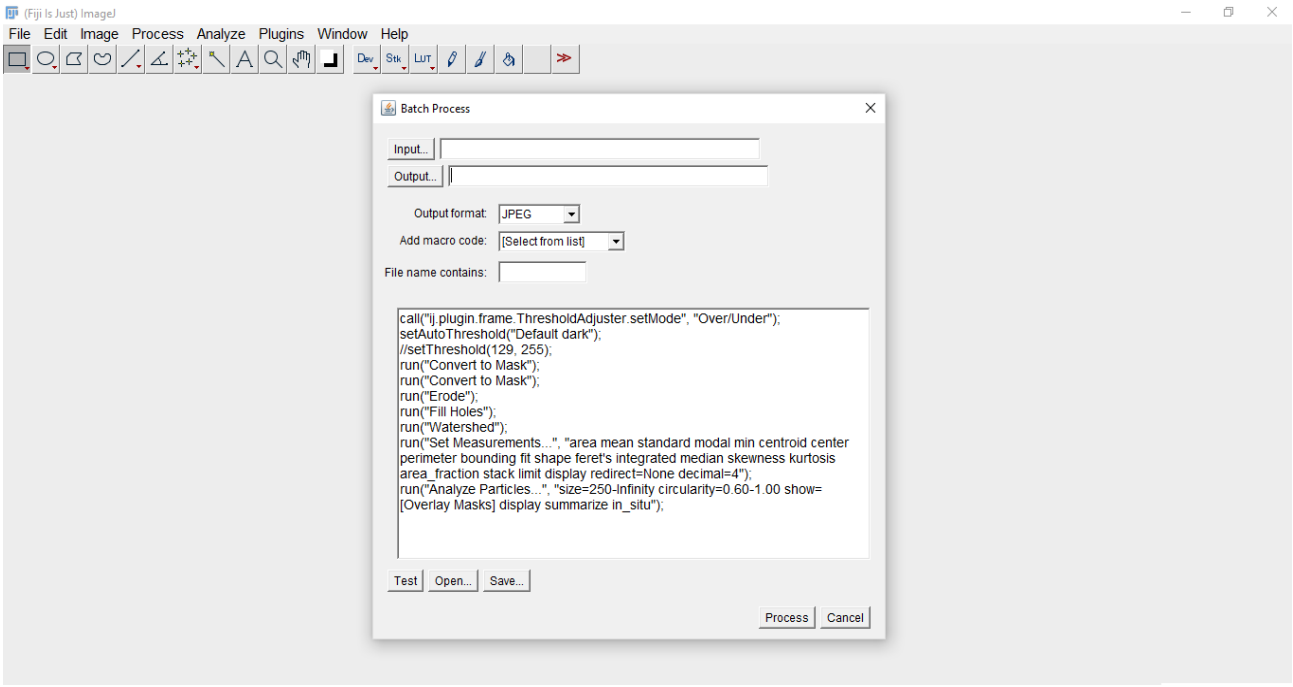

Figure 53.-Fiji Image-G: running a macro. Step 2

3.3.3.4. Sand proppant calculations.

Using the sand proppant measurement procedure, get a correlation of the measured area of sand proppant versus the mass of the 40/70-mesh or 100-mesh sand proppant. The above procedure should be followed:

1. Take sand proppant samples between 0.0300 gr and 0.2000 gr.
2. Using the “sand proppant measurements” procedure, take pictures of the area where the particles are spread.
3. Repeat every measurement three times to obtain the deviation standard of the measurements.
4. Using the “Fiji Image-G code”, quantify the total area of every sample of sand proppant.

5. Correlate the mass of every sample to its measured area.
6. The correlation obtained will be used to quantify the amount of sand proppant in every sample of a mixture of drill cuttings and sand proppant.

The concentration of sand proppant in a drill cutting mixture is determined as follow:

1. Weight between 0.2000 and 2.0000 grams of drilled cutting mixture samples.
2. Using the “sand proppant measurements” procedure, take pictures of the area where the particles are spread.
3. Using the “Fiji Image-G code”, quantify the total area of the sand proppant particles in every sample.
4. Using the correlation of mass of sand proppant to its measured area the sand proppant concentration in the sample can be determined.
5. The sand proppant concentration in the whole sample, this is, before the sample is divided into 4 different groups in “Sampling Preparation”, step 7, can be obtained by a mass balance.

3.4. Results.

The results reported here correspond to synthetic drill cuttings samples, prepared using the lower Eagle Ford drill cuttings from the well “Gus Tips Runge 1-D3H”.

3.4.1. Field sampling.

Theoretical drilling parameters were assumed to calculate the proppant concentration in the hydraulic fractures and determine the number of samples. The lateral length completion corresponds to the lateral wellbore of the legacy well. The values are shown in **Table 2**.

INPUTS		
Parameters	**Symbol**	**Value**
Rate of Penetration, ft/h	ROP	138
Circulation Rate, gpm	CR	300
Hole Size, in	D	6
Lateral Length Completion, ft	L	7000
Rock Porosity	Φ_R	0.05
Rock Density, gr/mL	ρ_R	2.71
Sand Proppant 30/50-mesh (average values)		
Porosity	Φ_S	0.2
Sand density, gr/mL	ρ_S	2.65
Proppand Pack Density, g/mL	ρ_{PP}	2.21
Fracture Width, in	W	0.2

Table 2.-Theoretical drilling inputs parameters

The **Table 3** presents the sampling parameters calculated for a sampling interval distance of 20 ft and a sample length of 10 ft.

Calculations		
Parameter	**Calculation**	**Value**
Drilling time, min/ft	(1/ROP)*60	0.4
Volume of Mud Circulated, gal/ft	CR/(ROP/60)	130.4
Proppant mass, Kg	$(1- \Phi_S)*\pi*D^2/4*W*0.01639$	0.20
Sampling		
Sampling interval distance (SID), ft	-	20
Sample Length (SL), ft	-	10
Total number of samples	L/SID	350
Sampling time, min	(1/ROP)*60*SL	4.3
Time between samples, min	SID/ROP*60	9
Cuttings volume, gal/min	$(1-\Phi_R)*D^2*ROP/0.41$	3.2
Cuttings mass, Kg/min	$(1-\Phi_R)*D^2*ROP*\rho_R*0.0026$	32.9
Proppant Concentration, w%	proppant mass/(proppant mass+sampling time*cuttings mass)*100	**0.1369**
Mud volume circulated per sample, Gal	Volume of Mud Circulated*SL	1304

Table 3.-Sampling parameters calculated

The theoretical sand proppant concentration in the drill cuttings and the sampling time as a function of the sample length are shown in **Figure 54**.

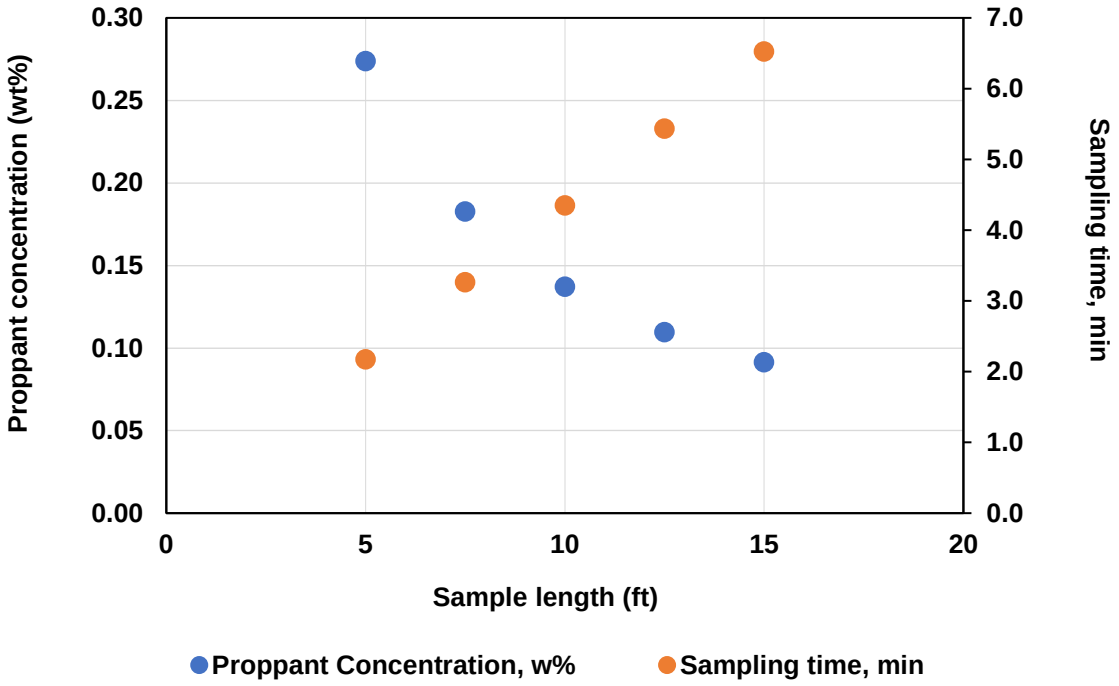

Figure 54.-Calculated proppant concentration and sampling time as a function of sample length

The theoretical sand proppant concentration in the drill cuttings varies from 0.274 to 0.091 wt%, for sample length from 5 to 15 ft, respectively. The calculated total mass of drill cuttings is 72 kg for 5 ft sample length, and 215 kg for 15 ft sample length.

3.4.2. Sand proppant concentration measurements in drill cuttings.

Two calibration curves, one for sand particles 40/70 mesh size and another one for 100 mesh size, were prepared to quantify sand proppant in synthetic drill cuttings samples. The sand proppant quantification was done using samples of known sand concentration to test the method, and blind samples to test the validity of the measurements.

3.4.2.1. Calibration curve of 40/70 mesh sand proppant.

A calibration curve of mass of sand proppant 40/70-mesh vs total area measured under the microscopy was built, obtaining a square coefficient of correlation larger than 0.99 (see **Figure 55**). The largest standard deviation obtained in the measurements was 0.033.

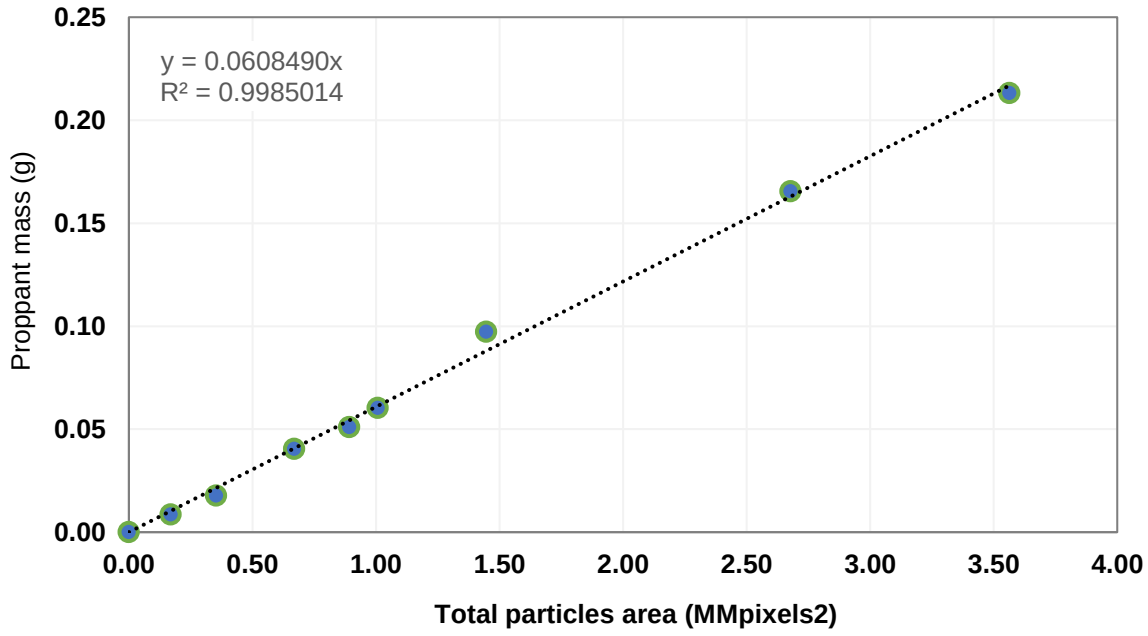

Figure 55.-Calibration curve: mass of 40/70 mesh sand vs total area

3.4.2.2. Quantification of sand proppant 40/70 mesh in drill cuttings.

Samples of known sand proppant concentration (to test the method) are shown as red marks, while the blind samples (used to test the validity of the measurement process) are shown as blue marks in **Figure 56**. The error bars denote the standard deviations obtained.

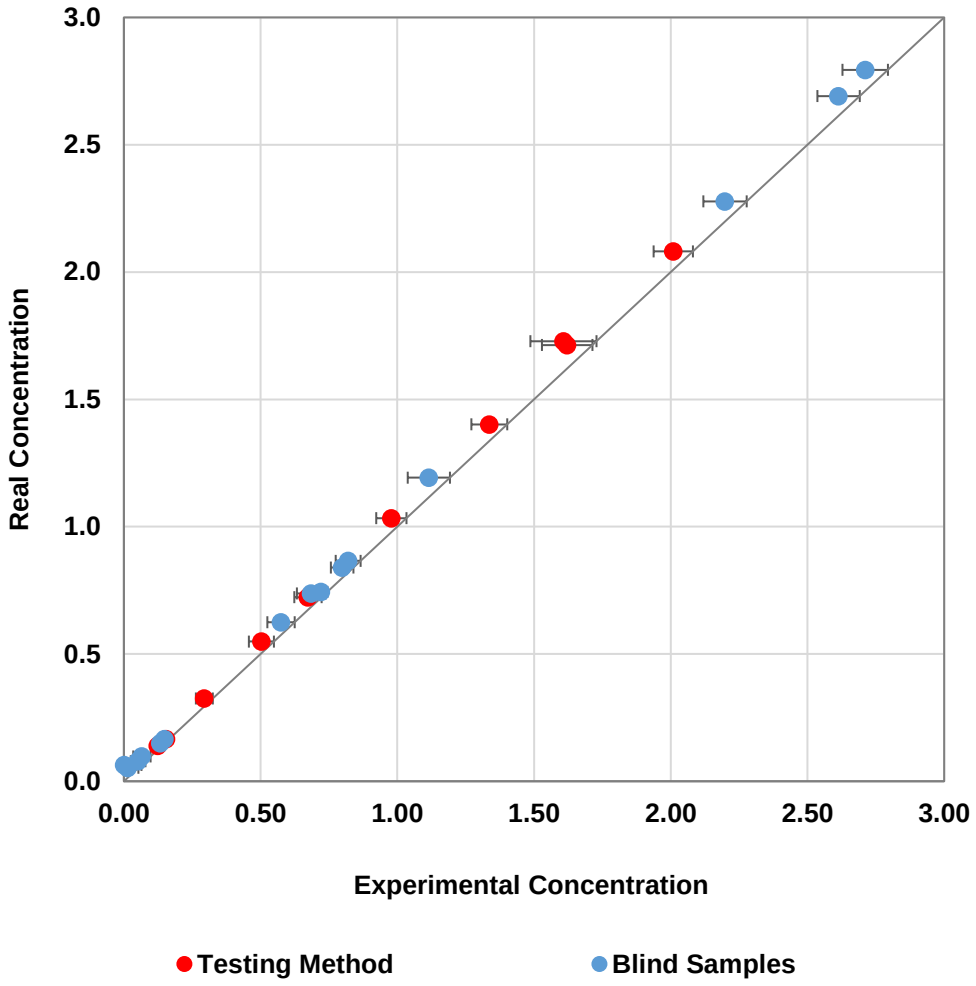

Figure 56.-Measuring of 40/70-mesh sand proppant concentration in drill cuttings samples

The biggest issue found was to get the synthetic sample mixtures (sand proppant-drill cuttings) homogeneously mixed, especially for the smallest sand proppant concentrations. The lower the sand proppant concentration the larger the relative errors.

3.4.2.3. Calibration curve of 100 mesh sand proppant.

To quantify smaller sand proppant particles, like 100 mesh sand particles pumped during a hydraulic fracturing operation or those produced as a result of crushing of the 40/70 mesh sand particles, the microscope magnification was adjusted to test proppant 100 mesh.

A calibration curve of mass of sand proppant 100-mesh vs total area measured under the microscopy was built, obtaining a square coefficient of correlation larger than 0.99 (see **Figure 57**). The largest standard deviation obtained in the measurements was 0.086.

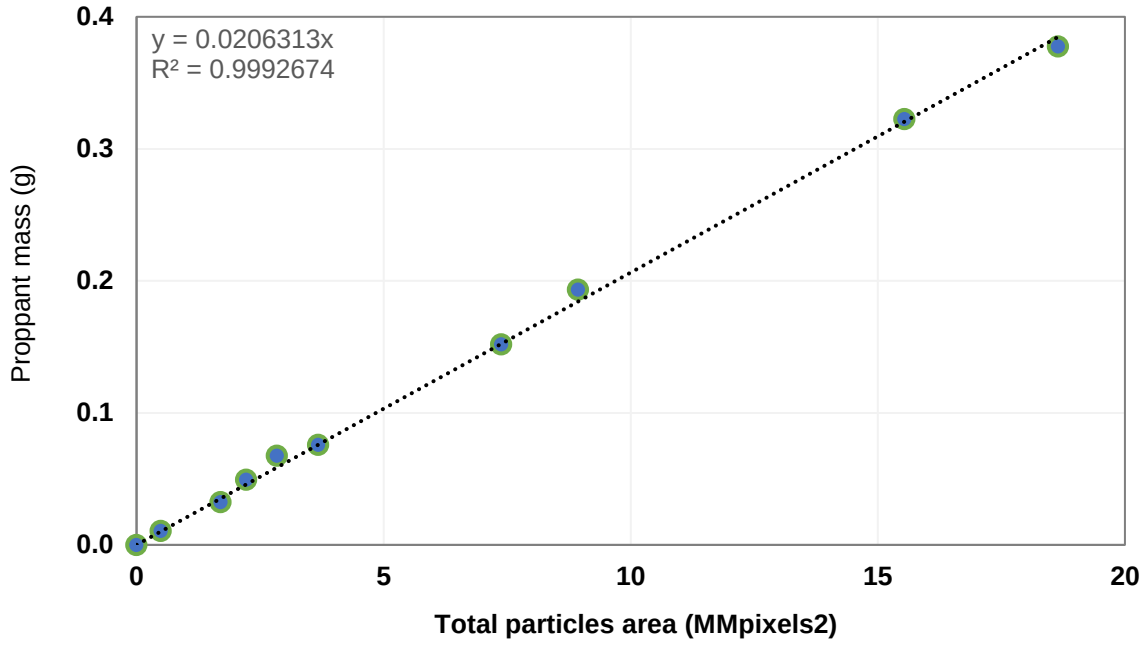

Figure 57.-Calibration curve: 100-mesh mass sand proppant vs total area

3.4.2.4. Quantification of sand proppant 100 mesh in drill cuttings.

Samples of known sand proppant concentration (to test the method) are shown as red marks, while the blind samples (used to test the validity of the measurement process) are shown as blue marks in **Figure 58**. The error bars denote the standard deviations obtained.

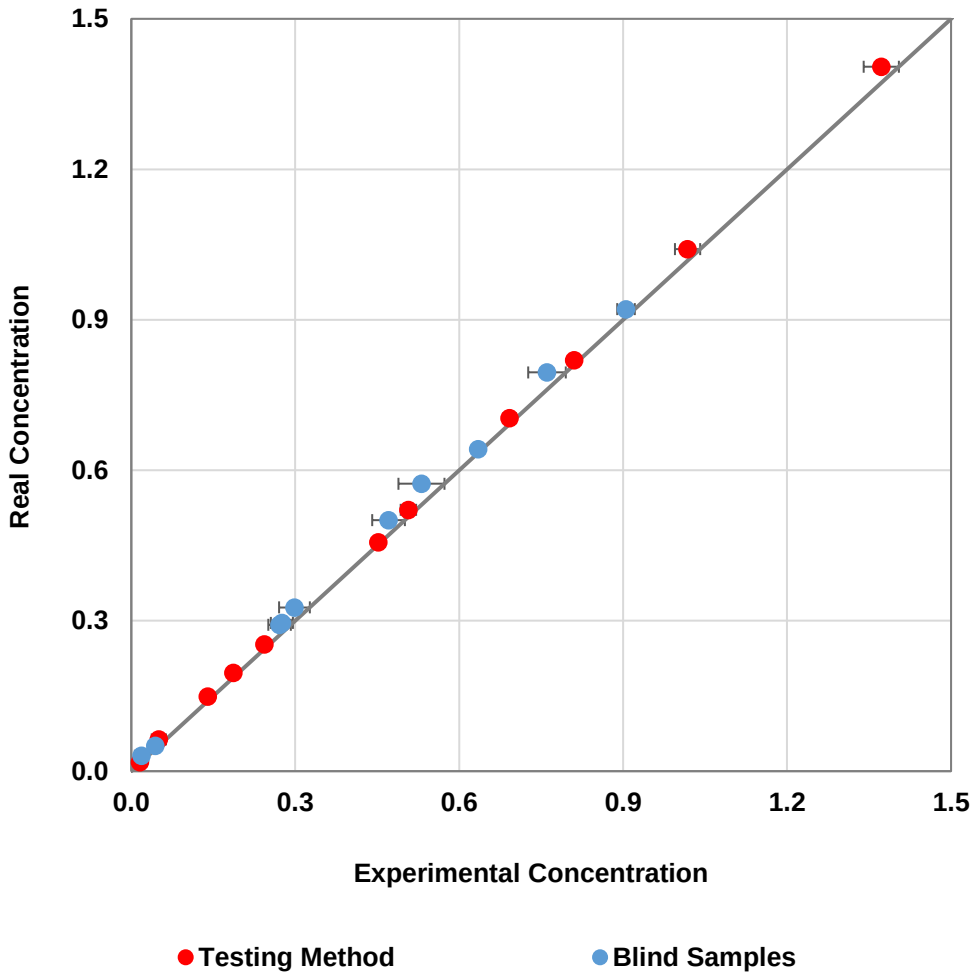

Figure 58.-Measuring of 100-mesh sand proppant concentration in drill cuttings samples

The biggest issue found was to get the synthetic sample mixtures (sand proppant-drill cuttings) homogeneously mixed, especially for the smallest sand proppant concentrations. As a result, variation in relative error results was obtained, ranging between 0 – 10% for larger sand proppant concentrations, and between 11 - 30 % for concentrations smaller to 0.1 wt%.

3.5. Analysis of results.

The physical properties of the sand proppant on the concentration measurements in drill cuttings, and the detection limit in the sand proppant 40/70 and 100 mesh was analyzed.

3.5.1. Sand proppant quality effect on concentration measurements in drill cuttings.

White sand, also known as silica sand, was the sand proppant used to complete the legacy well and used in this research. Sand is mainly made up of silicon and oxygen atoms bonded covalently in a tetrahedral crystal structure (Bernadis, S. 2005) to form silicon dioxide -SiO_2. **Figure 59** shows the chemical structure of SiO2, with silicon as grey marks, and oxygen in red.

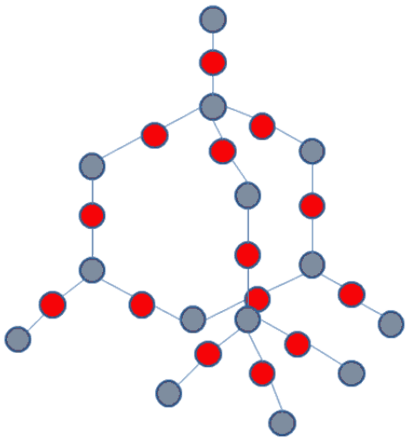

Figure 59.-Chemical crystalline structure arrangement of SIO_2 (Reprinted from Godino, 2013)

To consider sand as silica sand, the material must contain at least 95% SiO_2 and less than 0.6% iron oxide. If the sand does not meet this criterion, it will be classified as what is often called ‘regular’ sand. Regular sand, also known as feldspathic sand, or brown sand, will always contain some silica, but only in amounts less than 95%, along with varying amounts of iron, carbonate, potassium, and other trace elements and/or minerals which can occupy the silicon positions in its crystal structure, affecting its physical-chemical properties. These ‘impurities’ make regular sand more chemically reactive and often darker in color when compared to silica sand (Bernadis, S. 2005). Some of those darker sand particles were found in the sand proppants used in this research, and are highlighted with green circles in **Figure 60**.

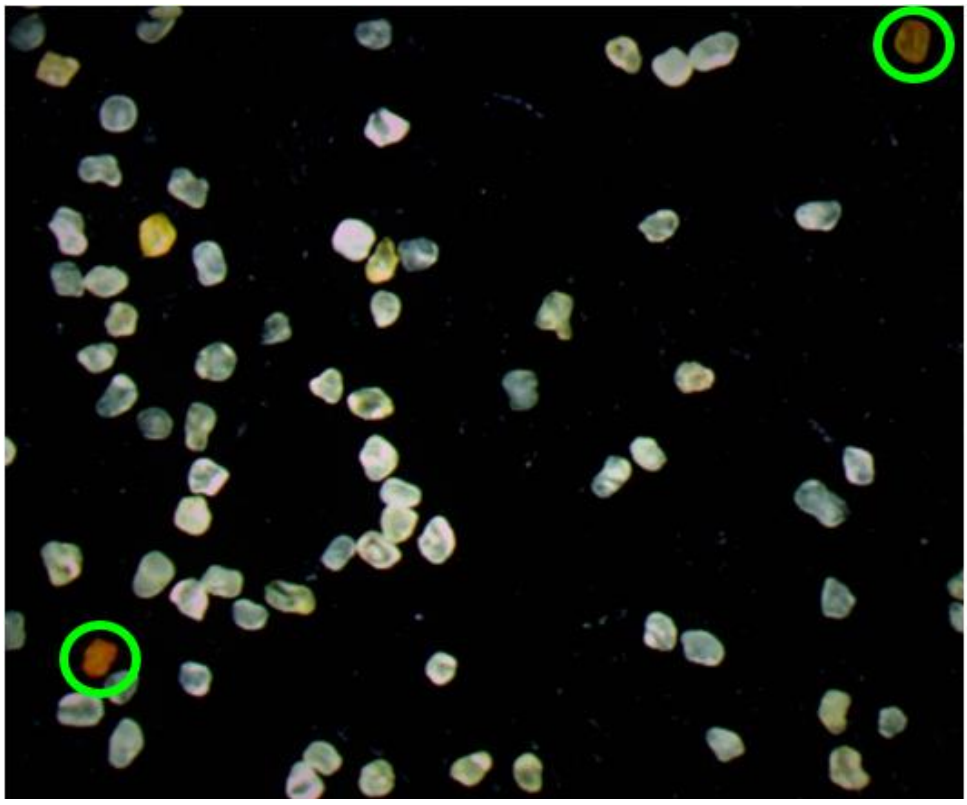

Figure 60.-Sand proppant 40/70 mesh

The presence of those darker particles in the sand proppant, because of impurities in the crystalline system of the sand, makes that they absorb more of the visible light spectrum, compared to silica sand particles, because of the valence electrons in the crystalline system change. As a result, the measured sand proppant concentration was always lower than the real concentration.

Light absorption is a function of the chemical composition of the system since every chemical element has its specific wavelength absorption.

3.5.2. Detection limit for 40/70 mesh sand proppant in drill cuttings.

The detection limit was found at a sand proppant concentration of 0.14 wt%, with a relative error margin lower than 10%, defined as the ratio of the absolute error (difference between the measured value and actual value) to the actual value. For lower concentrations, as expected, the relative error increases. Concentrations between 0.14 and 0.08 wt% produced relative errors between 11 and 35%. Concentrations as low as 0.06 wt% could not be detected. **Figure 61** presents the results obtained. The green circle marks, enclosing the results of the blind samples, corresponding to the measurement with a relative error larger than 10%, and the dashed line represents the detection limit.

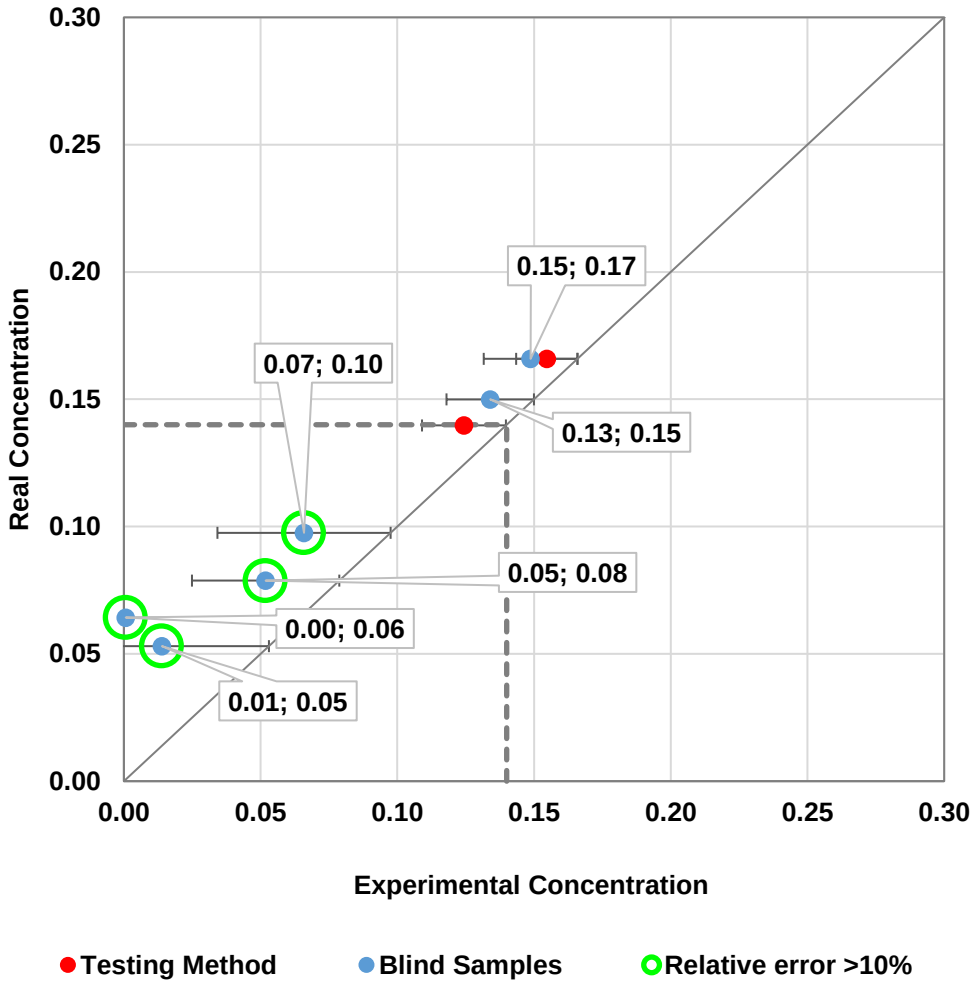

Figure 61.-40/70-mesh sand proppant concentration in drill cuttings samples (zoom-in)

3.5.3. Detection limit for 100 mesh sand proppant in drill cuttings.

A larger magnification was required, as the particle sizes were smaller, to capture the features of the particles and to measure their area. By increasing the magnification, the sensitivity of the method was improved. Sand concentrations as low as 0.02 wt% were detected with a relative error of 39%. The concentration of 0.06 wt% was measured with a 20% relative error.

Concentrations above 0.09 wt% were measured with relative errors lower than 10%. The 0.09 wt% concentration was defined as the detection limit, based on the relative error result. **Figure 62** illustrates the results obtained. The red and blue marks are the samples used to test the method and the blind samples, respectively. The green circles highlight the results with relative errors larger than 10%. The dashed line denotes the detection limit for proppant 100 mesh concentration.

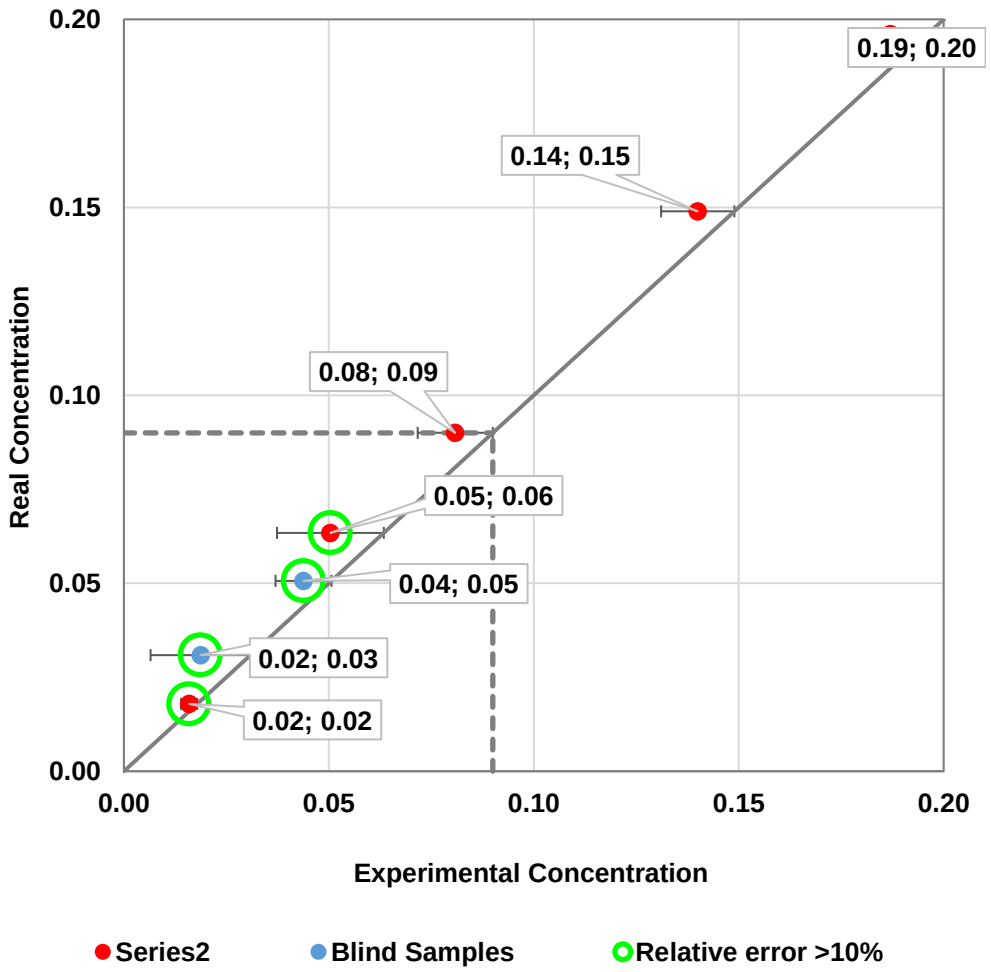

Figure 62.-100-mesh sand proppant concentration in drill cuttings samples (zoom-in)

3.6. Field application.

The detection limits for sands 40/70 and 100 mesh quantification in drill cuttings correspond to a fraction of the total drill cuttings sample. This means that the sand concentration detection limit is smaller when considering the whole sample size distribution.

The Eagle Ford drill cuttings particles 40/70 mesh were found to be on average around 20 wt% of the whole sample. Extrapolating the detection limit obtained to the whole sample, the detection limit for the 40/70 sand is 0.028 wt %. This value is smaller than the theoretical sand proppant 40/70 mesh concentration in the hydraulic fractures, which is equal to 0.14 wt% for a fracture width of 0.2 inches and a sample length of 10 ft.

The Eagle Ford drill cuttings particles 70/170 mesh were found to be on average around 20 wt% of the whole sample. Extrapolating the detection limit obtained for the 100 mesh sand proppant quantification to the whole sample, this value is 0.018 wt %. This methodology would be effective to quantify the sand proppant in the drill cuttings if the well would be completed using only sand 100 mesh. However, if this methodology would be used to quantify the crushing of the sand proppant 40/70 mesh, this methodology would be effective only for crushing larger than 15 wt%.

The results reported in this chapter are applicable for white sand proppants, where the physical phenomenon evaluated was light absorption/transmission in the sand proppant particles. Other proppants have different physical optical properties, and adjustments in the RGB microscope and Fiji code will be necessary. For example, resin-coated proppants, different from sand particles, tend to reflect more of the visible light spectrum. The specific wavelengths reflected will depend on the chemical composition of the resin.

A statistical sampling method in the field should be followed to decrease the uncertainty in the sand proppant concentration in the drill cuttings. Assuming a sample length of 10 ft, with a rate of penetration of 138 ft/h and a hole size of 6 ft, approximately 143 kilograms of drill cuttings would be obtained per sample, and theoretically sand proppant concentration in the drill cuttings would be 0.14 wt%. Samples of 200-500 grams are normally sampling in the field, which represents a low fraction of the total drill cuttings produced when drilling a well. A statistical sampling method can help avoid a large standard deviation from the sand proppant concentration in the drill cuttings. **Figure 63** to **Figure 65** exhibit how the sand proppant concentration deviates from the theoretical concertation in a form of a t-score distribution probability chart.

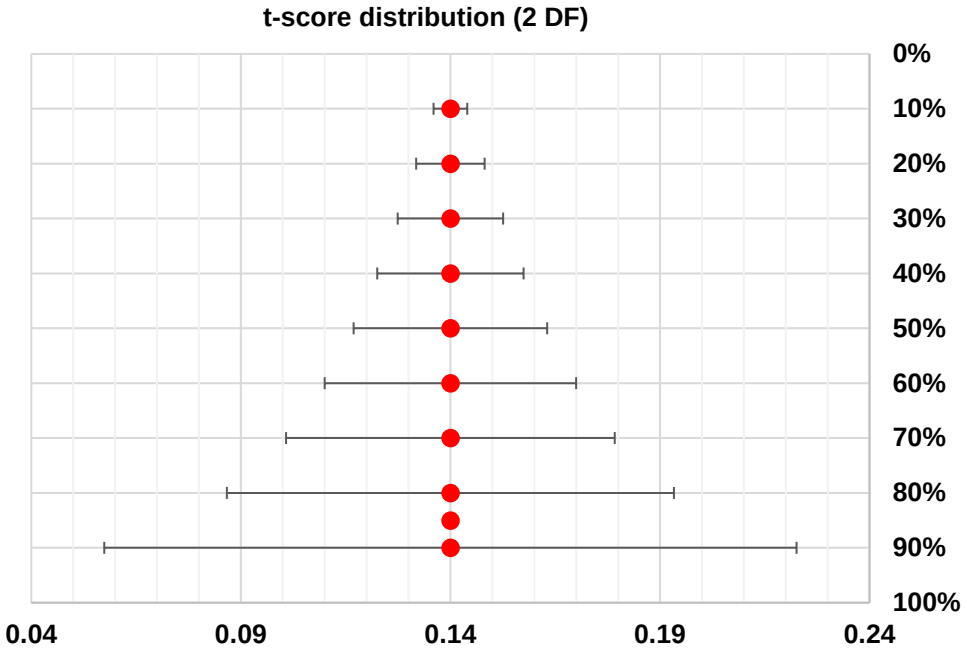

Figure 63.-t-score distribution for 2 degrees of freedom

When only two degrees of freedom are considered, a large deviation from the theoretical proppant concentration is got for a 90% of probability (Figure 57). However, Figure 58 shows that by increasing the degrees of freedom to 5 the sand proppant distribution for a 90% probability shows a lower deviation from the theoretical concertation (+/- 0.038).

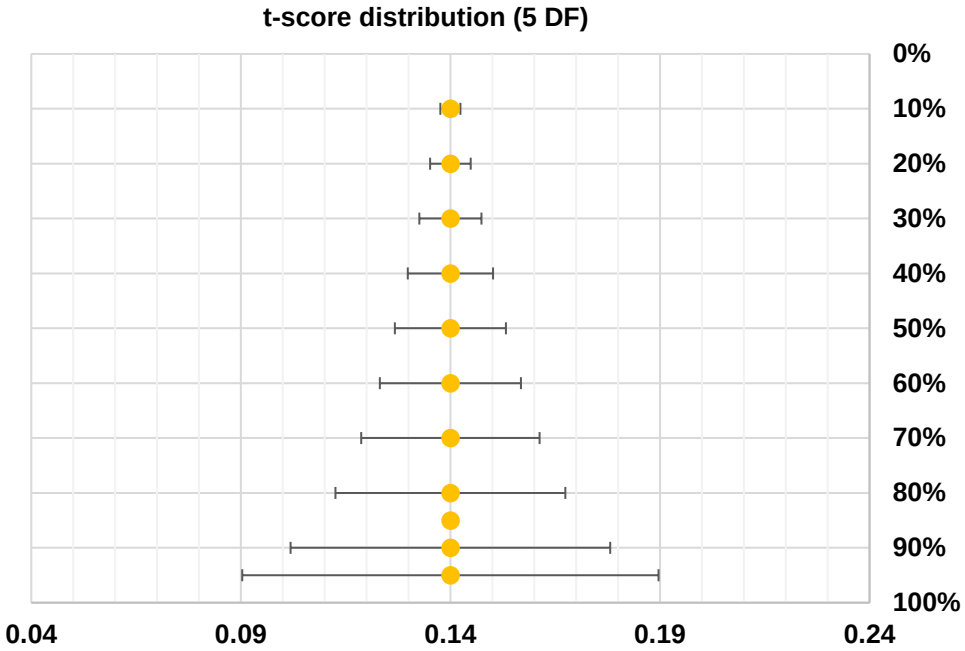

Figure 64.-t-score distribution for 5 degrees of freedom

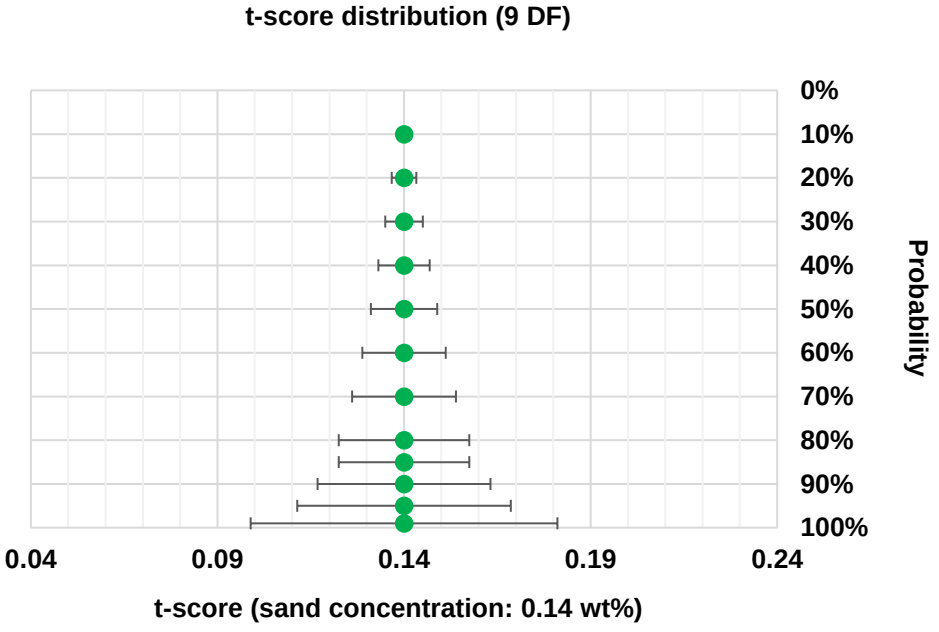

Figure 65.-t-score distribution for 9 degrees of freedom

When 10 degrees of freedom are evaluated, the deviation from the theoretical concentration for 90% of probability is +/- 0.024. These results show that a well-planned and organized sampling method needs to be followed in the field to reduce the uncertainty in the sand proppant concentration in the drill cuttings.

By increasing the number of sub-samples the t-score distribution decreases, which is highly recommended.

3.7. Conclusions.

The drill cuttings sample length, or sampling time, must be carefully registered in the field since sand proppant concentration in the drill cuttings is depending on the amount of drill cuttings sampled.

The sand proppant concentration measurements were always lower than the real value. This was caused by impurities present in the sand proppants utilized in this study which are the result of the substitution of silicon in the crystal structure of the silicon dioxide. Those impurities cause the crystals have a different electron valence number, changing the light absorption wavelength of the visible spectrum.

The detection limit for sand proppant 40/70 mesh quantification was 0.028 wt%, and for sand proppant 100 mesh was 0.018 wt%. These values are smaller than the theoretical sand proppant concentration in the hydraulic fractures, which was 0.14 wt% for a fracture width of 0.2 inches and a sample length of 10 ft.

The sensitivity of the method was improved when using larger microscopy magnification to quantify sand particles 100 mesh. Concentrations as low as 0.01 wt% were identified with a relative error of 14%.

The methodology to quantify sand particles 100 mesh can be used to quantify the crushing of sand particles 40/70 mesh for crushing larger than 15 wt%.

The proppant quantification results presented in this study are applicable to white sand proppants, as the physical phenomenon evaluated was light absorption/transmission by the silicon dioxide system. The same methodology can be applied to other types of proppants by adjusting the light configuration parameters in the microscope and Fiji code, according to the characteristic wavelength light absorption of the proppant material or resin-coated material.

A well-planned and organized drill cuttings sampling method needs to be followed in the field to reduce the uncertainty in the sand proppant concentration in the drill cuttings. By increasing the number of sub-samples of drill cuttings, the t-score distribution decreases, decreasing the uncertainty in the results.

4. HYDRAULIC FRACTURING SIMULATIONS

StimPlan™ V8, from NSI Technologies, LLC, a commercial hydraulic fracturing simulator, was used to simulate the hydraulic fractures in the well Klattenhoffunitlas-1H, called in this research the legacy well. The main objective was to get a simulated extent of the proppant in the hydraulic fractures after the legacy well was completed.

4.1. Introduction.

Modeling hydraulic fracturing is challenging since a variety of physical processes are involved. These include fracture propagation and inflation, fluid flow within the fracture, proppant transport and settling, followed by fracture deflation, closure, and proppant capture. These processes may be represented by making appropriate simplifying assumptions in the analysis. For the fracture propagation and fluid flow within it, it is typical to include simplification of the fracture geometry as a plane form, treating the inflating fluid as Newtonian, and assuming flow to be laminar. Various models follow this formalism to approximately define the development of fracture geometry, among which the PKN and KGD models are the most popular (Wang and Elsworth, 2019).

Understanding proppant transport plays a critical role in estimating propped fracture dimensions (Kou, et al., 2018). Proppant transport is a very complicated multi stage process, in which the effective transport of proppant in fractures has a dominant effect on well productivity. The proppant placement in the fractures largely

determines the productivity of the well because it affects the fracture conductivity. (Kim et al., 2021).

In this study, the hydraulic fractures in the legacy well were simulated by using as input; the reported information in drillinginfo (www.enverus.com), such as the well trajectory, a high viscosity guar-borate cross-linked fracturing fluid volume and the proppant mass pumped. The geomechanical model was built by using the literature reports for wells close to the legacy well. The geomechanical model and the perforation design were adjusted by matching the bottom hole injection pressure treatment and micro seismic events reported in the literature for wells close to the legacy well.

4.2. Literature review.

Three of the most common hydraulic fracture geometry models are presented: the KGD model, the PKN model, and the Penny-Shaped or Radial Model.

4.2.1. KGD Model

The KGD model was developed by Khristianovitch and Zheltov (Khristianovitch and Zheltov, 1955) and Geertsma and de Klerk (Geertsma and Klerk, 1969).

Assumptions: 1) flow rate and pressure in the fracture are constant, except for a small region close to the tips, 2) the fracture height is constant and is much greater than fracture length (Khristianovitch and Zheltov, 1955), then 3) the plane

strain is assumed to be in horizontal direction i.e., all horizontal cross-sections act independently, 4) the fracture width does not change along the fracture face and all section are identical, 5) fluid flow and fracture propagation are in one dimension (Xian, 2011) 6) No leak-off (Geertsma and Klerk 1969). **Figure 60** presents an illustration of this model.

4.2.2. PKN Model

Perkins and Kern (Perkins and Kern, 1961) presented a model to calculate the fracture length and width with a fixed height. Later, Nordgren (Nordgren 1972) added to the Perkins and Kern model by adding fluid loss to the calculation. This combination is called the PKN model.

Assumptions: 1) fracture toughness is neglected (Perkins and Kern, 1961) because the energy required for a fracture to propagate is significantly lower than that required for fluid to flow along fracture length 2) the fracture has a constant height, and it is much smaller than the created fracture length which propagates along the horizontal direction (Perkins and Kern, 1961), 3) the plane strain is considered in the vertical direction, and the rock response in each vertical section along the x-direction is assumed to be independent on its neighboring vertical planes 4) the fluid flow problem is considered in one dimension in an elliptical channel and 5) the fluid pressure is assumed to be constant in each vertical cross-section perpendicular to the direction of propagation (Xian, 2011). **Figure 66** presents an illustration of this model.

4.2.3. Penny-Shaped or Radial Model

In this model, the fracture is assumed to propagate within a given plane and the geometry of the fracture is symmetrical with respect to the point at which fluids are injected (Xian, 2011).

Assumptions: 1) vertical distribution of the minimum in-situ stress is uniform, 2) fracture growth follows elliptical shape, 3) no leak-off. Figure 60 presents an illustration of this model.

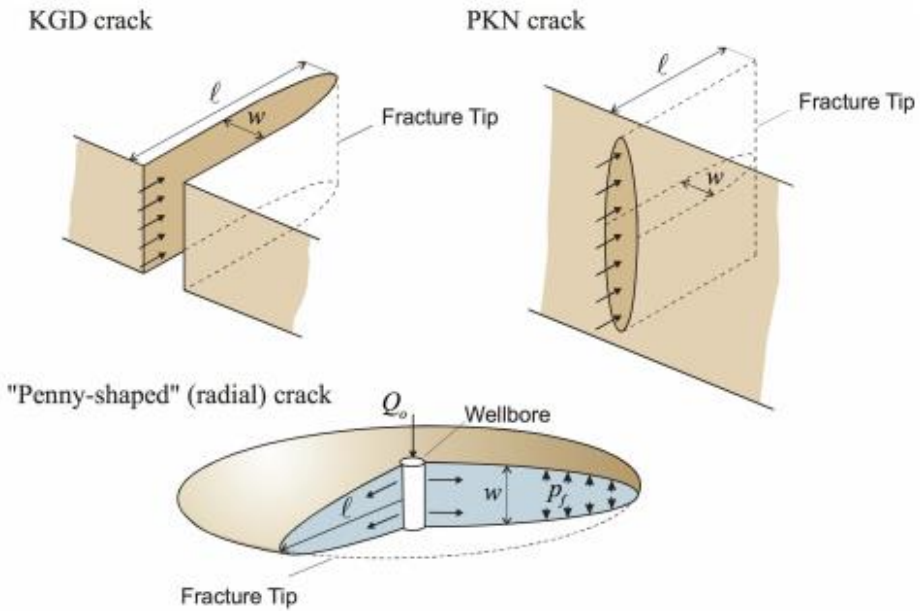

Figure 66.-Schematic representation of the Classical Models for Hydraulic Fracturing: KGD, PKN, and Penny-shaped (Reprinted from Kusmierczyk, 2015)

4.3. Methodology.

The description to run the hydraulic fracturing simulator, as well as the required inputs are presented. Additionally, micro seismic events after hydraulic

fracture operations in a well close to the legacy well, and those used to complete in the well in a similar way to the legacy well, are presented and were used to calibrate the geomechanical model of the legacy well.

4.3.1. Running the hydraulic fracturing simulator.

The procedure to use the software is as follow:

1. Select Advanced Options and High Angle for deviated wells.
2. Click on the Well Data tab.
3. Click on Deviation Data.
4. Select “Separate TVVD/MD data” and “TVD/MD” data.
5. Load/paste the well trajectory.
6. Load the well logs: resistivity, density, and sonic logs, at least.
7. Click on “Perforations” to add clusters/perforations characteristics.
8. Select “Automatic Initiation” and fracture orientation “Transverse”.
9. Add the top and bottom of perforations, type the number of shots/ft, the effective fraction which relates to the number of perforations effectively open, and the perforation diameter.
10. In the “Reservoir” tab, input the wellbore radius, initial and current reservoir pressure, and bottom hole pressure.
11. In the “Geologic Layering” tab, complete the description of all layers to be considered in the simulation.
12. In the “Fluid Data” tab, complete with the characteristics of the fracturing fluid to simulate.

13. In the “Proppant Data” tab, complete the information with the characteristics of the proppant to simulate.
14. Complete the friction data created by the fluid along with the completion by clicking on the tab “Friction Data”.
15. Finally, go to the main menu and click on “Run Frac Simulator”.
16. After the simulation is completed, the output data is displayed.

4.3.2. Input parameters.

Input data from papers SPE-170827-MS (Centurion, 2014), and SPE-170707-MS (Mokhtari, 2014), were used to calibrate the geomechanical model. Reported data in drillinginfo (https://www.enverus.com/) was used for well trajectory, volumes of fracturing fluid, and sand proppant used to complete the legacy well were used as inputs.

4.3.2.1. Building the geomechanical model.

The paper SPE-170827-MS, which corresponds to an Eagle Ford well located at La Salle County, approximately 17.47 miles north-east away from the well legacy well **(Figure 67)**, presents some rock mechanical properties which are illustrated in **Table 4**.

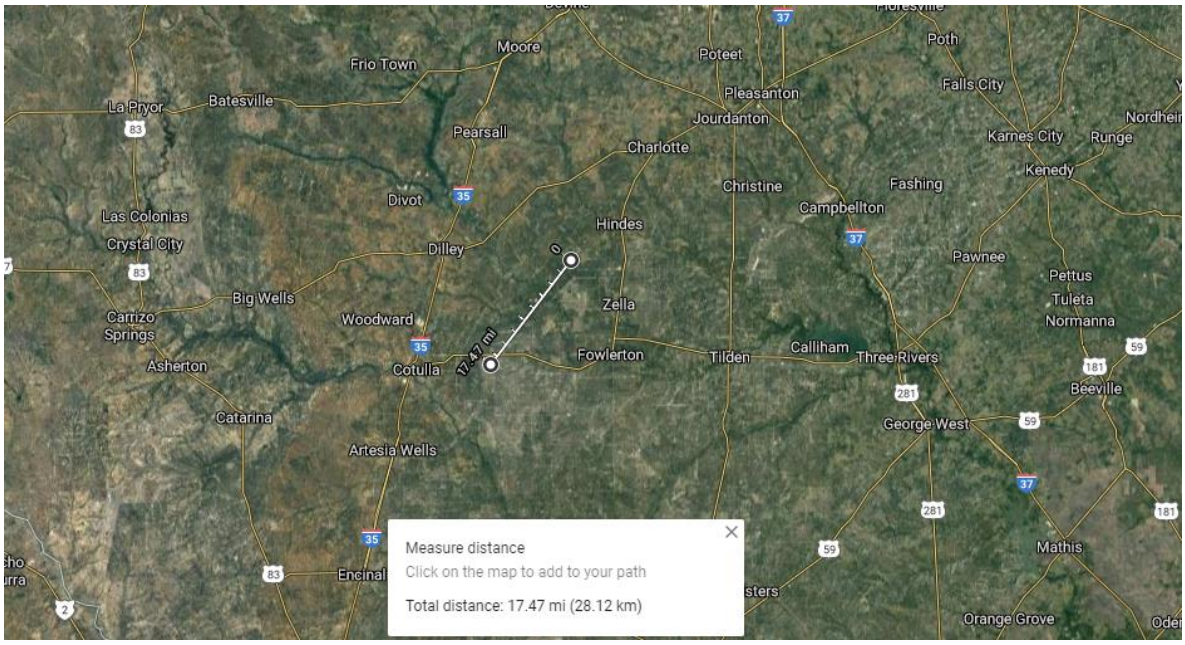

Figure 67.-Well location reported in paper SPE-170827-MS (https://www.google.com/maps)

Formation	TVD at Bottom (ft)	Stress Gradient (psi/ft)	Stress (psi)	Young´s Modulus (psi)*10^6	Poisson´s Ratio	Fracture Toughness (psi-in^1/2)
	9147	0.59	5411	2.4777	0.32	1329
	9200	0.62	5717	3.3711	0.31	1540
	9266	0.65	6065	3.7219	0.31	1572
	9277	0.84	7783	5.0293	0.36	1513
	9367	0.69	6482	5.3244	0.28	1890
Upper Eagle Ford	9407	0.67	6258	4.0652	0.31	1629
Lower Eagle Ford	9519	0.55	5219	2.6641	0.28	1414
	9616	0.96	9246	9.5610	0.29	2293
	9670	0.73	7047	4.3146	0.33	1608

Table 4.-Rock mechanical properties for the Eagle Ford and the adjacent formations

(Reprinted from Centurion, et al., 2014)

Additionally, this paper provides the well profile and the fracture stage locations, which are shown in **Figure 68**. Also, it describes a completion procedure followed in the Eagle Ford by the year 2012, the same year that the legacy well was completed, the fracturing fluid type, volume, and amount of sand proppant used (**see Table 5**), as well as the calculated bottom hole pressure (BHP) during the operation, a plan view, and a side view of the micro seismic events during the hydraulic fracturing operations, which are shown in **Figure 69, Figure 70**, and **Figure 71**, respectively. All this information will be used to match the simulated hydraulic fracturing results.

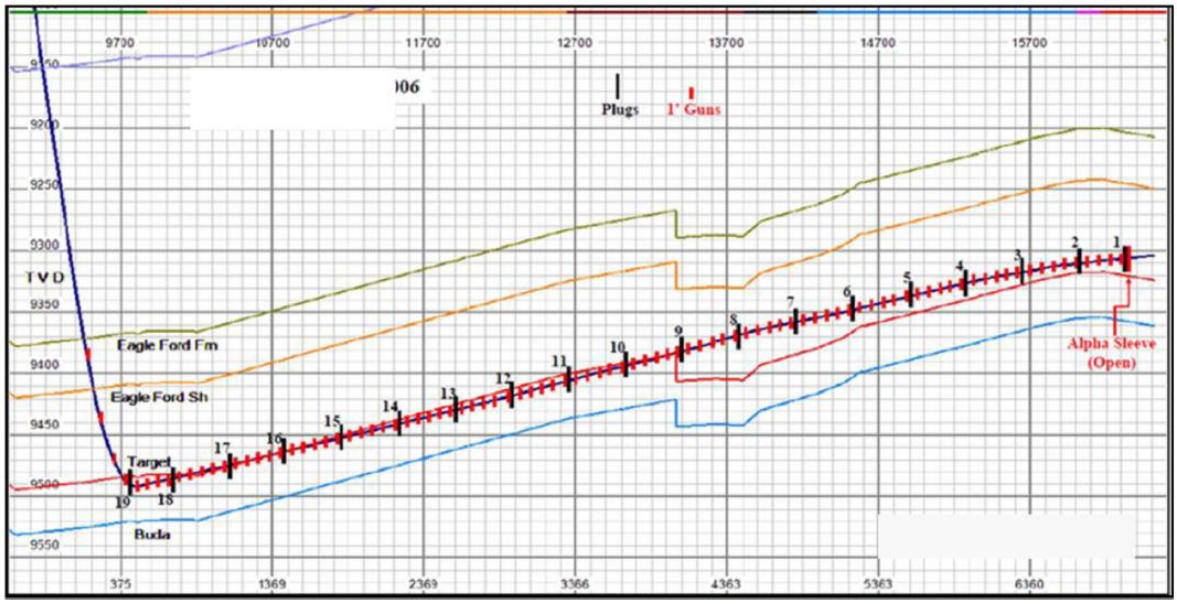

Figure 68.-SPE-170827-MS: well profile and fracture stage locations (Reprinted from Centurion, et al., 2014)

Stage	Slurry Volume (M-Gal)	Fluid volume (M-Gal)	Proppant Conc (PPG)	Rate (BPM)	Proppant (M-Lbs)	Pump Time (min)	Cumulative Time (min)
1	50.00	50.00	0.00	70.00	0.00	17.01	17.01
2	21.00	20.94	1.00	70.00	20.10	7.14	24.15
3	30.00	27.51	2.00	70.00	55.00	10.20	34.35
4	37.70	33.19	3.00	70.00	99.60	12.82	47.17
5	47.60	40.30	4.00	70.00	161.20	16.19	63.36

Table 5.-Downhole pump schedule

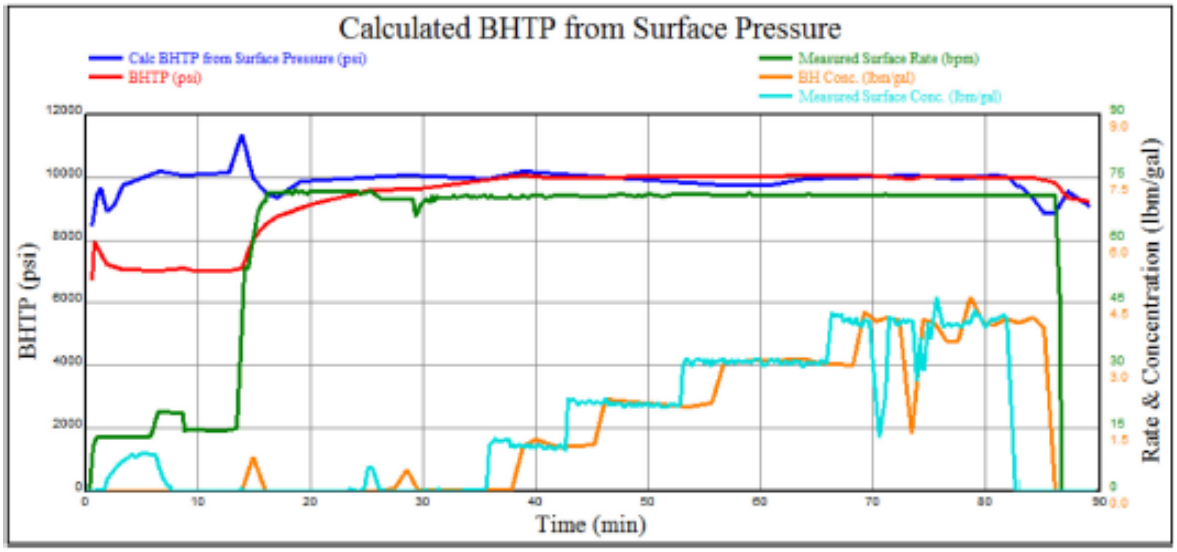

Figure 69.-Hydraulic fracturing bottomhole treating pressure (Reprinted from Centurion, et al., 2014)

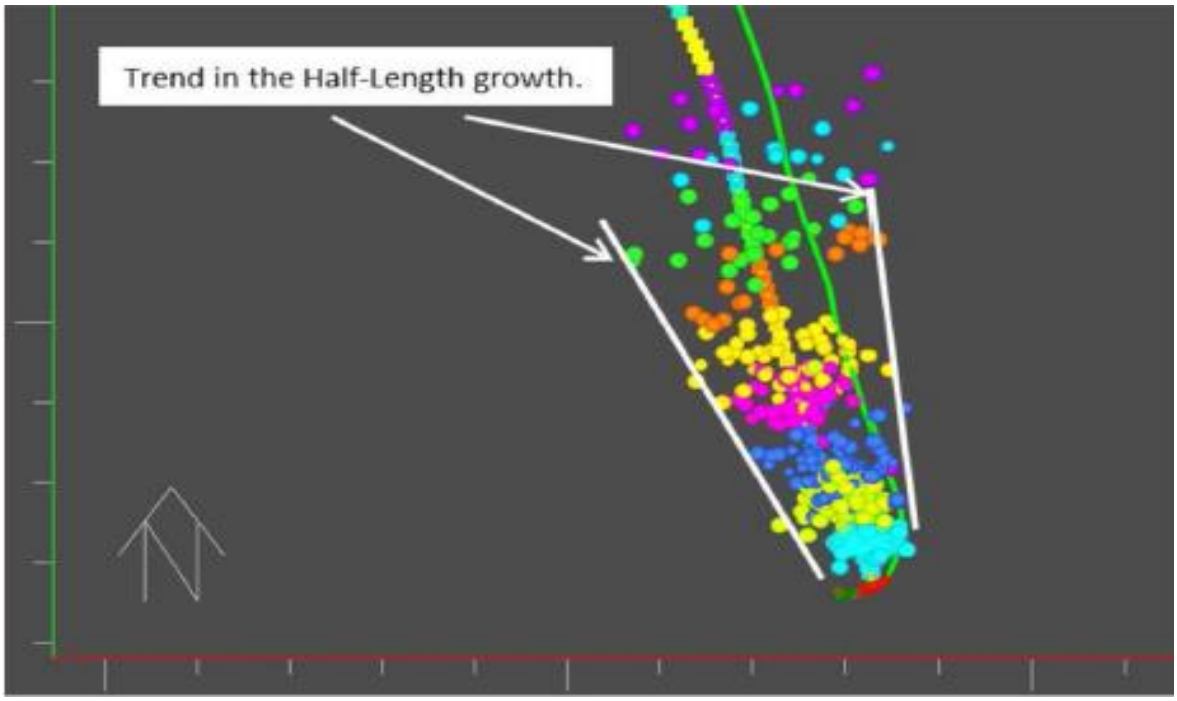

Figure 70.-Plan view of the micro seismic events. (Reprinted from Centurion, et al., 2014)

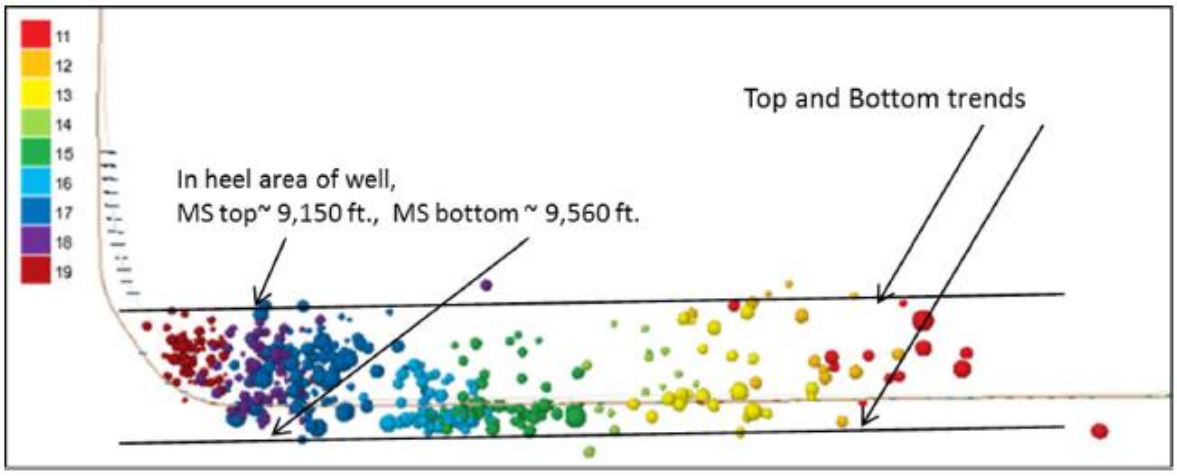

Figure 71.-Side view of the micro seismic events (Reprinted from Centurion, et al., 2014)

Additionally, the well logs presented in the paper SPE-170707-MS (Mokhtari 2014) were digitalized and used later as input in the hydraulic fracturing simulator. These well logs were obtained at a location between 13 – 20 miles away from the legacy well.

The Brown Texas Sand 40/70 mesh, which was the sand used to complete the legacy well, was used to run the simulations. The sand properties are shown in **Table 6**.

Confining Stress (psi)	Conductivity (md-ft)	Propped Width (in)	Beta (1/ft)
1000	5742.5	0.2502	11002.5458
2000	4578.5	0.2502	12302.6978
3000	2966	0.2394	21319.1775
4000	2099	0.2326	32241.2564
5000	1470	0.2268	48238.8335
6000	1071	0.2225	67673.1713

Table 6- Brown Texas Sand 40/70 Mesh (Reprinted from Fernandez 2019)

4.3.2.2. Hydraulic fracturing simulation in the legacy well

Different simulations were run in different zones in the Eagle Ford formation to know the different extents where the proppant could be placed when the legacy well was completed.

The well trajectory, the fracturing fluid volume and proppant mass will correspond to the reported in drillinginfo (https://www.enverus.com/) for the legacy well.

4.4. Results.

The first step was to execute the completion well data required. Different simulations were run to get an appropriate number of perforations per cluster, and its diameter. All other parameters were reported in the paper SPE-170827. The results are shown in **Figure 72**.

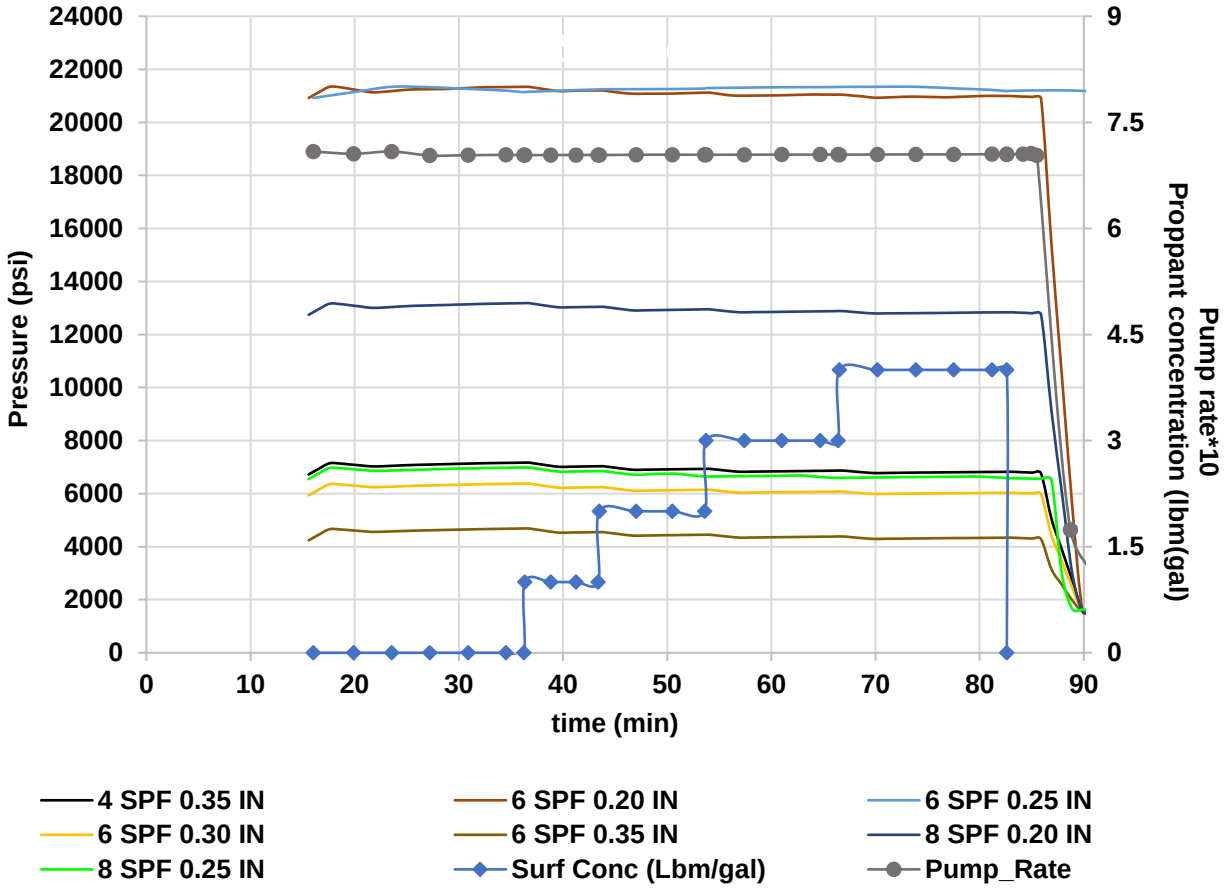

Figure 72.-Sensitivity evaluation for perforations configuration

The configurations, 6 shoots per foot (SPF) / 0.25 in, and 8 SPF / 0.20 in, produced surface pressures during the operation close to the value reported in the paper. 6 SPF / 0.25 in was selected and used in the next simulations.

Different leak-off multipliers were evaluated in the target zone, and above and below this zone. Also, the perforation erosion option in the simulator was considered. **Figure 73** shows the results.

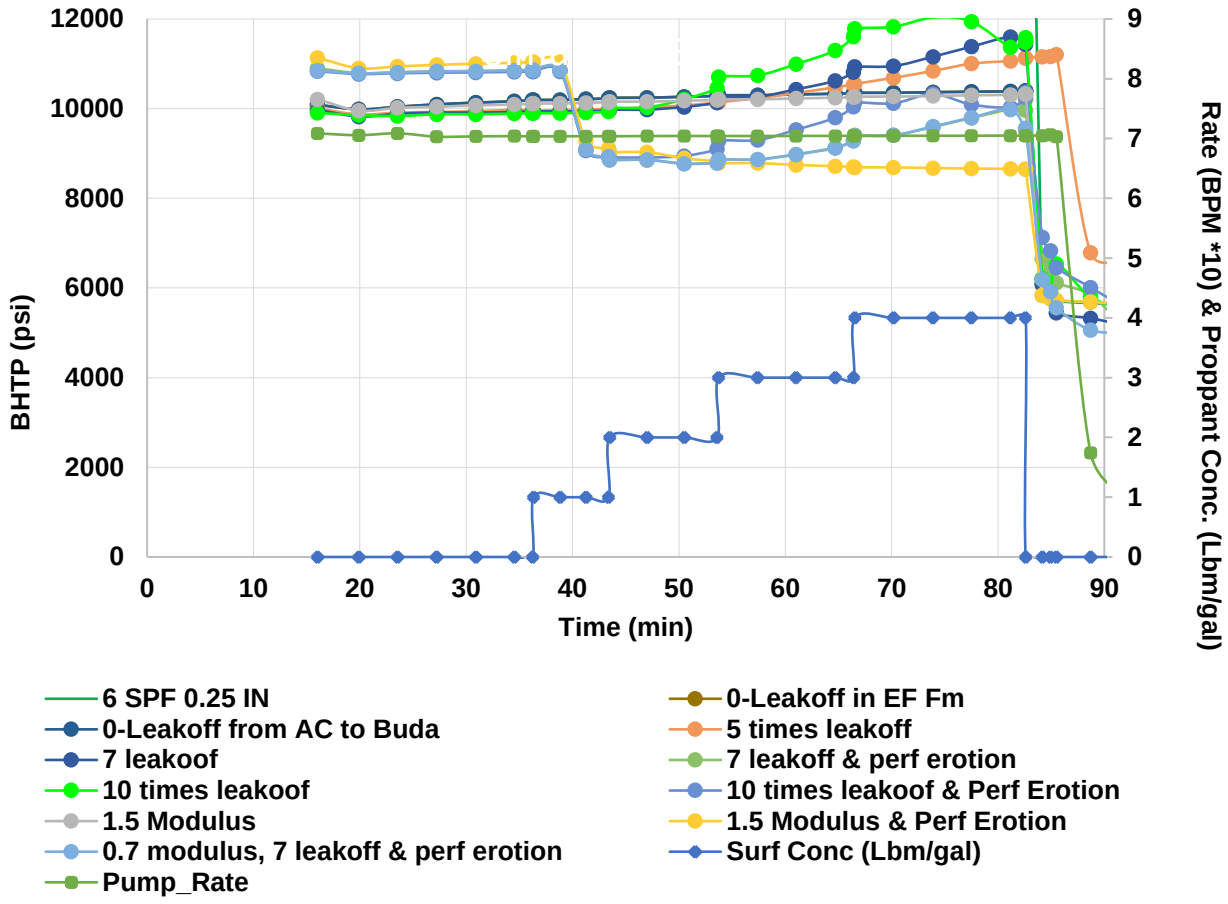

Figure 73.-Sensitivity for leak-off from Austin Chalk to Buda formations

It was possible to match the reported BHTP, but not the reported micro seismic events. To match the reported BHTP and the micro seismic events, a value multiplier was applied to the reported Young´s Modulus, fracture toughness, changes in the SPF, and perforation diameter. The different configurations (cases) ran are presented in **Table 7**.

Case	Shift Depth (ft)	Stress Gradient (psi/ft)	Modulus (MMpsi)		K-ic (psi*ïn^1/2)	SPF	Perf diameter (in)
			LEF	UEF			
1	0	0.55	1.8649	4.0652	990	8-8-8-8	0.25
2	0	0.55	2.6641	4.0652	1414	4-4-5-4	0.35
3	0	0.65	2.6641	4.0652	1414	5-5-5-5	0.35
4	0	0.65	3.5000	4.0652	1414	4-5-5-5	0.35
5	0	0.65	3.5000	4.5000	1414	4-5-5-5	0.35
6	0	0.65	3.5000	4.0652	1832	4-5-5-5	0.35
7	0	0.65	3.5000	3.8000	1414	4-5-5-5	0.35
8	50	0.55	2.6641	4.0652	1414	4-5-4-4	0.35

Table 7.-Sensitivity cases for properties reported in paper SPE-170827 (Reprinted from Centurion, et al., 2014)

The results from running the different cases showed a match in the BHTP, but not in the micro seismic events. **Figure 74** shows a schematic representation of the hydraulic fracturing simulation cases results.

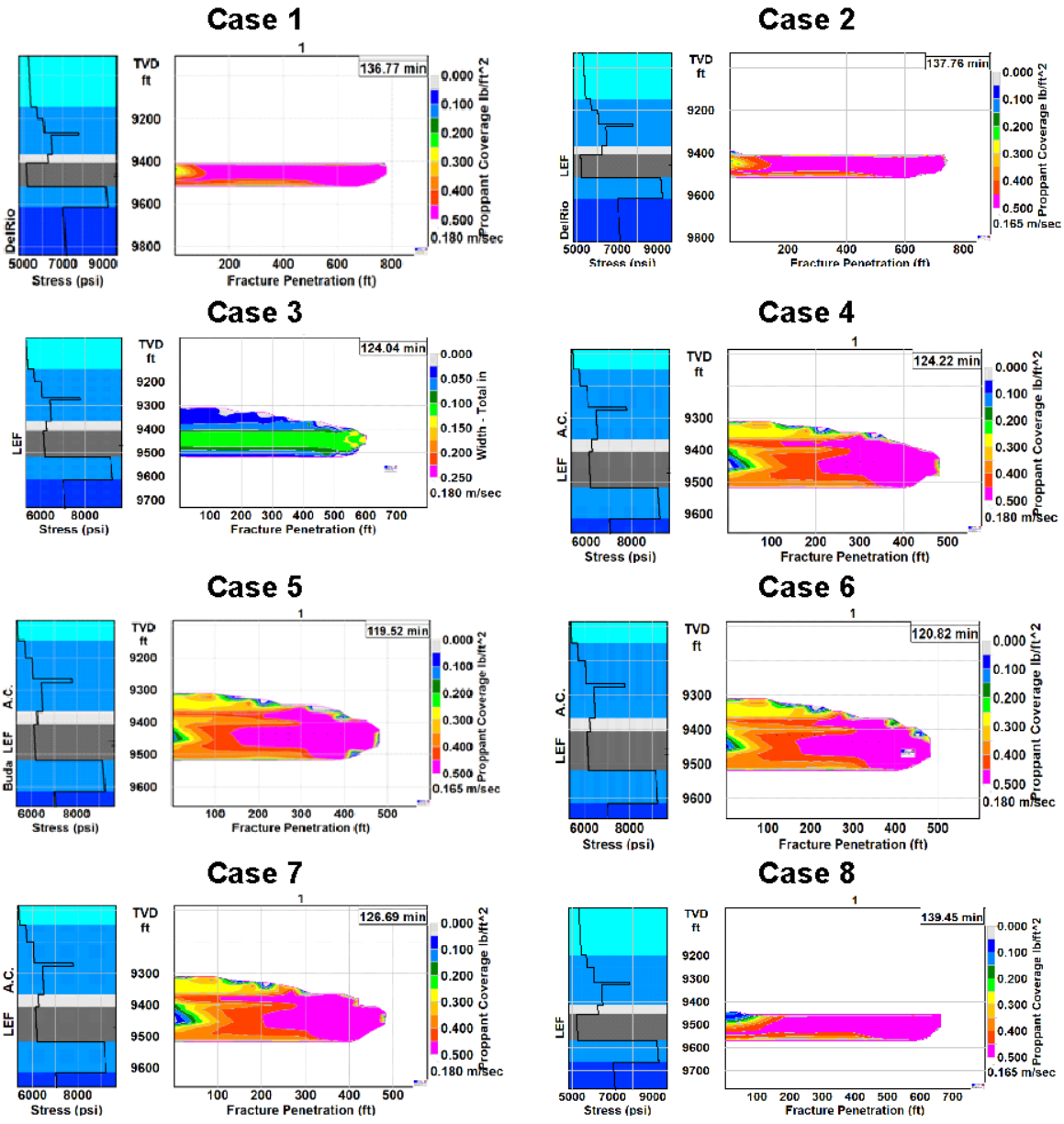

Figure 74.-Simulated hydraulic fracturing for the cases simulated using the geomechanical model in SPE-170827

Using the digitalized well logs from the paper SPE-170707 as inputs in the geomechanical model, the BHTP and micro seismicity reported in the paper SPE-

170827 were matched. **Figure 75** illustrates the matches obtained when evaluating stage 18 in the paper SPE-170827, which was completed with 4 clusters, with the simulated hydraulic fracturing.

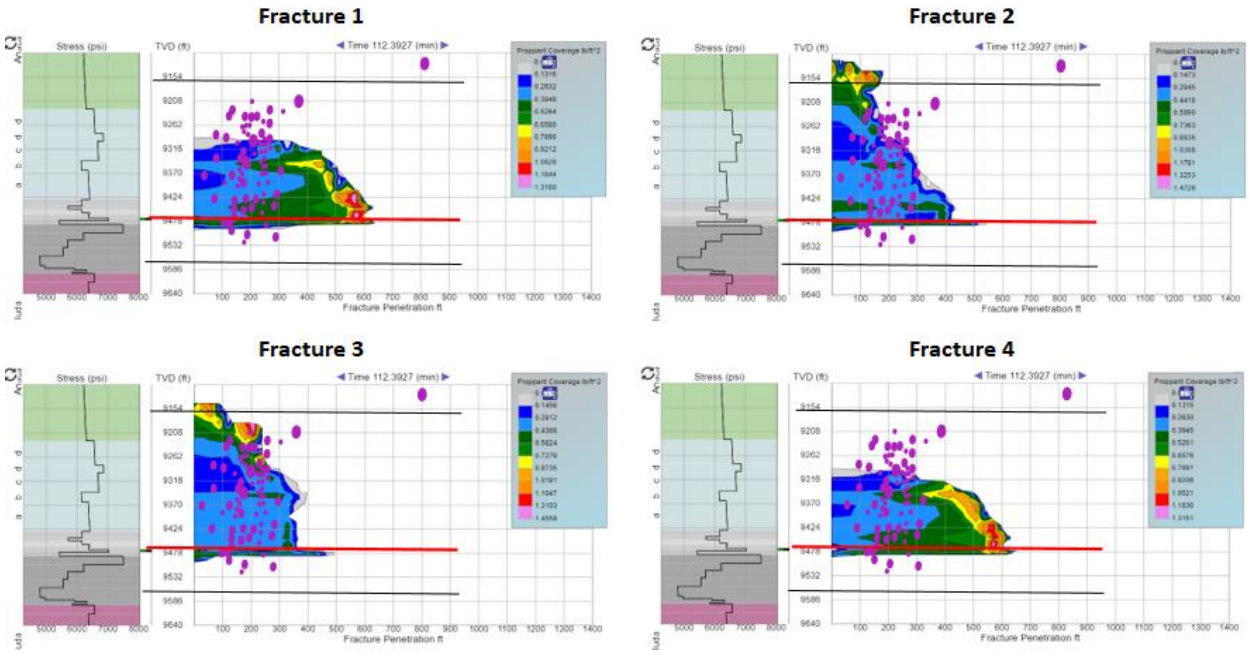

Figure 75.-Match of the hydraulic fracturing simulations and micro seismicity events reported in paper SPE-170827

By using this geomechanical model, the hydraulic fracturing in the legacy well was simulated. The fracturing fluid volume and proppant quantity simulated corresponded to the reported values in drillinginfo for the legacy well. The completion of the legacy well was simulated with 6 clusters per stage. The different zones in the Eagle Ford were simulated, results are presented in **Figure 76** to **Figure 81**.

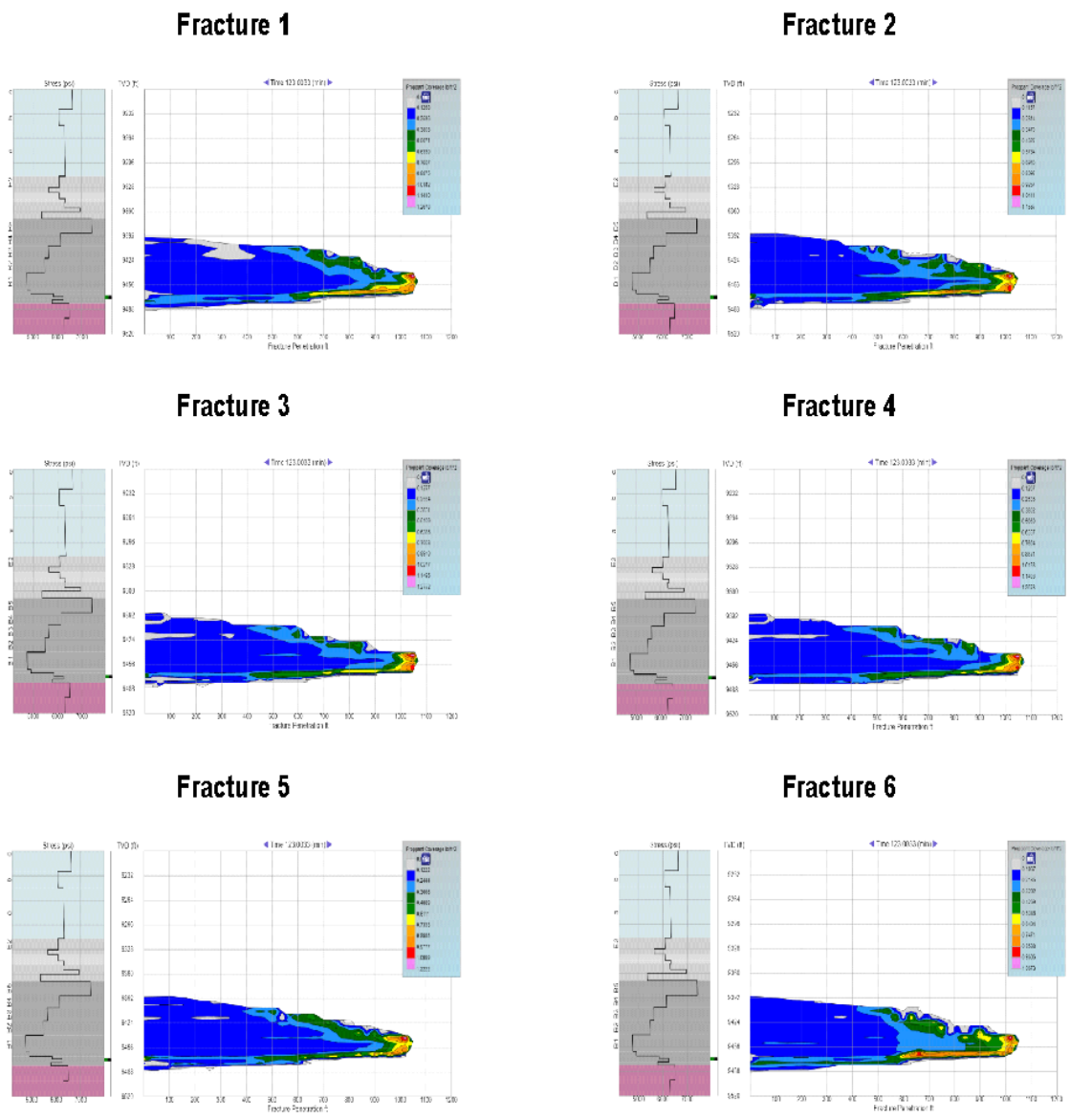

Figure 76.-Hydraulic fracturing simulation in the Eagle Ford for the legacy well, zone A2

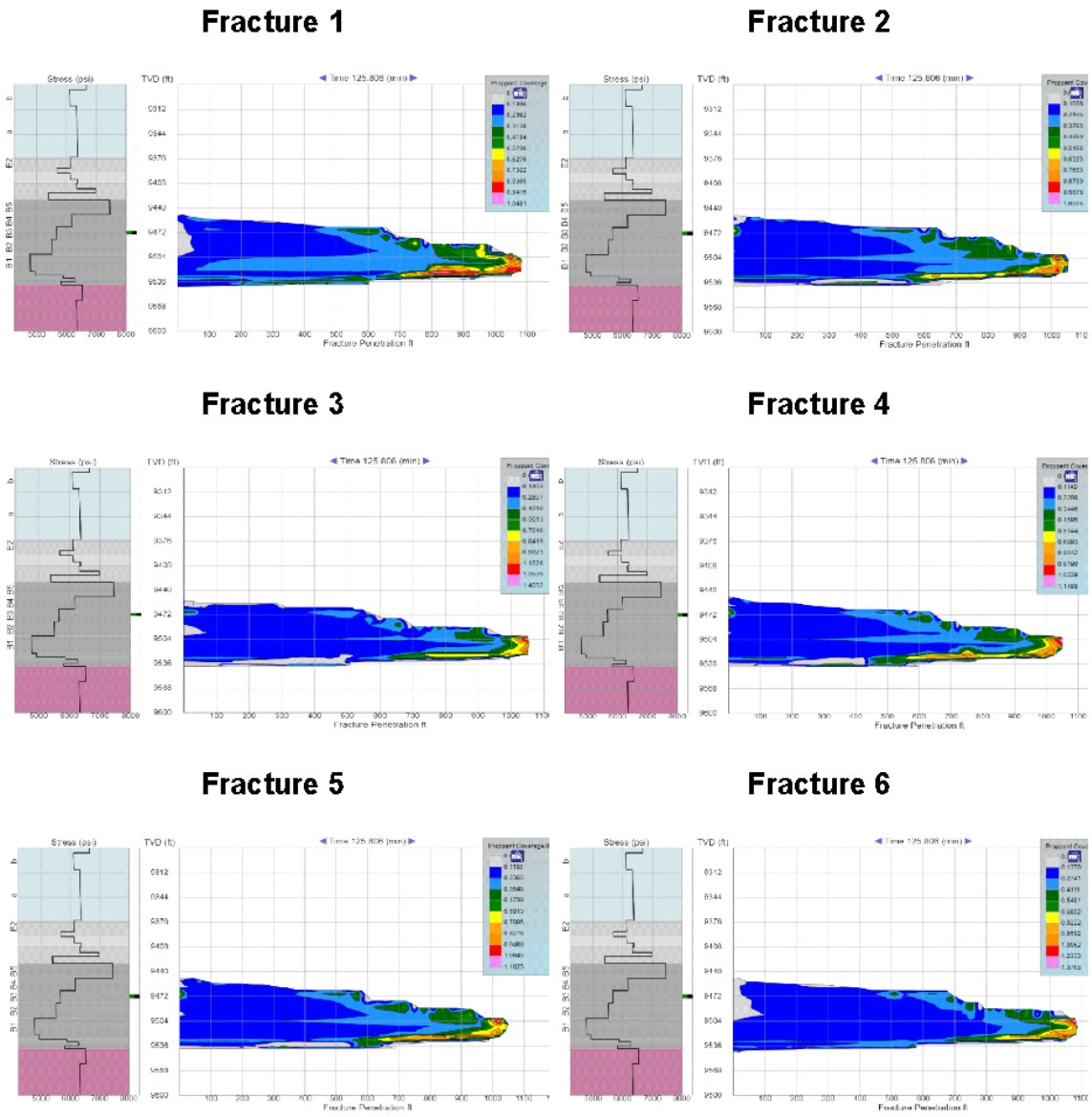

Figure 77.-Hydraulic fracturing simulation in the Eagle Ford for the legacy well, zone B3

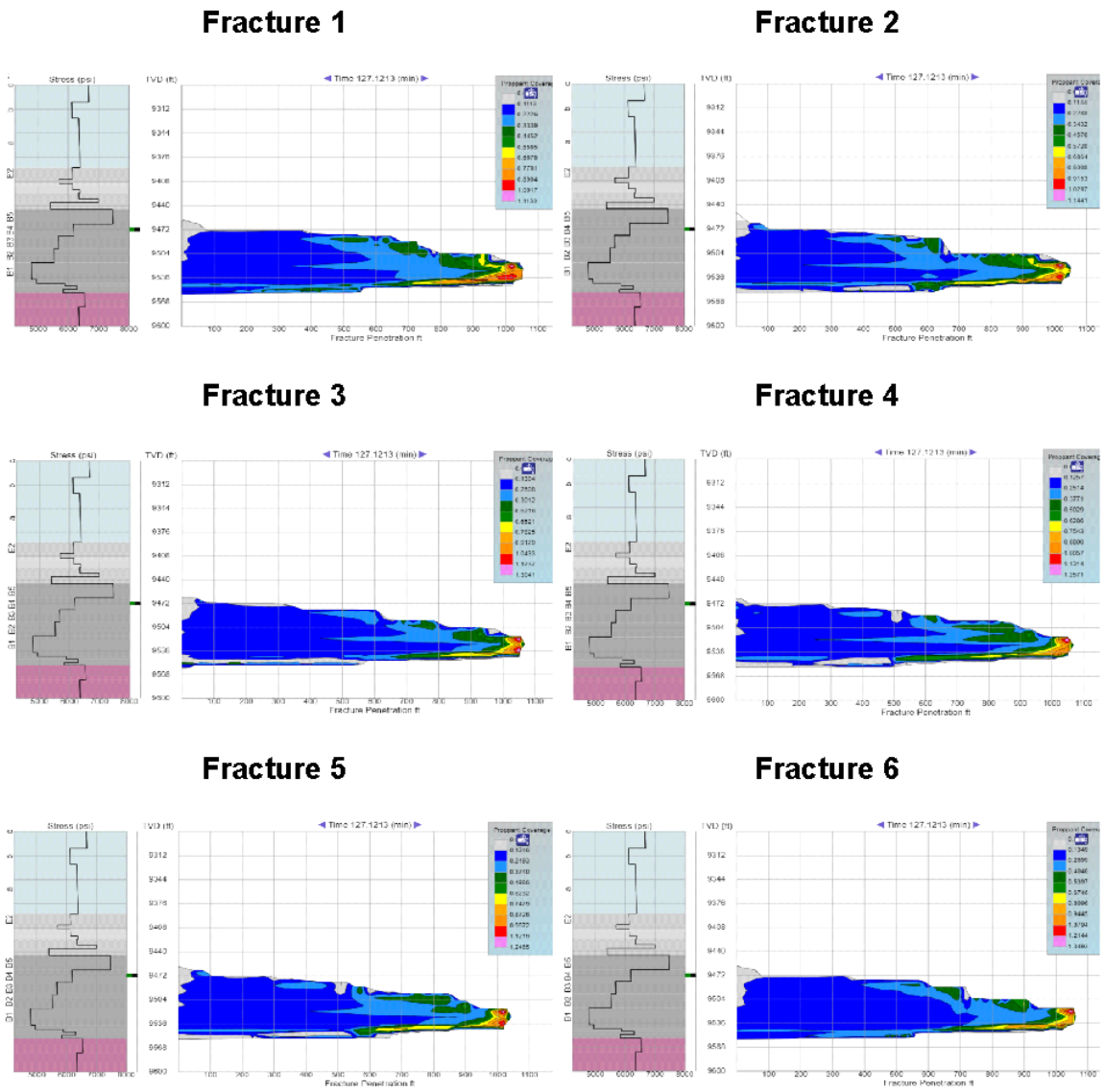

Figure 78.-Hydraulic fracturing simulation in the Eagle Ford for the legacy well, zone B4

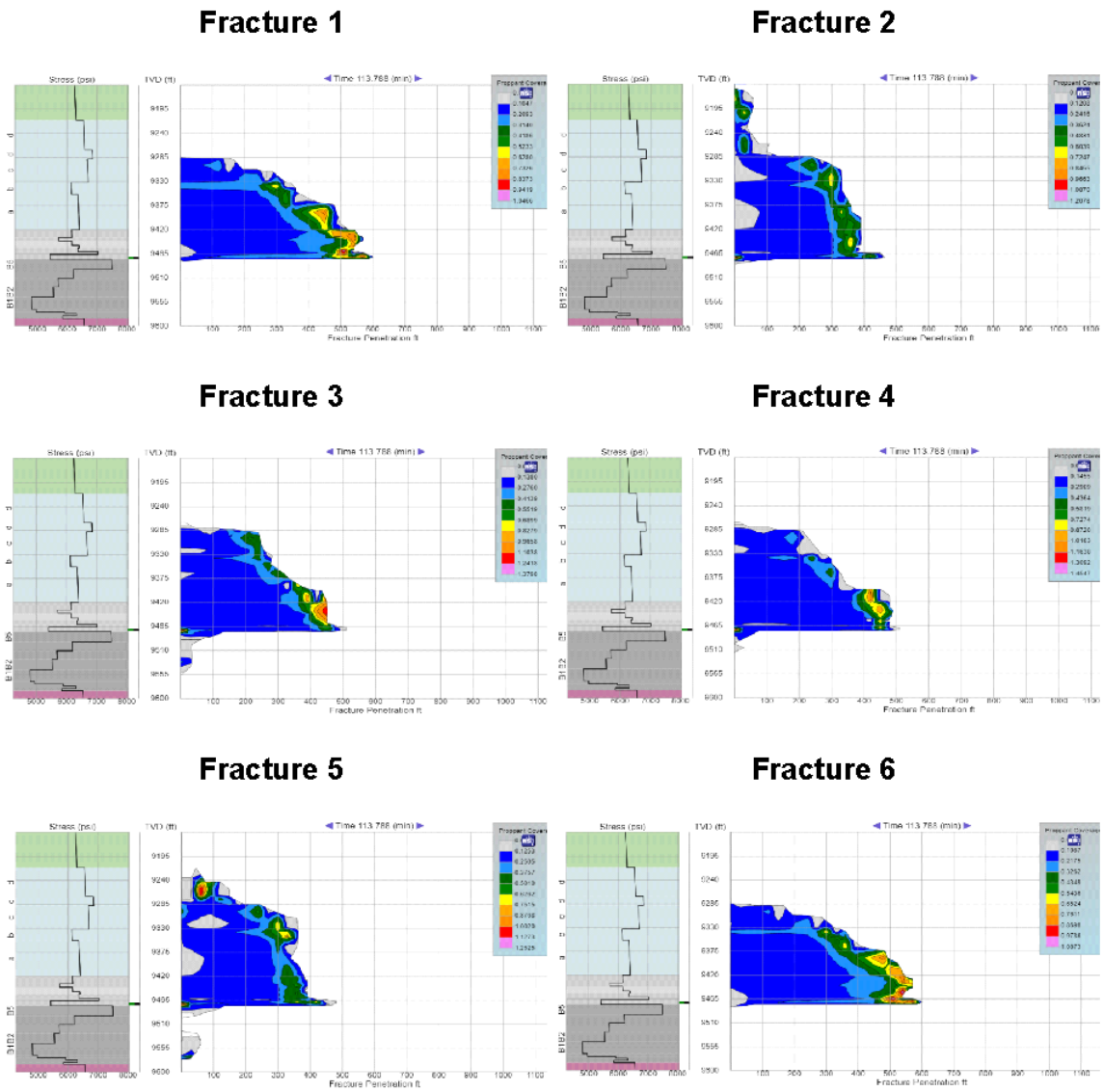

Figure 79.-Hydraulic fracturing simulation in the Eagle Ford for the legacy well, zone C1

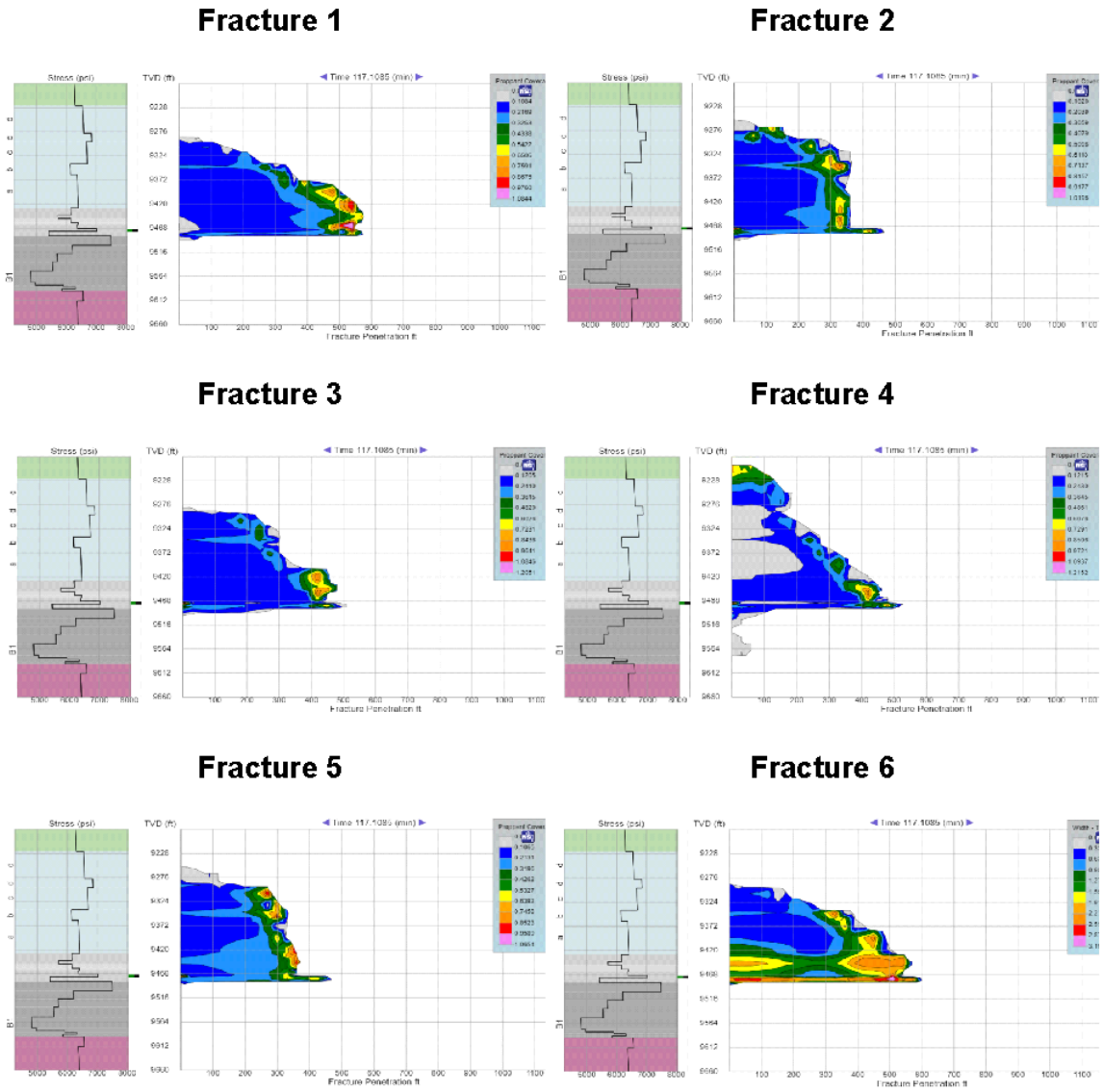

Figure 80.-Hydraulic fracturing simulation in the Eagle Ford for the legacy well, zone C2

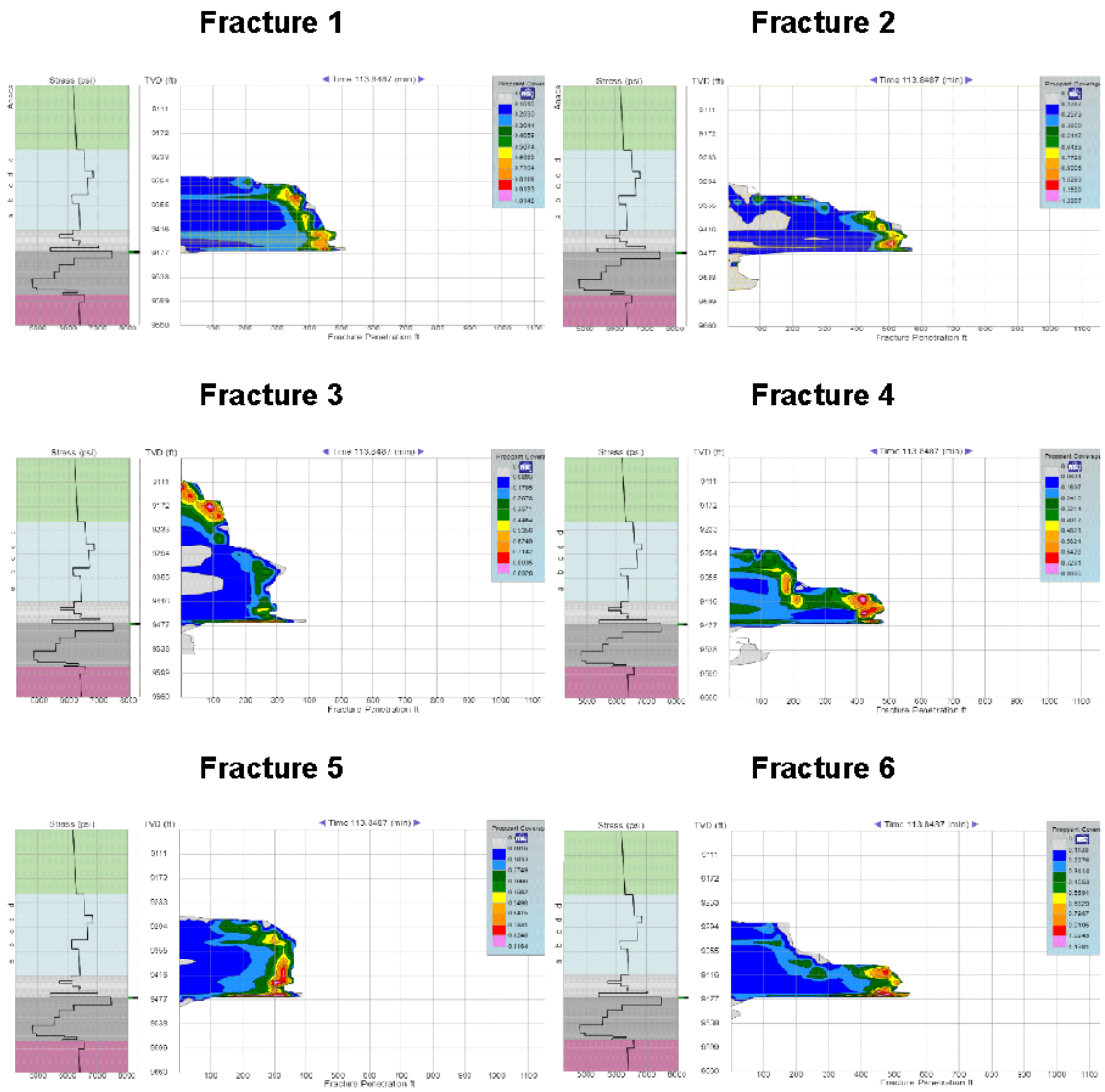

Figure 81.-Hydraulic fracturing simulation in the Eagle Ford for the legacy well, zone C1/B5

4.5. Analysis of results.

This section presents the summary of the simulated extents of the proppant placement in the legacy well, as well as the bottom hole injection pressure treatments, and fracture heights.

The legacy well was fractured using a borate cross-linked fracturing fluid, it was reported as landed in the lower Eagle Ford zone. Considering this, different simulations were run in the different zones of the lower Eagle Ford zone, as reported by Donovan et al. (2012). Simulations were also run in the C zones of the upper Eagle Ford zone, which are closer to the lower Eagle Ford.

4.5.1. Simulated extent of the sand proppant in the hydraulic fractures.

The simulated results showed that the proppant was distributed along the fracture half-length. According to this, the minimum extent of the proppant was found at a distance of 500 ft, corresponding to landing zones between the B5 zone of the lower Eagle Ford and the C1 zone of the upper Eagle Ford. The results are shown in Figure 82.

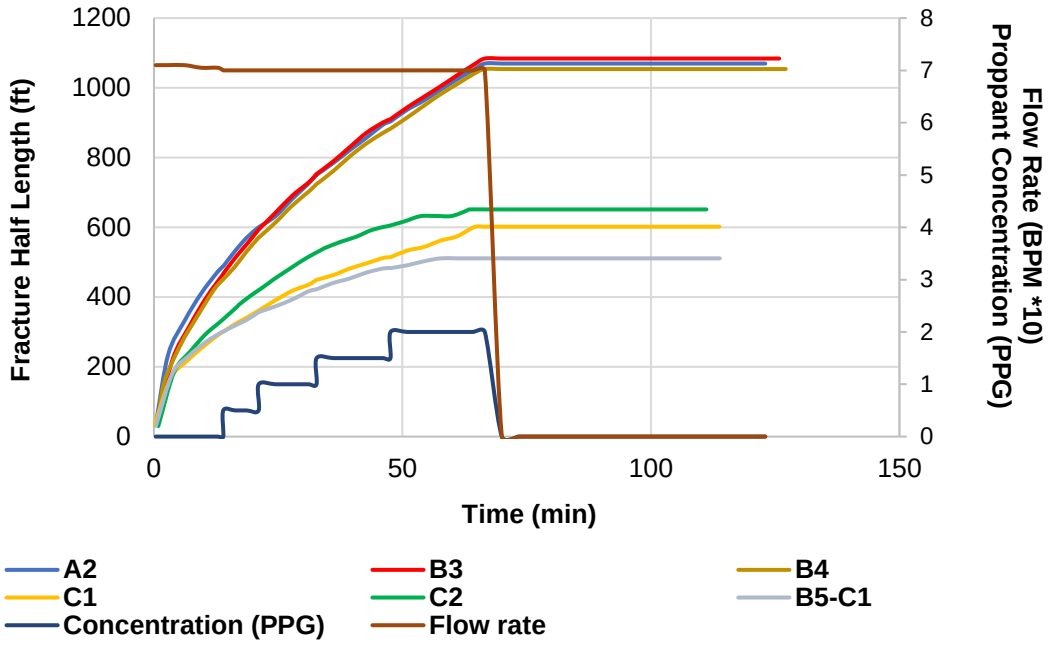

Figure 82.-Simulated fracture half-length of the hydraulic fractures in the legacy well

When landing in the other zones of the lower Eagle Ford, the extent of the proppant in the simulated hydraulic fractures is larger than 1000 ft. The lower Eagle Ford zone is highly confined, which makes the simulated hydraulic fractures tend to have larger fracture half lengths.

4.5.2. Simulated fracture height.

The simulated hydraulic fractures in the lower Eagle Ford zones showed the lower fracture heights, not being larger than 100 ft. As explained before, these are

because of the high confinement of this zone. The simulated fracture heights in the C1 zone through B5 produced fracture heights as large as 270 ft. The results are presented in **Figure 83**.

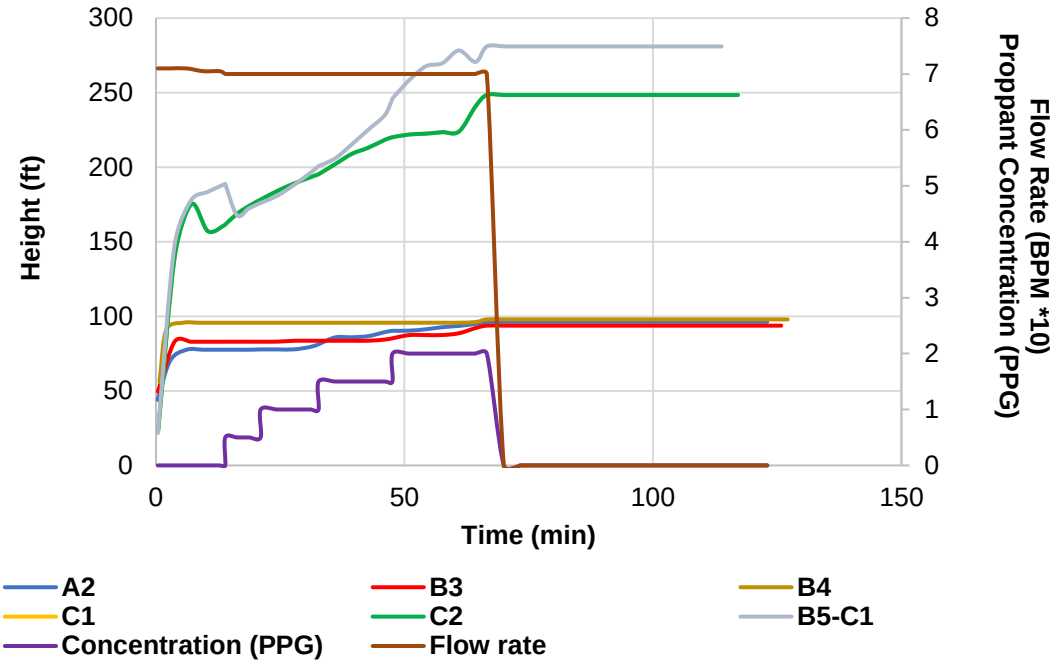

Figure 83.-Simulated fracture height of the hydraulic fractures in the legacy well

4.5.3. Simulated bottom hole injection.

The simulated bottom hole injection pressures of the treatments produced reasonable pressures, which are comparable to pressures reported in the literature. **Figure 84** exhibits the results obtained.

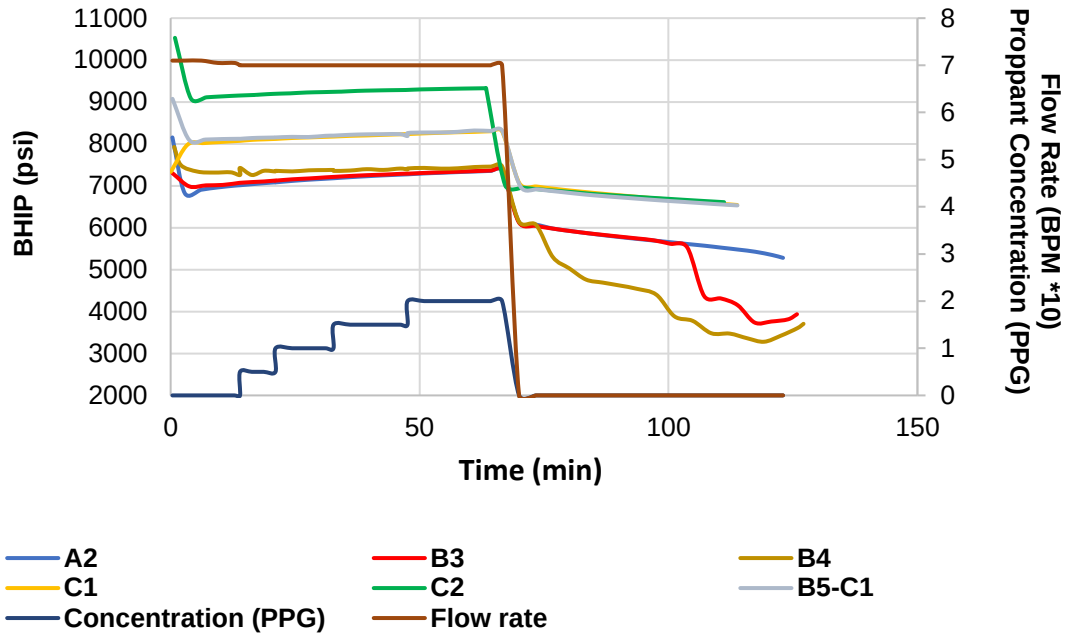

Figure 84.-Simulated bottom hole injection pressure of the hydraulic fractures in the legacy well

4.6. Conclusions.

According to the simulated hydraulic fracturing results, drilling a parallel well up to 500 ft away from the legacy well is enough to find proppant in the drill cuttings. This is the minimum extent that might be found when the hydraulic fracture occurs between the B5 zone of the lower Eagle Ford and the C1 zone of the upper Eagle Ford.

When landing in the other zones of the Eagle Ford formation, simulated extent of the proppant after hydraulic fracturing is larger than 1000 ft because these zones are highly confined.

The high confinement of the lower Eagle Ford zones produces the lower simulated fracture heights, not more than 100 ft. On the other hand, the B5 to C1 zones of the Eagle Ford produced simulated fracture height as large as 270 ft.

5. SUMMARY

This dissertation presents the research results of two applications of drill cuttings in hydraulic fracturing related operations: the use of drill cuttings as propping agents, and proppant quantification in drill cuttings. Additionally, hydraulic fracturing simulations in an Eagle Ford well completed with a borate crosslinked fracturing fluid to determine the minimum extent at which sand proppant can be found in the drill cuttings when drilling a parallel well.

Use of drill cuttings as propping agents

Shale formations are drilled through using synthetic or oil-based drilling mud because these types of fluids are more suitable for sensitive formations, allowing drilling to be faster, providing high temperature and pressure stability (Xie et al, 2013; Al Beshr et al., 2016), high salt concentration resistance beneficial to the stability of the borehole wall, and small damage to the oil and gas layer (Wu et al., 2019). However, the main disadvantage of these drilling fluids is related to their environmental impact. The drill cuttings produced using synthetic or oil-based drilling mud are referred as non-water cuttings (NWC), which may contain complex hydrocarbons, heavy metals, dissolved minerals, and naturally occurring radioactive materials that, released to the surrounding ground and aquatic environments, may cause deleterious effects on them (Somee et al., 2018).

Disposal of NWC is a costly operation, requiring to undergo a cleaning process to remove any remaining drilling mud before disposal (Cedola et al., 2020). NWC are treated first at the rig site, by a series of solid-control equipment, to remove the drilling fluid. Later, a second treatment is applied to reduce the drilling fluid content to less than 1% to satisfy most regional emission policies (Huang et al., 2018).

This problem brought us the idea of re-injection of the produced NWC. This operation has been done for years. However, reinjecting the NWC along with the proppant during the hydraulic fracturing operations has not been published yet. In this research, the use of NWC as propping agents was evaluated by conducting fracture conductivity experiments following a modified API RP-61 procedure. We used a modified API fracture conductivity cell with steel plates, to measure conductivity. Drill cuttings from an Eagle Ford well were used in two different conditions, first as received from the field (with oil-based drilling mud), and second washed and dried at room temperature to eliminate the drilling fluid. The drill cuttings were mixed at different concentrations with sand proppants for testing. Three different sand proppants were used to investigate the effect of the sand proppant in the fracture conductivity response of the mixture of drill cuttings-sand proppant.

Drill cuttings as propping agents were evaluated by conducting fracture conductivity experiments utilizing a modified API fracture conductivity cell and flowing dry nitrogen. Eagle Ford drill cuttings were used as received from the field (with oil-based mud drilling fluid) and washed and dried at room temperature to eliminate the drilling fluid. The drill cuttings were mixed at different concentrations

with sand proppants and they were tested. Three different sand proppants were used to investigate the effect of the sand proppant in the mixture of drill cuttings and sand proppant fracture conductivity response. The results show that the closer the sand proppant size particle distribution to the drill cuttings, the better the results; the drilling fluid present in the drill cuttings can improve the fracture conductivities results in the mixtures evaluated while keeping it lower than 5 wt%.

The use of oil-based drill cuttings as propping agents was investigated by mixing them with 40/70 mesh and 100 mesh sand proppants. Fracture conductivity experiments were performed following a modified API RP-61 procedure, doing short-term conductivity experiments and applying dry nitrogen gas as fluid, with closure stress applied in incremental steps of 1000 psi from 1000 to 6000 psi. The drill cuttings were used both as received from the rig site after mechanical separation on site, and also after being washed for removal of the oil-based drilling fluid, to compare the effect of drilling fluid in conductivity responses.

In general, 12.5 wt% drill cuttings concentration in sand proppant produced fracture conductivity results close to the baseline of proppant without mixed with cuttings. Drill cuttings concentration up to 25 wt% produced acceptable results. At high closure stress, proppant with high cutting percentage shows faster decline rate in conductivity compared with low cutting percentage.

Wet drill cuttings mixed with sand proppants showed, in general, better results than dried cuttings. The oil-based drilling fluid might act as an agglomerating agent to avoid the fine particles to move in the proppant pack.

Further studies are recommended to extend the scope and findings of this research. It is advisable to use rock samples, instead of steel plates, to evaluate the cuttings-proppant mixture embedment and its effect on the fracture conductivity response. Additionally, using downhole fluids will give an approximation of the real conditions and its impact on the fracture conductivity response.

Proppant quantification in drill cuttings

The general approach to estimate the proppant concentration in the hydraulic fractures, and the fracture conductivity, is by using hydraulic fracturing simulations. Modeling of hydraulic fracturing is a complex problem, which includes the description of many physical processes, including the fluid flow in the fracture, deformation of the rock, fracture of the rock, proppant flow, etc. An effective solution to this problem requires a considerable number of simplifications and assumptions (Khasanov et al., 2017). Many of these process are not very predictable because of the strong uncertainties concerning subsurface heterogeneities (Chen et al., 2015), and proppant transport mechanism. Understanding of the mechanisms and effects of the coupled fracture/proppant system is greatly limited by insufficient direct observations (Chen et al., 2015) to calibrate the models (Raterman et al., 2018), and justify any intent to measure the proppant concentration in the hydraulic fractures.

When the matter interacts with a beam in the visible region of the electromagnetic spectrum, the spectroscopic method is referred as to visible molecular spectroscopy. It can lead to light absorption, scattering, diffraction or

emission of radiation at certain wavelengths. When the silicon dioxide interacts with a beam in the visible region of the electromagnetic spectrum, it leads to light absorption. The light absorption is produced by the electron excitation of the bonding or nonbonding electrons of the silicon dioxide molecule.

Light absorption is a two steps process: absorption and relaxation (Todoli, 2008).

a) Absorption: a beam interacts with the external electrons of the matter, changing its energy levels, generating a transition state of the matter and producing light absorption of specific wavelength.

$$M + h\upsilon \quad M^*$$

The transition state (M*) has a lifetime of 10-8 – 10-9 seconds.

b) Relaxation: the transition state of the matter liberates the absorbed energy and returns to its originally state, generating heat, photochemical reactions or luminescence.

$$M^* \quad M + \text{Heat}$$

$$M^* \quad B \text{ (Photochemical reactions)}$$

$$M^* \quad M + h\upsilon \text{ (Luminescence)}$$

Every atom (and molecule) has its specific wavelength absorption values. It is determined by their external electron configuration. It is useful to identify atoms or molecules. The silicon dioxide molecule has σ electrons, corresponding to the electrons in the σ bonding between silicon and oxygen, and nonbonding electrons (called n electrons) which are the lone pair in the oxygen atom. These electrons are involved in the light absorption process of the silicon dioxide.

Light absorption measurements of silica sand, in various silica sand samples, showed that more absorption takes place around in the blue range of the visible light within the visible region of the electromagnetic spectrum (Coblentz, 1912, Ketheeswaren, 2004; Kitamura, 2007; Kowalsky, 2009; Yang et al., 2010; Rodríguez, 2018). This absorption occurs because when a beam (photon) with the appropriate energy interacts with a silica crystal, then the photon is absorbed by the external electronic configuration of the system, increasing their kinetic and vibration random movement.

In this research, it was investigated the use of drill cuttings to quantify the proppant concentration in hydraulic fractures when drilling through it. A visible molecular spectroscopy method was used to quantify the proppant particles. Synthetic samples, using Eagle Ford drill cuttings, were used to test and validate the methodology developed. Additionally, in this dissertation a field sampling procedure is presented to illustrate how the operation can be performed at the field.

The main conclusions of this research are:

The detection limit for sand proppant 40/70 mesh quantification was 0.028 wt%, and for sand proppant 100 mesh was 0.018 wt%. These values are smaller than the theoretical sand proppant concentration in the hydraulic fractures, which was 0.14 wt% for a fracture width of 0.2 inches and a sample length of 10 ft.

The sensitivity of the method was improved when using larger microscopy magnification to quantify sand particles 100 mesh. Concentrations as low as 0.01 wt% were identified with a relative error of 14%.

The methodology to quantify sand particles 100 mesh can be used to quantify the crushing of sand particles 40/70 mesh for crushing larger than 15 wt%.

Hydraulic fracturing simulations

Modeling hydraulic fracturing is challenging since a variety of physical processes are involved. These include fracture propagation and inflation, fluid flow within the fracture, proppant transport and settling, followed by fracture deflation, closure, and proppant capture. These processes may be represented by making appropriate simplifying assumptions in the analysis. For the fracture propagation and fluid flow within it, it is typical to include simplification of the fracture geometry as a plane form, treating the inflating fluid as Newtonian, and assuming flow to be laminar. Various models follow this formalism to approximately define the development of

fracture geometry, among which the PKN and KGD models are the most popular (Wang and Elsworth, 2019).

StimPlan™ V8, from NSI Technologies, LLC, a commercial hydraulic fracturing simulator, was used to simulate the hydraulic fractures in the well Klattenhoffunitlas-1H, called in this research the legacy well. The main objective was to get a simulated extent of the proppant in the hydraulic fractures after the legacy well was completed.

In this study, the hydraulic fractures in the legacy well were simulated by using as input; the reported information in drillinginfo (www.enverus.com), such as the well trajectory, a high viscosity guar-borate cross-linked fracturing fluid volume and the proppant mass pumped. The geomechanical model was built by using the literature reports for wells close to the legacy well. The geomechanical model and the perforation design were adjusted by matching the bottom hole injection pressure treatment and micro seismic events reported in the literature for wells close to the legacy well.

The legacy well was fractured using a borate cross-linked fracturing fluid, it was reported as landed in the lower Eagle Ford zone. Considering this, different simulations were run in the different zones of the lower Eagle Ford zone, as reported by Donovan et al. (2012). Simulations were also run in the C zones of the upper Eagle Ford zone, which are closer to the lower Eagle Ford.

The simulated results showed that the proppant was distributed along the fracture half-length. According to this, the minimum extent of the proppant was found

at a distance of 500 ft, corresponding to landing zones between the B5 zone of the lower Eagle Ford and the C1 zone of the upper Eagle Ford.

When landing in the other zones of the lower Eagle Ford, the extent of the proppant in the simulated hydraulic fractures is larger than 1000 ft. The lower Eagle Ford zone is highly confined, which makes the simulated hydraulic fractures tend to have larger fracture half lengths.

The simulated hydraulic fractures in the lower Eagle Ford zones showed the lower fracture heights, not being larger than 100 ft. As explained before, these are because of the high confinement of this zone. The simulated fracture heights in the C1 zone through B5 produced fracture heights as large as 270 ft.

The simulated bottom hole injection pressures of the treatments produced reasonable pressures, which are comparable to pressures reported in the literature.

According to the simulated hydraulic fracturing results, drilling a parallel well up to 500 ft away from the legacy well is enough to find proppant in the drill cuttings. This is the minimum extent that might be found when the hydraulic fracture occurs between the B5 zone of the lower Eagle Ford and the C1 zone of the upper Eagle Ford.

When landing in the other zones of the Eagle Ford formation, simulated extent of the proppant after hydraulic fracturing is larger than 1000 ft because these zones are highly confined.

The high confinement of the lower Eagle Ford zones produces the lower simulated fracture heights, not more than 100 ft. On the other hand, the B5 to C1 zones of the Eagle Ford produced simulated fracture height as large as 270 ft.

REFERENCES

Acharya, R. 1988. Hydraulic-Fracture-Treatment Design Simulation. J Pet Technol 40 (02): 139–142. SPE-17175-PA. https://doi.org/10.2118/17175-PA

AlBeshr, K., Al-Hammadi, S., Bhaskar, R., et al. 2016. Treatment of Legacy Oil Based Mud OBM Drill Cuttings and Sustainable Use of Recovered Materials. Presented at the Abu Dhabi International Petroleum Exhibition & Conference held in Abu Dhabi, UAE, 7-10 November. SPE-183140-MS. https://doi.org/10.2118/183140-MS

API RP 19D (2008). Recommended Practices for Measuring the Long Term Conductivity of Proppants; Washington D.C., American Petroleum Institute.

API RP 61 (1989). Recommended Practices for Evaluating Short Term Proppant Pack Conductivity, Washington D.C., American Petroleum Institute.

B. M. Smirnov, 2018. Atomic Particles and Atom Systems, Springer Series on Atomic, Optical, and Plasma Physics 51, https://doi.org/10.1007/978-3-319-75405-5

Bernardis, S., 2012. Engineering Impurity Behavior on the Micron-Scale in Metallurgical-Grade Silicon Production. PhD Dissertation, Massachusetts Institute of Technology, Massachusetts.

Cedola, A., Nygaard, R., and G. Hareland. 2020. Cuttings Disposal in Cement: Investigation of the Effect on Mechanical Properties. Presented at the 54th US Rock Mechanics/Geomechanics Symposium held in Golden, Colorado, USA, 28 June-1 July. ARMA 20–1677.

Chen, C., Martysevich, V., O'Connell, P. et al. 2015. Temporal Evolution of the Geometrical and Transport Properties of a Fracture/Proppant System Under Increasing Effective Stress. SPE J. 20 (03): 527–535. SPE-171572-PA. https://doi.org/10.2118/171572-PA

Clark, J. 1949. A Hydraulic Process for Increasing the Productivity of Wells. Journal of Petroleum Technology 1 (01): 1–8. SPE-949001-G. https://doi.org/10.2118/949001-G

Coblentz, w. 1912. Absorption, reflection, and dispersion constants of quartz. https://nvlpubs.nist.gov/nistpubs/bulletin/11/nbsbulletinv11n3p471_A2b.pdf

Donovan, A., Staerker, S., Pramudito, A. 2012. The Eagle Ford outcrops of west Texas: A laboratory for understanding heterogeneities within unconventional mudstone reservoirs. GCAGS Journal, v. 1 (2012), p. 162–185. https://doi:10.2118/178595-MS

Economides, M. and Nolte, K. 2000. Reservoir Stimulation, third edition. Hoboken, New Jersey: John Wiley and Sons.

Elliott, S., and Gale; J. 2018. Analysis and Distribution of Proppant Recovered from Fracture Faces in the HFTS Slant Core Drilled through a Stimulated Reservoir. Presented at the Unconventional Resources Technology Conference held in Houston, Texas, USA, 23–25 July. URTeC: 2902629. https://doi.org/10.15530/urtec-2018-2902629

Elsarawy, A. and Nasr-El-Din H. 2018. Propped Fracture Conductivity in Shale Reservoirs: A Review of its Importance and Roles in Fracturing Fluid Engineering. Presented at the SPE Kingdom of Saudi Arabia Annual Technical Symposium and Exhibition held in Dhahran, Saudi Arabia, 23–26 April. SPE-192451 -MS. https://doi.org/10.2118/192451-MS

Fan, M., McClure, J., Han, Y., et al. 2019. Using an Experiment/Simulation Integrated Approach to Investigate Fracture-Conductivity Evolution and Non-Darcy Flow in a Proppant-Supported Hydraulic Fracture. SPE J. 24 (04): 1912–1928. SPE-195588-PA. https://doi.org/10.2118/195588-PA

Geertsma, J. and Klerk, F. 1969. A Rapid Method of Predicting Width and Extent of Hydraulically Induced Fractures. JPT 21 (12): 1571–1581. SPE-2458-PA. https://doi.org/10.2118/2458-PA

Gianoutsos, N., et al. 2020. Results of the 2019 U.S. Geological Survey Assessment of Water and Proppant Associated with Petroleum Production from the Eagle Ford Group, Texas. Presented at the Unconventional Resources Technology Conference held in Austin, Texas, USA, 20-22 July. URTeC: 3080. https://doi.org/10.15530/urtec-2020-3080

Gillis, B., Arbieva Z., and Gavin, I. 2012. Analysis of Lead Toxicity in Human Cells. BMC Genomics 344 (13): 93-102. https://doi:10.1186/1471-2164-13-344

Godino, G. 2017. Silica - Molecule of the Month November. Journal contribution. https://doi.org/10.6084/m9.figshare.5414581.v1

Greetesma, J., de Klerk, F. 1969. A rapid method of predicting width and extent of hydraulic induced fractures. J. Pet. Technol. 21, 1571–81. https://doi.org/10.2118/2458-PA

Guerra, J., Zhu, D., and Hill, D. 2018. Impairment of Fracture Conductivity in the Eagle Ford Shale Formation. SPE Production & Operations 33 (04): 637–653. SPE-184857-PA. https://doi.org/10.2118/184857-PA

Holditch, S. 2006. Tight Gas Sands. JPT 58 (06): 86-93. SPE-103356-JPT. https://doi.org/10.2118/103356-JPT

Huang, Z., Xu, Z., Quan, Y. et al. 2018. A Review of Treatment Methods for Oil-Based Drill Cuttings. IOP Conference Series: Earth and Environmental Science 170: 1-7. https://doi:10.1088/1755-1315/170/2/022074

ISO 13503-2:2006. Completion Fluids and Materials - Part 2: Measurement of Properties of Proppants Used in Hydraulic Fracturing and Gravel-Packing Operations. Petroleum and Natural Gas Industries.

Jansen, T.A. 2014. The Effect of Rock Properties on Hydraulic Fracture Conductivity in the Eagle Ford and Fayetteville Shales. MS Thesis, Texas A&M University, College Station, Texas, U.S.A. (December 2014).

Ketheeswaren, S. 2004. Optical absorption of quartz. Master thesis, University of Jaffna, Department of Physics.

Khasanov, M., Paderin, G., Shel, E. et al. 2017. Approaches to modeling hydraulic fracturing and their development. OIJ (12): 37–41. Paper Number OIJ-2017-12-037-041-RU. https://doi.org/10.24887/0028-2448-2017-12-37-41

Khristianovitch, S. and Zheltov, Y. 1955. Formation of Vertical Fractures by Means of Highly Viscous Fluids. Presented at the 4th World Petroleum Congress, Rome, Italy, June. WPC-6132. https://onepetro.org/WPCONGRESS/proceedings/WPC04/All-WPC04/WPC-6132/203824

Kim, J., Zhou, L., and Morita, N. 2021. Study of Degradable Fibers with and without Guar Gum as a Proppant Transport Agent Using Large-Scale Slot Equipment. SPE Journal 26 (01): 262–280. SPE-195808-PA. https://doi.org/10.2118/195808-PA

Kitamura, R., Pilon, L., and Jonasz, M. 2007. Optical constants of silica glass from extreme ultraviolet to far-infrared at near room temperature. Optical Technology, 20 November 2007 Vol. 46, No. 33 applied optics. https://doi.org/10.1364/ao.46.008118

Kleppe, S., Michelsen, E., Handgraaf, P. et al. 2009. Reusing Recovered Base Oil from OBM Cuttings. Presented at 2009 SPE Asia Pacific Health, Safety, Security, and Environment Conference and Exhibition, Jakarta, Indonesia, 4-6 August. SPE-123559. http://doi:10.2118/123559-MS

Kou, R., Moridis, G, and Blasingame, T. 2018. Field Scale Proppant Transport Simulation and Its Application to Optimize Stimulation Strategy. Paper presented at the Unconventional Resources Technology Conference held in Houston, Texas, USA, 23-25 July. URTeC: 2878230. https://doi.org/10.15530/URTEC-2018-2878230

Kusmierczyk, P., 2015. Numerical simulation of hydraulic fractures. Various leak-off regimes and multi-fracturing. Ph.D. dissertation. http://pure.aber.ac.uk/ws/files/10624978/Kusmierczyk_P.pdf

Lippman, M., Ito, K., Hwang, J. et al. 2006. Cardiovascular Effects of Nickel in Ambient Air. Environmental Health Perspectives 114: 1662-1669. https://doi.org/10.1289/ehp.9150

Liu X., Song Q., Tang, Y. et al. 2013. Human Health Risk Assessment of Heavy Metals in Soil–Vegetable System: A Multi-Medium Analysis. Science of The Total Environment 463-464: 530-540. http://dx.doi.org/10.1016/j.scitotenv.2013.06.064

Mack, M, and Cokerc, C. 2013. Proppant Selection for Shale Reservoirs: Optimizing Conductivity, Proppant Transport, and Cost. Presented at the SPE Unconventional Resources Conference-Canada held in Calgary, Alberta, Canada, 5–7 November. SPE 167221. https://doi.org/10.2118/167221-MS

Maity, D., Ciezobka, J., and Eisenlord, S. 2018. Assessment of In-situ Proppant Placement in SRV Using Through-Fracture Core Sampling at HFTS. Presented at the Unconventional Resources Technology Conference held in Houston, Texas, USA, 23-25 July. URTeC: 2902364. https://doi.org/10.15530/urtec-2018-2902364

Mandal, A., Sarma, P., Singh, B. et al. 2012. Bioremediation: An Environment-Friendly Sustainable Biotechnological Solution for Remediation of Petroleum Hydrocarbon Contaminated Waste. ARPN Journal of Science and Technology 2: 1-12.

McGinley, M. 2015. The Effect of Fracture Orientation and Anisotropy on Hydraulic Fracture Conductivity in the Marcellus Shale. MS thesis, Texas A&M University, College Station, Texas (May 2015).

Meeker, S., Gadon, A., Abdelouahab, N. et al. 2020. Proppant Transport in a Newtonian Fluid Under Laminar Flow. SPE 201097 Journal Paper. https://doi.org/10.2118/201097-PA

Morillo, M. and Machado, H. 2020. Changing the Paradigm of Hydraulic Jet Lift Selection on Unconventional Applications: Eagle Ford Case Study. Originally scheduled to be presented at the SPE Annual Technical Conference & Exhibition held in Denver, Colorado, USA, 5 – 7 October. SPE-201780-MS. https://doi.org/10.2118/201780-MS

Nordgren, R.P. 1972. Propagation of a Vertical Hydraulic Fracture. SPE J. 12 (04): 306–314. SPE-3009-PA. https://doi.org/10.2118/3009-PA

Ouyang, L; Petalas, N.; Arbabi, S.; et al. 1998. An experimental study of single-phase and two-phase fluid flow in horizontal wells. Presented at the SPE Western Regional Meeting, Bakersfield, California, CA, USA, 10–13 May. https://doi.org/10.2118/46221-MS

Pearson, M., Fowler, G., Stribling, M. et al. 2020. Near-Wellbore Deposition of High Conductivity Proppant to Improve Effective Fracture Conductivity and Productivity of Horizontal Well Stimulations. Presented at the SPE Annual Technical Conference & Exhibition originally scheduled to be held in Denver, Colorado, USA, 5 – 7 October. SPE-201641-MS. https://doi.org/10.2118/201641-MS

Perkins, T. and Kern, L. 1961. Widths of Hydraulic Fractures. JPT 13 (09): 937–949. SPE-89-PA. https://doi.org/10.2118/89-PA

Presley, J. 2019. Eagle Ford Soars On. https://www.hartenergy.com/exclusives/eagle-ford-soars-182323

Profit, M., Dutko, M., and Yu, J. 2015. Developing a Framework to Simulate the Hydraulic Fracturing of Tight Gas Reservoirs Based on Integrative Adaptive Remeshing and Combined Finite/Discrete Element Approach. Presented at the 49 US Rock Mechanics / Geomechanics Symposium held in San Francisco, CA, USA, 28 June 1 July. ARMA 15-293. https://doi.org/10.1002/(SICI)1097-0363(19970415)24:7<645::AID-FLD458>3.0.CO;2-Z

Quentin, M. 2013. Unlocking the Earth - A Short History of Hydraulic Fracturing. GeoExPro, Vol. 10, No. 6. https://www.geoexpro.com/articles/2014/02/unlocking-the-earth-a-short-history-of-hydraulic-fracturing

Raterman, K. et al. 2018. Sampling a Stimulated Rock Volume: An Eagle Ford Example. SPE res Eval & Eng: 927-941. SPE-191375-PA. https://doi.org/10.15530/urtec-20172670034

Raterman, K., Liu, Y., Royet, B. et al. 2020. Analysis of a Multi-Well Eagle Ford Pilot. Presented at the Unconventional Resources Technology Conference held in Austin, Texas, USA, 20-22 July. URTeC: 2570. https://doi.org/10.15530/urtec-2020-2570

Reyes, R., Kyzym, I., Rana, P. et al. 2015. Cuttings Analysis for Rotary Drilling Penetration Mechanisms and Performance Evaluation. Presented at 49th US Rock Mechanics / Geomechanics Symposium, San Francisco, CA, USA, 28 June - 1 July. ARMA 15-764.

Rodríguez, E. 2018. Desarrollo de la técnica de espectroscopia de reflexión óptica difusa para evaluar los cambios en piel de pacientes oncológicos sometidos a teleterapia de fotones de 6 mv. Master thesis, instituto venezolano de investigaciones científicas, I.V.I.C.

Seixas, M., de Ávila C., Leibsohn, A. et al. 2014. Microwave Treatment of Drilled Cuttings Contaminated by Synthetic Drilling Fluid. Separation and Purification Technology 124 (March 18): 68-73. https://doi.org/10.1016/j.seppur.2014.01.011

Shiozawa, S. and McClure, M. 2016. Simulation of proppant transport with gravitational settling and fracture closure in a three-dimensional hydraulic fracturing simulator. J. Pet. Sci. Eng. 138, 298–314. https://doi.org/10.1016/j.petrol.2016.01.002

Siddique, S., Kwoffie, L., Afoakwa, K. et al. 2017. Oil Based Drilling Fluid Waste: An Overview on Highly Reported but Less Explored Sink for Environmentally Persistent

Pollutants. IOP Conf. Series: Materials Science and Engineering 195: 1-9. http://doi:10.1088/1757-899X/195/1/012008

Smith, M. and Montgomery, C. 2015. Hydraulic Fracturing. First Edition, June 9, 2015. Boca Raton, Florida, U.S.A.: CRC Press, Taylor & Francis Group.

Somee, M., Shavandi, M., Mehdi, S. et al. 2018. Bioremediation of Oil-Based Drill Cuttings by a Halophilic Consortium Isolated from oil-contaminated Saline Soil. Biotech 8 (229). https://doi.org/10.1007/s13205-018-1261-8

Suzart, W., Kateb, M., Mohammed, O. et al. 2016. Enhance Production by Infinite Conductivity Technique Applied in Tight Formations. Presented at the Abu Dhabi International Petroleum Exhibition & Conference held in Abu Dhabi, UAE, 7-10 November. SPE-182926-MS. https://doi.org/10.2118/182926-MS

Temizel, C., Energy, A., Betancourt, D. et al. 2016. Optimization of Hydraulic Fractures in Tight-Oil Reservoirs Using Different Numerical Fracture Models. Presented at the SPE Asia Pacific Hydraulic Fracturing Conference held in Beijing, China, 24-26 August. SPE-181824-MS. https://doi.org/10.2118/181824-MS

Todoli Torró, José Luis. 2008. Métodos Espectroscópicos de Análisis. http://rua.ua.es/dspace/handle/10045/7619

Ugueto, G., Huckabee, P., Wojtaszek, M. et al. 2019. New Near-Wellbore Insights from Fiber Optics and Downhole Pressure Gauge Data. Presented at the SPE Hydraulic Fracturing Technology Conference and Exhibition held in The Woodlands, Texas, USA, 5-7 February. SPE-194371-MS. https://doi.org/10.2118/194371-MS

Wang, J., and Elsworth, D. 2019. Proppant Transport in a Propagating Hydraulic Fracture and the Evolution of Transport Properties. Presented at the 53rd US Rock Mechanics/Geomechanics Symposium held in New York, NY, USA, 23–26 June. ARMA 19-1800. https://doi.org/10.1017/jfm.2018.670

Wu, J.; Pan, J., Wang, H. et al. 2019. The Application of Cyclone Desorption Technology for OBM Drill Cuttings Disposal. Presented at the International

Petroleum Technology Conference held in Beijing, China, 26 – 28 March. IPTC-19223-MS. https://doi.org/10.2523/IPTC-19223-MS

Xiang, j. 2011. A PKN hydraulic fracture model study and formation permeability determination. Master of Science Thesis. Texas A&M University.

Xie, S., Deng, H., Wang, R. et al. 2013. Useful Recycling and Safe Disposal Technology of Waste Oil-Based Drilling Fluids and Its Application. Presented at the International Petroleum Technology Conference held in Beijing, China, 26–28 March. IPTC 16623. https://doi.org/10.2523/IPTC-16623-MS

Xu H, Han S., Bi X. et al. 2016. Atmospheric Metallic and Arsenic Pollution at an Offshore Drilling Platform in the Bo Sea: A Health Risk Assessment for the Workers. Journal of Hazardous Materials 304: 93-102. https://doi.org/10.1016/j.jhazmat.2015.10.065

Xu, T., Wang, L., Wang X. et al. 2018. Heavy Metal Pollution of Oil-Based Drill Cuttings at A Shale Gas Drilling Field in Chongqing, China: A Human Health Risk Assessment for the Workers. Ecotoxicology and Environmental Safety 165: 160-163. https://doi.org/10.1016/j.ecoenv.2018.08.104

Yang, S., Matthews, M, Elhadj, S. et al. 2010. Comparing the use of mid-infrared versus far-infrared lasers for mitigating damage growth on fused silica. APPLIED OPTICS / Vol. 49, No. 14 / 10 May. https://doi.org/10.1364/AO.49.002606

Yi, S., Zhiming, W., Yi, X. et al. 2013. The Fundamental Characteristics on Particle Size Distribution of Drilling Rock-cuttings. *Applied Mechanics and Materials* 275-277**.** 2411-2414. http://doi:10.4028/www.scientific.net/AMM.275-277.2411

Yousef, K, AlQallaf, Y., and Fouzy, H. 2017. Oil Based Mud and Drill Cuttings (OBM) Treatment and Management at KOC. International Journal of Waste Resources 7 (3). https://doi.org/10.4172/2252-5211-C1-006

Zhang, G., Li, M., Gutierrez, M., 2017. Numerical simulation of proppant distribution in hydraulic fractures in horizontal wells. J. Nat. Gas Sci. Eng. 48, 157–168. https://doi.org/10.1016/j.jngse.2016.10.043